Stony Brook University

Evaluation of synthetically and naturally derived polymers for drug delivery and adhesion reduction applications

A Dissertation Presented

By

Christine Angelica Falabella

To

The Graduate School

In Partial Fulfillment of the

Requirements

For the Degree of

Doctor of Philosophy

In

Biomedical Engineering

Stony Brook University

May 2011

Stony Brook University

The Graduate School

Christine Angelica Falabella

We, the dissertation committee for the above candidate for the

Doctor of Philosophy degree, hereby recommend

acceptance of this dissertation.

Weiliam Chen – Dissertation Advisor
Associate Professor of Surgery
New York University
Associate Professor of Biomedical Engineering
Stony Brook University

Michael Hadjiargyrou - Chairperson of Defense
Associate Professor of Biomedical Engineering

Sanford Simon
Professor of Biochemistry

Perena Gouma – Outside Member
Associate Professor of Materials Science and Engineering
Stony Brook University

This dissertation is accepted by the Graduate School

Lawrence Martin
Dean of the Graduate School

Abstract of the Dissertation

Evaluation of synthetically and naturally derived polymers for drug delivery and adhesion reduction applications

by

Christine Angelica Falabella

Doctor of Philosophy

in

Biomedical Engineering

Stony Brook University

2011

Polymeric materials have a wide application of use in biomedical applications. The evaluations of several polymers (synthetically and naturally derived) are presented in this dissertation as drug/protein delivery vehicles and solid adhesion barriers. A blended polymer matrix consisting of poly(ethylene glycol)-grafted-chitosan (PEG-g-CHN) and poly(lactic-co-glycolic acid) (PLGA) was used to produce microspheres for therapeutic protein delivery. The release kinetics of a model protein was also investigated as PEG-g-CHN content was varied. A hamster cheek pouch microvascular model was utilized to evaluate the inflammatory potential of both the PEG-g-CHN/PLGA microspheres and released basic fibroblast growth factor (bFGF). We found the protein release rate is regulated by PEG-g-CHN content, and the bFGF released from the microspheres did not produce an inflammatory response in the hamster cheek pouch

blood vessels. Next, in order to reduce post surgical abdominal adhesions in rats, we evaluated the efficacy of two different barrier materials: crosslinked hyaluronan (HA) films and oxidized dextran/N-carboxyethyl chitosan (Odex/CEC) hydrogel. Use of either barrier resulted in significantly lower adhesion severity scores than untreated animals. Finally, microgels composed of Odex/CEC were synthesized to deliver anti-inflammatory drugs (guanidinoethyl disulfide) with the goal of reducing nitric oxide production and oxidative damage following injury. The microgels were characterized after synthesis by measuring the release kinetics of drug and effective diameter. The inflammatory potential of the microgels were evaluated using both a macrophage cell culture model and a murine subdermal implantation model. The drug release kinetics experiments demonstrated a burst release of drug within 24 hours *in vitro* and moderate drug release up to 9 days. The microgels with and without encapsulated drug produced a mild inflammatory response *in vitro* when the particles were co-incubated with macrophage cells. The results of the subdermal implantation study suggested that the drug attracted more inflammatory cells into the implant site compared with the microgel vehicle alone, but produced less capsule fibrosis with the high dose of drug. Overall, the results presented in this dissertation indicate that the polymers studied were promising materials for use as drug/protein delivery vehicles and adhesion barriers.

This dissertation is dedicated to my family.

Table of Contents

List of Tables

List of Figures

Acknowledgements

I would like to thank my research adviser, Weiliam Chen, for his support and guidance throughout the dissertation process. I would also like to thank my committee chair and academic adviser, Michael Hadjiargyrou, for allowing me to continue working in his laboratory to complete my experiments. I am very thankful for the patience and guidance of my other committee members, Perena Gouma and Sanford Simon for their insights and encouragement.

I would also like to thank my labmates, both past and present that have helped me greatly in my research: Hui Pan, Lihui Weng, Evon (Yick) Lee, Eunok Cho, Qiong Zeng, Hanwei Zhang, Ayesha Qadeer, and Sarah Kantharia. I am also thankful for the help of Molly Frame and Aparna Kadam who allowed me to use their microscope equipment for polarized light microscopy during my last few weeks of experiments. Of course, the polarizing light microscopy could not have even started without the polarizer filters which were lent to me by Richard Clark and use demonstrated to me by Lauren Macri.

I am also thankful to the many individuals outside my lab that have aided me in my research: Jim Quinn (SEM), Martin Schoonen (DLS and zeta potential), Mark Melendez (small animal surgical models), Jonathan Chiu (cell culture), Robert Gersch (cell culture), and Joel Israel (histology). I would like to extend a most humble thank you to Suzanne Ferreri for her guidance and patience with me as she helped me prepare for my QE and dissertation proposal. I will never be able to pay her back fully

for her time and energy, but I hope to be able to give back even a fraction of her wisdom as I help others in the future.

Portions of the text of this dissertation are in part reprints of materials as it appears in the following journals: Falabella et al. 2009. J Biomater Sci Polym Ed. 20(7-8): 903-22 (Chapter 2), and Falabella CA and Chen W. 2009. Dig Surg. 26(6):476-81 (Chapter 3), Falabella et al. 2010. J Surg Res. 159(2):772-8 (Chapter 4). I would like to thank the publishers for granting me permission to reprint figures and text from these manuscripts.

I am most grateful for the unwavering support of my family, who saw me through very tough times during my time in graduate school. My brother, James, always encouraged me to do my best and to trust my intuition during the experimental phase of the dissertation. My father was always there to be my “extra adviser” and taught me the art of technical writing in the years before starting my PhD. I am especially thankful for my mother’s positive encouragement through even the most difficult portions of my studies and always seeing the best in me even when I could not. This dissertation is also dedicated to both of my grandmothers, Angeliki and Martha, who passed away in February 2008 and March 2009, respectively.

Lastly, but surely not the least, I want to thank my fiancé, Jesse Muir, for his unconditional love and mutual understanding of how truly terrifying the dissertation process can be.

Chapter 1

Introduction and Specific Aims

1.1 Growth factor delivery using blended polymer microspheres

The delivery of growth factors, proteins that mediate many different processes from wound healing to angiogenesis, is a very promising area of research. Clinical uses of growth factors include the application of vascular endothelial growth factor (VEGF) to promote angiogenesis in ischemic tissue [5], bone morphogenetic protein-2 (BMP-2) to promote fusion between vertebrae [6], and regeneration of smooth muscle using basic fibroblast growth factor (FGF-2) [7]. Development of recombinant therapeutic proteins (e.g. antigens for vaccines) from bacterial or mammalian cell culture by pharmaceutical companies has expanded in the last 25 years. Although some treatments utilizing these therapeutic proteins and growth factors require only a single intravenous delivery, some conditions require a more sustained and localized delivery of these proteins. In some vaccines, immunity to a disease is produced after a series of antigen administrations over a few months. Most antigens and therapeutic growth factors have a brief half-life *in vivo* after administration, therefore shortening their therapeutic window of efficacy [8].

The development of a device to deliver a sustained dose of antigens over time would reduce the need for the patient to return at specific time points to receive booster shots and also reduce the costs to the patient or the patient's health insurance costs.

A delivery vehicle for therapeutic proteins must satisfy a few key requirements: 1) protection of the protein during the vehicle's implantation, 2) vehicle must modulate the release of the protein over time, and 3) the vehicle must be synthesized from a material that has low immunogenicity. There are a vast number of different polymeric delivery vehicles that have been studied, including self-gelling hydrogel solutions [9,10]. electrospun scaffolds [11-13], and micron-sized particles [5,14].

1.1.1 Synthetic polymers for protein delivery

Poly(lactic-co-glycolic acid) (PLGA) is a frequently researched delivery vehicle for both drug and protein delivery because of its degradation characteristics and long record of biocompatibility [15,16]. The polymer is composed of monomer units of glycolic and lactic acid, which are assembled into linear polymers through ester linkages. The mode of PLGA degradation is hydrolysis and the degradation is increased as the localized pH becomes more acidic from the free lactic acid monomers released from the PLGA bulk [17]. The ratio of the two monomers can determine the degradation speed; decreasing the amount of glycolic acid relative to lactic acid greatly increases the degradation resistance of the polymer in aqueous solution [16]. Therapeutic proteins are typically incorporated into PLGA by adding the aqueous solution directly into the organic solvent containing the PLGA [18,19]. After the protein solution is dispersed into the solvent/polymer solution by mechanical stirring, a larger

volume of aqueous solution is added to the same mixing vessel to produce an emulsion. The aqueous solution also contains a stabilizer, such as poly(vinyl alcohol), to maintain the emulsion and prevent polymer droplet coalescence. The organic solvent evaporates from the emulsion resulting in the formation of hard, micron-sized polymer/protein spheres. The particles are extracted from the emulsion by several washes with water or alcohols and then dried by air or by lyophilization.

A major drawback of using pure PLGA in protein delivery is the polymer's intrinsic hydrophobic nature. Because of the hydrophobic characteristic of PLGA, microspheres have a low loading capacity for proteins and display a high initial "burst" release of proteins when placed in an aqueous environment [20]. A high initial release of proteins also suggests that the proteins are located primarily on the microsphere surface, instead of homogenously distributed throughout the particle bulk [21]. The low loading capacity measured in PLGA microspheres may also be due in part to some destruction of the protein due to their exposure to harsh solvents (e.g. methylene chloride) which are routinely used in PLGA microparticle and scaffold synthesis [8]. In general, protein loading is favored by hydrophilic polymers or the addition of hydrophilic polymers blended into a hydrophobic polymer bulk, such as PLGA [22].

The blending of hydrophilic polymers which are either synthetically or naturally derived with PLGA is one method to increase protein loading and modulate the release of those proteins over time. In some early studies, modification of PLGA by adding poly(ethylene glycol) (PEG) to the structure greatly increased the hydrophilic characteristics of the PLGA polymer; however no increase in the loading capacity of the polymer vehicle was observed [23]. In fact, the loading capacity was significantly

decreased with PEG-PLGA polymers compared with pure PLGA polymers alone [23]. These results suggest that simply increasing the hydrophilicity of the polymer bulk alone is not sufficient to improve total protein loading. Despite the decrease in loading efficiency, one positive effect observed of the addition of PEG to the PLGA structure was a decrease in inflammation occurring at the site of vehicle implantation. PEG is a polymer known to circumvent much of the immune system's reaction, giving it the nickname of "stealth molecule" by some biomaterials researchers [24]. While adding PEG to PLGA's structure did not leverage better protein loading or protein release modulation, PEG may be more important in preventing moderate inflammatory reaction upon implantation, an important factor in delivery vehicles.

1.1.2 Blending PLGA with natural polymers to improve loading capacity and modulate release of proteins

Alginate and chitosan are two naturally derived polymers that are frequently combined with PLGA to increase protein loading and modulate protein release over time. Both polymers are hydrophilic and have demonstrated excellent protein binding characteristics when utilized in a delivery vehicle [25] or by themselves [9]. However, both polymers are insoluble in organic solvents that are necessary to process PLGA into microparticles. One method of incorporating alginate and chitosan into PLGA involves the combination of the desired protein payload with either alginate or chitosan, producing microparticles, and then combining the dried alginate/chitosan microparticles with the PLGA dissolved in organic solvent [26,27]. This produces a physical composite of the alginate/chitosan and PLGA. Even though alginate is insoluble in organic

solvents, some researchers have incorporated this polymer as an internal aqueous phase in the PLGA microsphere emulsion process [28]. To prevent the alginate from dissolving, calcium chloride is added to the emulsion to crosslink the alginate inside the PLGA microspheres. These physical blends do not guarantee the homogenous distribution of the natural polymers inside the PLGA, since the alginate is still not easily dissolved in organic solvent solution.

The direct chemical modification of synthetic polymers, such as PEG, with natural polymers may aid in improving the distribution inside PLGA while also modulating protein release over time. In Chapter 2, PEG-grafted-chitosan (CHN) will be introduced as a part-synthetic, part-natural polymer that will be blended with PLGA to study the protein loading characteristics of a model protein, bovine serum albumin. The proposed structure of PEG-g-CHN has a long backbone of positively-charged chitosan with grafted side groups of PEG attached to the backbone molecule [29]. Unlike chitosan and alginate aqueous solutions, PEG-g-CHN is relatively insoluble in water at physiological pH, but it is readily soluble in several organic solvents. The PEG-g-CHN can be easily incorporated into an organic solvent/PLGA solution for producing microspheres using a simple emulsion process. PEG-g-CHN has been previously blended with PLGA to synthesize electrospun scaffolds to deliver ibuprofen [30]. The release kinetics of ibuprofen from scaffolds demonstrated that as PEG-g-CHN percent weight was increased, the initial burst release of ibuprofen was decreased. Additionally, the PEG-g-CHN was retained inside the polymer bulk during the release kinetics experiments when the scaffolds were maintained inside neutral pH buffer for up to 16 days [30]. This last result is important for the maintenance of sustained release of a

drug or protein from the scaffold fibers, since the PEG-g-CHN is electrostatically binding the payload.

1.2 Adhesion reduction barriers synthesized from naturally-derived polymers

Complications from abdominal adhesions cost the US health care system $1.33 billion per year [31]. In the United States, approximately 90% of patients undergoing intra-abdominal procedures will experience some type of tissue adhesions, ranging from thin and filmy to extremely fibrotic [32,33]. Adhesions typically occur when injured tissue come into direct apposition after surgery and incomplete hemostasis deposits fibrin on the visceral surface. The typical window for prophylactic treatments of adhesions is 12-36 hours following surgery [34]. During the inflammation phase of healing, macrophages will migrate into the fibrin network between the two visceral surfaces and secrete cytokines that will promote later fibroblast infiltration into the same fibrin matrix [35-37]. The fibroblasts lay out collagen precursors and later restructure them into Collagen Type I fibers that act as a “bridge” between the two surfaces. In about 10% of adhesion cases, bowel tissue can become twisted as the free tissue pivots around the adhered tissue and cause tissue ischemia and eventually leading to tissue necrosis [31,32,38]. Adhesions that result in strangled bowel or severe pain must be treated by lysing the adhered tissues surgically; however the incidence of adhesion re-occurrence after surgical treatment is significantly higher for these patients [39,40]. Thus, a method to prevent de-novo adhesions would decrease patient

discomfort and decrease hospitalization costs by reducing the need for these follow-up surgeries.

In the last 2 decades, various academic and industrial research groups have investigated different prophylactic treatments for intra-abdominal adhesions to be applied to surgical insults before the operating field is closed. A consensus in the prevention of de-novo adhesions favors the use of a physical barrier to separate injured tissues inside the abdomen [41,42]. The barrier material must meet several requirements for successful implementation: 1) facile application/handling by the surgeon, 2) maintenance of the barrier between healing tissues in the post-operative period (12-36 hours), 3) non-interference with the tissue healing process, and 4) non-promotion of additional adhesions or severe inflammatory response.

1.2.1 Current adhesion barriers utilized in the clinic

The adhesion barriers currently utilized in the clinic are categorized as either non-degradable or degradable. One non-degradable barrier that has shown some success in adhesion prevention is a woven, polytetrafluoroethylene membrane (Preclude™, WL Gore and Associates) [43]. Although it shown to be efficacious in preventing adhesions, it is not a permanent implant and must be removed at a later date [44]. Additionally, the process of removing the Preclude membrane may cause new tissue injury and further adhesions of the newly injured tissue [41]. In contrast, degradable adhesion barriers are more desirable from the standpoint of patient safety/comfort and hospital/insurance costs since it eliminates the need for a second operation. One resorbable barrier that was developed to reduce adhesions in both

pelvic and abdominal surgeries was synthesized from oxidized regenerated cellulose (Interceed, Ethicon, Somerville, NJ). Recently, the FDA has recommended that Interceed only be used in open pelvic surgeries, not abdominal surgeries because of a lack of efficacy reported in this application [45]. Interceed also has specific instructions that dictate how the film must be placed on the injured tissues. The surgeon must insure complete hemostasis [46,47] in the operating field and the pelvic cavity must be free of superfluous peritoneal fluid before placing the Interceed film [46]. In both cases, the anti-adhesive properties of Interceed are rendered ineffective upon contact with blood and excess peritoneal fluid, which will dissolve the barrier prematurely. Additional small animal studies also showed Interceed to be ineffective in reducing adhesions in the abdomen [48,49] and that it caused additional, strong inflammatory reactions [43].

Another FDA-approved barrier is a non-crosslinked film composed of carboxymethylcellulose and sodium hyaluronate (Seprafilm, Genzyme Corporation, Cambridge, MA) that is applied to the injured abdominal or pelvic tissue as a dry film. The film re-hydrates to a gel-like consistency during the 24 hours following surgery and produces a lubricious surface that separates damaged tissues while allowing the tissue to heal under the film. However, the dehydrated film is very brittle and aggressively adheres to any wet surfaces (including surgeon's gloves), making application during surgery difficult [50]. It is also not possible to re-position Seprafilm after it is placed; post-implantation adjustments cause the film to fall apart due to the lack of any crosslinking between the two polymer components. The rigidity of the film also limits the ability to manipulate film to fit small geometries, restricting its use to open surgeries,

not laparoscopic procedures [51]. The next generation of adhesion barriers to be used in the clinic must be mechanically flexible and tolerate rehydration by not degrading after contact with wet tissues or gloves.

1.2.2 Alternate solid film barrier research

Hyaluronic acid (HA) has been previously researched as an adhesion barrier in the abdomen. In early studies, aqueous solutions of HA were applied to injured visceral tissue after surgery in order to measure adhesion occurrence [52,53]. The rationale for using HA is based mainly on its reported anti-inflammatory [54] and anti-cellular adhesion properties [55,56], both ideal characteristics for an adhesion barrier. However, animal surgical model results for the HA solutions were underwhelming at best when compared to untreated control animals [57]. The clearance of solutions of HA inside the abdomen occurs within 6 hours of application, well below the 36 hour window after surgery during which adhesions are reported to occur [58,59]. One solution to the rapid clearance of HA inside the abdomen would require the HA to be crosslinked into a solid film form. Crosslinking would slow the degradation and re-absorption of the HA, providing more residence time as a barrier between the injured tissues during the critical after surgery period. While some methods of crosslinking HA involve the incorporation of the crosslinking initiator into the polymer solution [60] prior to casting, Yeo et al. developed a two-part, self-crosslinking HA gel/film barrier composed of adipic dihydrazide and aldehyde-modified HA [61]. The self-crosslinking solution could be added directly to the site of abdominal tissue insult or the solution could be cast and dried before using it as a solid film barrier in the same application. A

possible downside to using modified HA to produce crosslinked barriers is the cost of processing and purification of the final polymer components before use.

In our lab, we previously developed crosslinked HA films for gene delivery applications to reduce abdominal adhesions [62]. The films were tested to deliver hyaluronic acid synthase (HAS) as the film acted as a physical barrier to adhesions. The modulation of HAS release would be dependent on the enzymatic degradation of the film inside the abdominal cavity. We proposed utilizing this film as a barrier material without therapeutic genes to reduce intra-abdominal adhesions. The films were synthesized by casting a 1% HA solution and the solution was then dried for several days. After the films were thoroughly dry, they were crosslinked using dihydrazide chemistry. This crosslinking chemistry was advantageous because it does not require extensive pre-processing of HA and the crosslinking reaction occurs after the film is cast and dried, not inside the cast HA solution. We tested the efficacy of the HA film using a 21 day, rat cecum abrasion model for post-surgical adhesions. The extent and severity of adhesions in the abdomen were evaluated on a graded scale and compared to control animals that did not receive any film treatment.

1.2.3 Crosslinked hydrogel barriers

The application of a self-crosslinking, liquid adhesion barrier would circumvent the rigidity issues of a solid film (e.g. Seprafilm), but also allow the barrier to be applied over a wide range of tissue geometries and in limited spaces (e.g. laparoscopy) [43]. Currently, there are no FDA-approved liquid or hydrogel barriers that have successfully been introduced into the market. Several different formulations of a crosslinking, liquid

HA barrier have been explored, including a spray form (SprayGel, Confluent Surgical, Waltham, MA) and a syringe applied solution made from ferric hyaluronate (Intergel, Ethicon, Somerville, NJ). SprayGel has shown great promise in clinical trials in preventing pelvic tissue adhesions; however a drawback to this device is the need for the hospital to purchase an additional piece of equipment to propel the solution for application. Inconsistency of clinical results across different HA derived liquid barriers has hindered the wide adoption of barriers of this type [63]. Intergel showed good efficacy in early laboratory tests and clinical trials, but was removed from market in 2003 because of wide-spread reports of severe complications in some patients, including pain, strong foreign body reactions, and additional tissue adhesions [64].

Other naturally derived polymers have been explored as adhesion barrier material, such as chitosan, a deacetylated derivative of chitin [65]. Chitosan is biocompatible and enzymatically degradable, [66] and it can be modified to enhance crosslinking activity [67]. This polymer is positively charged and has demonstrated excellent adhesion to negatively charged surfaces, such as mucosal membranes [68]. In its native form, chitosan also difficult to dissolve in water at a neutral pH (i.e., 7.4), requiring more acidic conditions to dissolve [65]. One method to achieve solubility at neutral pH is to modify the molecule with side groups on the chitosan's nitrogen and oxygen centers, such as by adding carboxymethyl groups to formulate N,O,-carboxymethyl chitosan (NOCC) [67]. This produces a self-crosslinking hydrogel that does not require an additional agent, such as glutaraldehyde [69], to initiate solution stiffening. The use of a secondary crosslinker in any biomaterials application can lead

to downstream toxicity and irritation if any un-reacted crosslinker remains inside the crosslinked polymer and leeches out over time.

NOCC has been previously studied as a reducer of adhesions in a rat small intestine [67] and rabbit large intestine (cecum) [70] surgical models. In both animal studies, NOCC was added to as a 1% gel to the injured tissue and 2% solution to the peritoneal cavity. The results demonstrated significance improvement in cecal (large intestine) adhesion severity scores of NOCC treated animals over untreated controls. However, the authors did not address whether the application of the 2% NOCC solution was necessary to prevent adhesions alongside the 1% NOCC gel. Yeo et al. also investigated the biocompatibility of a UV-crosslinked chitosan-based hydrogel inside the rabbit peritoneal cavity which could be used as a combination drug delivery vehicle and adhesion barrier [71]. The results of the study were less than desirable in terms of abdominal compatibility; both animals that received the UV-crosslinked gel or the un-crosslinked chitosan solution formed adhesions between and multiple nodules on the cecum and on the omentum (a section of the peritoneum) [71]. The nodules appeared to be granulomous and contain clusters of macrophage/lymphocyte cells and pieces of chitosan gel surrounded by a thick, fibrotic capsule. The results of this study suggest that the chitosan preparation used in the study would be unsuitable for intraperitoneal usage. Therefore, new crosslinking preparations of chitosan must be developed to increase biocompatibility of the polymer inside the abdominal cavity.

The derivatization of chitosan using acrylic acid to form carboxyethyl chitosan (CEC) is another reported method to increase chitosan's solubility in water [72,73]. Unlike NOCC, the chemical modification of chitosan to CEC does not create a self-

crosslinking material, however the presence of amine side groups in CEC allows for cross-linking with other polymers with complementary aldehyde side groups. Similar to chitosan, dextran can also be modified to present reactive functional groups. Oxidation is one method that adds aldehyde groups to the dextran molecules which allows for crosslinking with other polymer molecules presenting amine groups [72,74]. Aqueous solutions of oxidized dextran (Odex) and CEC have been combined to produce a stable, crosslinked hydrogel at room temperature [72,75]. The chemical bonds between the aldehyde and amine groups of Odex and CEC are characterized as “Schiff Base” linkages [72]. *In vitro* cytotoxicity studies have demonstrated that the Odex/CEC hydrogel formulation has excellent biocompatibility with dermal fibroblast cells in direct contact with the hydrogel surface and encapsulated inside the crosslinked hydrogel [75]. In Chapter 3, a 2% Odex/CEC hydrogel was investigated as an *in situ*, abdominal adhesion barrier using the same surgical adhesion model in rats as previously described. This experiment allowed us to assess the biocompatibility of the hydrogel inside the abdominal cavity and its interaction with healing visceral tissue surfaces.

1.3 Delivery of anti-inflammatory drugs using naturally-derived polymers

During the early stages of traumatic injury, the body produces inflammation to both notify the immune system about the presence of foreign pathogens and to signal the start of the healing process that will occur after the inflammatory period has come to an end. Shortly after injury, the rupture of blood vessel walls triggers the infiltration of polymorphonuclear cells (PMNs), including neutrophils and monocytes, to the trauma area. The neutrophils are present in the wound for a short time, but their main task is to

phagocytize and digest foreign pathogens (e.g. bacteria), foreign materials, and damaged cells in the wound area. The next phase of inflammation involves the differentiation of monocytes (from circulating blood) into macrophages. The macrophages are also strong phagocytes that help clear dead neutrophils and damaged tissue from the wound.

Once inside the wound area, macrophages also secrete a variety of pro-inflammatory cytokines and molecular mediators that help regulate the down-stream healing process, including wound closure (i.e. fibrosis). The nitric oxide (NO) is produced by inducible nitric oxide synthase (iNOS) in macrophages responding to certain secreted cytokines and endotoxins during inflammation (Figure 1) [76]. The up-regulation of iNOS is mediated by the activation of nuclear factor kB (NF-kB). The iNOS enzyme converts L-arginine and oxygen into L-citrulline and NO as products. The NO also combines with other oxidative metabolic products, such as superoxide (O_2^-), to synthesize reactive peroxynitrites that are toxic to invading bacteria and protect the patient from infection [77,78]. Peroxynitrites can also provide protection from viral infection by inhibiting the replication by crosslinking viral transcription proteins, thereby rendering them inactive [79]. iNOS is a potent synthesizer of NO and is more active than other NO synthases produced in the body [78]. Healing wounds require a certain level of NO production for collagen synthesis and wound contraction [80,81]. However, extended periods of inflammation and an over-exposure to peroxynitrites can be harmful to surrounding tissues/migrating cells and promote fibrotic tissue/scar formation [78,82,83]. When iNOS activity was inhibited specifically, collagen deposition and wound contraction were greatly decreased [84,85]. In this injury state, overabundant

peroxynitrites produced during the initial inflammatory period following spinal cord damage causes oxidative damage that leads to further nerve cell death and glial scarring which can hinder the implementation of stem cell therapy at later time points following the initial injury. In this section, the application of iNOS inhibitor application will be discussed in terms of reducing oxidative damage from peroxynitrites.

1.3.1 Reduction of peroxynitrite damage using inhibitors of iNOS

As previously mentioned, oxidative damage produced by peroxynitrites following spinal cord injury induces scar tissue formation and impairs neuronal cell repair. The application of a peroxynitrite scavenger, Manganese (III) Tetrakis (4-Benzoic Acid) Porphyrin (MnTBAP), has been studied as a method of reducing peroxynitrites after spinal cord injury [86,87]. MnTBAP reduces peroxynitrite by its strong affinity to bind peroxynitrite directly [86]. When MnTBAP was applied directly to a damaged spinal cord, researchers reported a significant decrease in both the oxidation and nitration of proteins in the spinal cord tissue [88]. However, the drug does not reduce any of the molecular pre-cursors to peroxynitrite formation, nitric oxide (NO) or superoxides (O_2^-), which are formed during the initial inflammatory phase following injury. Another approach to prevent peroxynitrite damage following spinal cord injury would include both the reduction of NO synthesis by iNOS during the inflammatory phase and the scavenging of any peroxynitrites that formed despite the reduction in NO synthesis.

In recent years, a group of anti-inflammatory drugs called mercaptoalkylguanidines (MAGs) have been investigated to inhibit NO generation associated with gingivitis/bacterial infection, chronic airway inflammation, and arthritis [83,89-91]. Mercaptoethylguanidine (MEG), a compound found in the MAG group, has

a dimeric form called guanidinoethyl disulphide (GED) that has a high specificity for inhibiting iNOS produced by macrophage cells [91]. GED inhibits iNOS through the competitive inhibition of L-arginine binding and conversion into L-citrulline and NO. Systemic administration of MEG has been studied to treat experimentally-induced periodontitis in rats and demonstrated a significant decrease in the severity of symptoms in the gum tissue [83]. GED has also demonstrated peroxynitrite scavenging properties in addition to reducing NO production [92]. The term scavenging refers to prevention of peroxynitrite oxidation through the direct interaction of GED's thiol groups with peroxynitrite [92]. Systemic administration of GED, a potent depressor and vasodilator, may not safe for patients since it could also cause undesirable system-wide side-effects [93]. The use of a locally administered, controlled release method for GED will allow the drug to be applied very close to the targeted tissue and decrease the undesirable systemic side-effects of GED.

1.3.2 Microgels composed of natural polymers to deliver iNOS inhibitors

Microspheres fabricated from natural polymers have been extensively investigated in drug delivery, including trans-scleral applications. In particular, microspheres produced from hydrogel formulations have been recently studied in the drug delivery field. The process sometimes involves adding a mixed solution of polymers (from original hydrogel formulation) to a temperature-controlled oil bath and mechanically agitated to break the polymer solution into smaller droplets (i.e. microspheres). An emulsion stabilizer is added to the oil phase to decrease droplet coalescence and maintain droplet dispersion inside the emulsion [94]. Agnihotri and

colleagues demonstrated a similar hydrogel microsphere fabrication process using poly-ethylene oxide-*grafted*-polyacrylamide (PEO-*g*-pAAm) and chitosan for the delivery of the anticancer drug Capecitabine [95]. The cross-linking process is not initiated when the chitosan/PEO-*g*-pAAm mixture is added to the light liquid paraffin/surfactant phase during the emulsion process; however additional glutaraldehyde and hydrochloric acid are added to the continuous phase of the emulsion to produce cross-linked microspheres [95]. As mentioned in the previous section, glutaraldehyde is an effective cross-linking agent, but it is also very toxic to cells and tissues even in small quantities.

As mentioned in Section 1.2, we have previously developed a macromolecular, self-crosslinking hydrogel system composed of Odex and CEC in our laboratory. Microgels synthesized from Odex and CEC could be developed for the encapsulation and delivery of an iNOS inhibitor, GED. The self-crosslinking properties of the two polymers would allow for the microgels to stiffen as individual droplets inside the emulsion without the addition of a secondary crosslinking initiator. This would also simplify the post-processing since there is only the innocuous oil phase of the emulsion to remove.

Hypothesis and Specific Aims

The overall goal of this study is to evaluate natural and synthetic polymers for adhesion reduction and drug/protein delivery applications.

Specific Aim 1:

Evaluate the release modulation of a model protein, BSA, from microspheres composed of different concentrations of PEG-g-CHN blended with PLGA and evaluate the effects of released bFGF from the microspheres in a microcirculation model.

Hypothesis 1.1: Increasing the weight percent of PEG-g-CHN will decrease the cumulative release of BSA and decrease the burst release of protein.

Hypothesis 1.2: PEG-g-CHN/PLGA microspheres and microsphere-released bFGF will not induce pre-conditioning or inflammation responses in a hamster cheek pouch blood vessel model.

Rationale: In a previous study by Yun et al, microspheres composed of PEG-g-CHN blended with PLGA was used to encapsulate plasmid DNA [96]. The researchers found that with increased PEG-g-CHN weight fraction, the burst release at the first sampling period was decreased [96]. PEG-g-CHN is a positively charged molecule with the potential to bind negatively charged proteins and modulate their release over time while also protecting the proteins from damage during microsphere synthesis. If the proteins become aggregated or denatured during processing, an inflammatory response in the tissue surrounding the microspheres can occur.

Specific Aim 2:

Evaluate the efficacy of a crosslinked, 1% HA film on the reduction of post-surgical adhesions in an experimental rat model.

Hypothesis 2: Crosslinked HA films will reduce the severity of intra- abdominal adhesions after 21 days compared with untreated control animals.

Rationale: Hyaluronan is considered to be very biocompatible, has been utilized in a variety of both wound healing and drug delivery applications, and can resist cell adhesion. Since aqueous solutions of HA are cleared quickly in vivo (<12 hours), we chose to evaluate a crosslinked, HA film to reduce post-surgical adhesion in a rat model. Crosslinking the HA should allow the film to remain in place during the first 36 hours following tissue injury and reduce the incidence and severity of cecal adhesions.

Specific Aim 3:

Evaluate a macromolecular, self-crosslinking hydrogel composed of Odex and CEC as a barrier for the reduction of post surgical adhesions in an experimental rat model and compare efficacy to a clinically available barrier, Seprafilm.

Hypothesis 3: The Odex/CEC hydrogel will reduce the severity of intra-abdominal adhesions compared with Seprafilm and the untreated controls.

Rationale: In this specific aim, we developed a self-crosslinking hydrogel that can conform to complex geometries inside the abdomen and be later adapted to laparoscopic procedures. This experiment allowed us to assess the biocompatibility of the hydrogel inside the abdominal cavity and its interaction with healing visceral tissue surfaces. In parallel, the hydrogel treated animals were benchmarked against a

clinically available barrier material (Seprafilm). This comparison allowed us to assess the adhesion prevention quality of the Odex/CEC hydrogel against a current and proven standard of care in the clinic.

Specific Aim 4:

Synthesize microgel particles produced from Odex and CEC to deliver an iNOS inhibitor drug and test the inflammation potential/biocompatibility of microgels (with and without drug) in a macrophage cell culture and in a murine subdermal implant model.

Hypothesis 4.1: An increase in GED loading of the microgels will reduce diameters of the microgels compared with microgels with a low dose of GED or no GED loaded.

Hypothesis 4.2: Microgels will elicit a mild foreign body reaction with macrophage cells in culture.

Hypothesis 4.3: Microgels that are subdermally implanted will demonstrate decreased inflammatory cell infiltration into the implant area and decreased fibrous tissue capsule surrounding the implant with increasing GED dose.

Rationale: As a bulk material, Odex/CEC hydrogel has shown good biocompatibility as a wound covering and the aldehyde side groups on Odex could be utilized to bind small molecule drugs with amine side groups, such as GED [75]. The self-crosslinking nature of Odex and CEC is adaptable to crosslinking as spherical microgels inside an single emulsion preparation

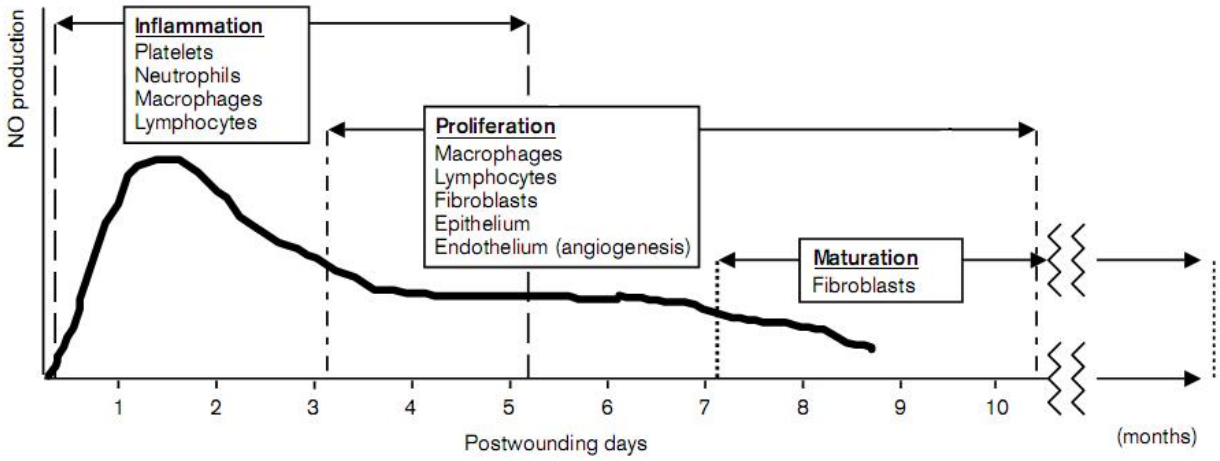

Figure 1: Temporal production of nitric oxide (NO) during wound healing and the cell types present during each phase. Figure reproduced with permission from Efron DT, Most D, and Barbul A. Role of nitric oxide in wound healing. *Curr Opin Clin Nutr Metab Care*. 3(3): 197-204 (2000).

The results presented in Chapter 2 have been previously published (Falabella CA, Jiang H, Frame MD, Chen W. J Biomater Sci Polym Ed. 20(7): 903-22. 2009). All tables and figures have been reproduced with written permission from Koninklijk Brill NV.

Chapter 2

In Vivo Validation of Biological Responses of bFGF Released from Microspheres Formulated by Blending Poly-lactide-co-glycolide and Poly(ethylene glycol)-grafted-Chitosan in Hamster Cheek Pouch Microcirculatory Models

2.1 Summary

Microspheres formulated from blending poly(lactide-co-glycolide) (PLGA) and poly(ethylene glycol)-grafted-chitosan (PEG-g-CHN), using a modified in-emulsion-solvent-evaporation method, was investigated for the delivery of protein. A model protein, bovine serum albumin (BSA), was incorporated into the PLGA/PEG-g-CHN microspheres and both initial burst and release kinetics could be modulated by varying the PEG-g-CHN content. Basic fibroblast growth factor (bFGF) was formulated into the microspheres containing 5% PEG-g-CHN and the bFGF contents in the releasates were determined by a receptor based ELISA with their in vitro bioactivities validated by fibroblast cell culture. The in vivo effect of the bFGF microspheres formulation was evaluated in a hamster cheek pouch model using a 7 day exposure (e.g., before significant vascular remodeling was expected). Using intravital microscopy, the tissue showed no evidence of inflammation with any formulation; deliberate activation of a preconditioning response linked to inflammation was attenuated by BSA microspheres

alone. Vasoactive responses (receptor-dependant and independent constriction and dilation) linked to nitric oxide were attenuated, and constriction to endothelin was enhanced in bFGF and not BSA containing microspheres. PLGA/PEG-g-CHN blended microspheres were also demonstrated to be non-inflammatory and non-thrombogenic in vivo by observing the vascular changes in the cheek pouch. In conclusion, the addition of PEG-g-CHN to PLGA microspheres can serve as a sustained delivery vehicle for bFGF and the released protein provides vasoactive changes consistent with chronic bFGF exposure.

2.2 Introduction

Synthetic and naturally derived biodegradable polymers are two classes of biocompatible materials that have been widely investigated as vehicles for delivery of bioactive agents, such as nucleic acids [97,98] and recombinant proteins [99,100]. Two representative materials that have been extensively investigated are poly(lactide-co-glycolide) (PLGA), a synthetic polymer, and chitosan, a natural polymer. Materials consisting of PLGA or chitosan have vastly different physicochemical properties, the former is mechanically strong, solvent soluble, and thus easy to process; in contrast, the latter is brittle and only soluble in acidic aqueous media [101].

PLGA has been utilized in formulating microspheres for protein encapsulation with the goal of achieving prolonged release while retaining protein bioactivity. This was exemplified by a reported formulation of encapsulating crystalline vascular endothelial growth factor (VEGF) into PLGA/poly(ethylene glycol) (PEG) microspheres [102]. The rationale for using solid protein particulates was the reduction of the protein's exposure

to shear stress during encapsulation which could cause denaturation if prepared in aqueous solution [102,103]. However, the encapsulation efficiency was greatly compromised partially due to the hydrophobicity of PLGA. It is possible that the solid protein crystals were incompletely encapsulated as signified by a measured rapid burst release of VEGF [103]. This phenomenon has also been observed in comparable microsphere formulations designed to encapsulate proteins [19,104-106]. Another issue that has not yet been adequately addressed is the inflammatory response evoked by PLGA upon in vivo administration [107]. The blending of PEG with PLGA increases biocompatibility [108-110], however, the encapsulation efficiency of proteins inside PLGA-PEG particles is decreased as compared with pure PLGA particles [111]. Conversely, chitosan has a polycationic backbone capable of electrostatically binding with charged molecules, such as protein [112]. However, native chitosan requires an acidic pH for processing [113] and this has compromised its potential uses in protein encapsulation and delivery.

Blending of PLGA and chitosan represents a strategy of leveraging the unique advantageous properties of the individual polymers with vastly different physicochemical properties while mutually compensating each other's limitations. Nonetheless, formulating these blends is not a trivial issue. We have previously demonstrated the feasibility of co-processing PLGA with chitosan rendered solvent soluble through grafting of PEG [96]. The grafting of PEG to chitosan also greatly enhanced its biocompatibility [114]. Accordingly, integrating PEG, which is recognized for its "stealth" characteristics, into the structure of the PLGA/PEG-grafted-Chitosan (PLGA/PEG-g-CHN) blend could potentially enhance its biocompatibility overall. In this chapter, we

characterize the in vitro and in vivo performance of PLGA/PEG-g-CHN blend microspheres, with basic fibroblast growth factor (bFGF) incorporated, formulated using a modified double emulsion solvent evaporation method.

A PLGA/PEG-g-CHN microspheres formulation was selected for in vivo validation of both its biocompatibility and efficacy in hamster check pouch model through a standard 7-day exposure protocol in our laboratory. The cheek pouch is a highly perfused structure with a very well-defined vascular architecture; it is a sensitive model for studying vascular functional changes. We have previously shown that local application of an adenoviral vector in the hamster cheek pouch produces localized genomic changes with minimal impact on the whole animal [115]. Accordingly, we examined both whole animal behavior, and microvascular function following chronic exposure to bFGF containing microspheres. The vasoactive responses that were examined included both receptor-dependent and independent constriction and dilation, responses requiring vascular communication [4], flow mediated dilation [3], and microvascular pre-conditioning, a response tightly linked to oxidative stress (e.g., inflammation) [1]. This spectrum of well characterized microvascular responses tested both the ability of individual arteriolar segments to constrict and dilate, and also tested how the arteriolar network functioned as a whole. Lastly, we compared the responses in adult hamsters treated with microspheres to those of juvenile hamsters with actively growing tissue, yet, receiving no treatment.

2.3 Methods

2.3.1 Synthesis of PEG-g-CHN

PEG-g-CHN was synthesized following a procedure modified from the method described by Nishimura et al [116]. Briefly, chitosan was modified to form 6-O triphenylmethyl-Chitosan. Activation of methoxy poly(ethylene glycol) (mPEG-OH, MW 2000) (Sigma-Aldrich, Saint Louis, MO) was performed at room temperature using 1,1-carbonyldiimidazole (CDI) dissolved in tetrahydrofuran. It was then coupled to 6-O-triphenylmethyl-Chitosan in dimethylformamide (DMF) at 75 °C with dimethylaminopyridine (DMAP) as a catalyst. PEG-g-6-O-triphenylmethyl-CHN formed was precipitated with ether; and removal of the triphenylmethyl groups was accomplished using 50% acetic acid. Thereafter, the acidic solution was neutralized with triethylamine (TEA). PEG-g-CHN was recovered by precipitation and collected by filtration; this was followed by washing thrice with water. De-protection of triphenylmethyl groups was confirmed by the absence of UV absorption at 265 nm (Lambda 12, Perkin-Elmer, Shelton, CT, USA). The pure PEG-g-CHN obtained was characterized following a method described elsewhere [30].

2.3.2 Formulation of Microspheres

Microspheres were formulated using a modified water-in-oil-in-water (W/O/W) in-emulsion-solvent evaporation technique. Briefly, PLGA (400 mg) and PEG-g-CHN were dissolved in a co-solvent of $CHCl_3$ and DMSO. The weight percents of PEG-g-CHN investigated were 0.5, 1, 5 and 10% (2, 4, 20, and 40 mg PEG-g-CHN, respectively). In this experiment, bovine serum albumin (BSA) was chosen as a model protein to investigate release kinetics of the PLGA/PEG-g-CHN microspheres. An aqueous BSA

solution (3 mg/mL) was emulsified at 4°C with the solution of PLGA and PEG-g-CHN under rapid stirring at 1,500 rpm (LR400 Lab Stirrer, Yamato, Tokyo, Japan) to form a primary W/O emulsion; it was further emulsified with a 2% polyvinyl alcohol (PVA) aqueous solution to form a W/O/W emulsion. This stirring speed was reduced to 1,000 rpm and maintained for an additional 4 hours at 4˚ C; then the stirring speed was further decreased to 500 rpm overnight to enable slow evaporation of chloroform. To recover the microspheres formed, the mixture was centrifuged at 1,500 rpm for 15 minutes and the microspheres pellet recovered was re-dispersed in water and centrifuged. This procedure was repeated thrice for removal of PVA. The washed microspheres were snap frozen, lyophilized (Freezemobile 6100, VirTis, Gardiner, NY), and stored in a desiccator at -20°C before use.

2.3.3 Microsphere BSA Release Kinetics

Various microspheres formulations composed of PLGA and PEG-g-CHN (content: 0.5, 1, 5 and 10%) were evaluated. Briefly, approximately 30 mg of each PLGA/PEG-g-CHN microsphere formulation was re-suspended in 1 ml of pH 7.4 phosphate buffered saline (PBS) in each vial. All vials were agitated vigorously (LabQuake shaker L-1237, Lab Industries, Berkeley, CA) at 37˚ C. At pre-stipulated time intervals (1, 2, 4, 8 hours, and 1, 2, 5, 7, and 14 days), each vial was centrifuged (Model 5682, Forma Scientific, Inc., Marietta, OH) for 10 minutes at 1,500 rpm at room temperature, supernatants were collected and stored at -20˚ C. Each vial was replenished with an aliquot of equal volume of fresh PBS solution. BSA concentrations in the releasates collected was determined by a bicinchoninic acid assay kit (Pierce

Biotechnology, Rockford IL) using a microplate reader (Biotek Instruments, Inc). Released BSA data was normalized to the average weight of microsphere aliquot used (µg BSA/mg microspheres).

2.3.4 bFGF Release Kinetics

These microspheres were formulated using a protocol comparable to the one used for preparing microspheres for BSA encapsulation (see above). A blend containing PLGA/5% PEG-g-CHN was used as the model preparation for in vitro characterization. Following the procedure described above, a 3 mg/mL BSA solution (with 100 µg of bFGF and 100 µg of heparin co-dissolved) was used to prepare the primary W/O emulsion. The microspheres prepared were lyophilized, and stored in a desiccator at -20° C before use. The release experiments were performed in triplicate exactly as the BSA microspheres. The bFGF contents of the releasates collected during the course of the study were quantified by a receptor based ELISA assay (Quantikine™ bFGF assay kit) acquired from R & D Systems (Minneapolis, MN).

2.3.5 In vitro verification of the bioactivities of bFGF releasate

Murine M.DUNNI dermal fibroblasts (clone III8C, CRL-2017) (ATCC, Manassas, VA) was used as model cell line to characterize changes in cell morphology in the presence of exogenous bFGF. Approximately 10,000 cells in Dulbecco's Modified Essential Medium (DMEM, Invitrogen, Carlsbad, CA) supplemented with 0.5% fetal bovine serum (FBS) (Hyclone, Logan, UT) and 100 units/mL Penicillin/100 µg/mL Streptomycin solution (Gibco, Grand Island, NY) were seeded in individual wells of 24-

well culture plates. Cells were incubated overnight at 37° C under a humidified atmosphere of 5% CO_2 air before adding exogenous bFGF. To dilute releasate samples and bFGF stock solutions, 0.1% bovine serum albumin (BSA) solution was utilized, as recommended by the manufacturer. After quantifying the released bFGF with an ELISA protocol, the 2 hour releasate samples from bFGF microspheres were diluted to a concentration of 10 ng/mL and 50 µL of the mixture (n=3) was added to the proper wells on the plate, similar to the method described by King et al [102]. In addition to the releasate samples, 10 ng/mL bFGF (R&D Systems, Minneapolis, MN) (n=3), 0.1% bovine serum albumin (BSA) (Sigma-Aldrich, St. Louis, MO) (n=3), or phosphate buffered saline (PBS) (Sigma-Aldrich, Louis, MO) (n=3) in 50 µL aliquots were added to separate wells on the same plate. At the end of a 48 hour incubation period at 37° C, the cells were rinsed with PBS and fixed with a 70% ethanol solution. Cells morphology was observed using light microscopy (Zeiss-Axiovert 200M, Carl Zeiss Micro Imaging GmbH, Germany) and images were digitally captured.

2.3.6 In vivo microsphere infiltration protocol

All in vivo studies were performed following protocols approved by the Institutional Animal Care and Use Committee (IACUC) of SUNY-Stony Brook. Golden hamsters (adult male: HSD:Syr, N=12, 72±13 days, 95±10 grams) were anesthetized with pentobarbital sodium (70 mg/kg ip). Using a previously described protocol [115], 1 mg of microspheres (PLGA/10%PEG-g-CHN with BSA only, or PLGA/10% PEG-g-CHN with bFGF) was suspended in 200 µl sterile media was infiltrated to the left cheek pouch. Over the next 7 days, animals were monitored for wellness [115]. No animals

were removed from the study; no animals showed clinical signs of lethargy or illness. Four animals received PLGA/10% PEG-g-CHN microspheres without bFGF, and eight animals received PLGA/10% PEG-g-CHN microspheres with bFGF (130 ng bFGF per mg of microspheres). On day 7, these 12 animals were observed with intravital microscopy in an acute animal preparation.

Acute animal preparation - Golden hamsters (adult males injected with microspheres 7 days prior: HSD:Syr, N=12, 79±13 days, 98±9 grams; adult males not injected with microspheres: HSD:Syr, N=7, 87±8 days, 107±8 grams; juvenile males: HSD:Syr, N=6, 43±4 days, 84±9 grams) were anesthetized with pentobarbital sodium (70 mg/kg ip), tracheostomized, and maintained on constant infusion of pentobarbital sodium (10 mg/kg at 0.50 ml/hr ip). Specific procedures used to prepare the left cheek pouch for in situ intravital microscopy are described elsewhere [1-3].

Arteriolar networks fed by an arcade arteriole (Figure 2.1) were chosen for this study [2,3,117]. Both local and remote vasoactive responses were examined. For local responses, the test agents were applied via micropipette to the location specified in Figure 2.1A, which was the entrance to the arteriolar network, and observations were made at this location. For remote responses, the test agents were applied to the location specified in Figure 2.1B, which was the distal end of the network, and observations were made upstream at the local response area (Figure 2.1A).

Micropipette techniques - Custom fabricated micropipettes (tip diameter: 15-20μm, Kopf Instruments) were backfilled with test agents, and placed within 25 μm of the arteriolar wall. Outflow of the micropipette was pneumatically controlled (PLI-100, Medical Systems, Corp., Greenvale, NY) at an ejection pressure range of 0.2-0.4 psi.

Each test agent solution contained 25 μM FITC-dextran (MW 40,000) as a flow marker, and the flow path was observed under a Chroma B1E filter set (Chroma Technology, Inc., Brattleboro, VT). Because of the placement of the micropipette, geometry of the chosen sites, and continuous flow of suffusate over the tissue (5ml/min), the micropipette's contents were carried away from the local exposure area when drugs were applied at remote exposure area, and were not re-circulated. Typical application times were 60 seconds (unless noted otherwise), and were always preceded by a 30 second baseline time-period. Test protocols 1-3 (below) were performed at different vascular locations.

Protocol 1 Local Responses - Local vasoactive responses were obtained by applying constrictors: 20 mM KCl (directly depolarizing smooth muscle), 10^{-8} M endothelin (ET, a vasoconstrictor acting via receptors), and dilators: 10^{-4} M sodium nitroprusside (SNP, a NO mimetic agent acting on smooth muscle via cGMP), 10^{-4} M adenosine (ADO, a vasodilator acting via receptors, cAMP mediated). Following a 30 second stable baseline diameter, the drug was micropipette applied for 60 seconds at the local exposure region (Figure 2.1A) while simultaneously observing the change in diameter of the vessel in the same area. The drugs were applied in random order, waiting for full recovery of diameter before the next exposure.

Protocol 1 was also used to test the bioefficacy of bFGF in microspheres in order to confirm that microsphere encapsulation did not compromise bFGF's capacity to elicit normal vasodilation response. While bFGF has numerous biological effects, we reasoned that if bFGF released from microspheres could induce vasodilation upon release, a specific biological effect involving binding of bFGF to its receptor was being

demonstrated. In conjunction with this we tested the microspheres with no bFGF to rule out material induced vasoactive response. In seven animals we evaluated the vasoactive response to the following micropipette applied formulations: native bFGF (native bFGF, 166 ng/ml), microspheres composed of only PLGA polymer with bFGF (166 ng /ml equivalent, these microspheres were formulated without PEG-g-CHN in order to exhibit a typical "burst-release" occurring over minutes), PLGA/10% PEG-g-CHN microspheres containing only bovine serum albumin, and PLGA/10% PEG-g-CHN microspheres containing no biological proteins.

Protocol 2 Remote Responses - Remote responses were obtained by applying SNP (10^{-4} M) [4], or LM609 (10μg/ml, acting on αvβ3 integrin receptors [3]). Following a 30 second stable baseline diameter, the drug was micropipette applied for 60 seconds at the remote exposure area downstream, while observing the local exposure area upstream. A remote response is observed within seconds of drug exposure, and only lasts the duration of drug exposure. The drugs were applied in alternate order, waiting for full recovery of diameter before the next exposure.

Protocol 3 Remote Vascular Pre-conditioning - This response involves both remote and local mechanisms. The arteriolar network could be preconditioned by an initiating signal, linked to NO or oxidative stress, at the remote exposure area; which results in a change in the local responses to many stimulations, including enhancement of dilation to SNP, attenuation of dilation to ADO and presence of dilation to L-arginine (L-arg) at the local exposure area[1,118] (Without preconditioning, micropipette applied L-arg is not vasoactive). Testing this response thus requires 3 separate exposures. First, L-arg (10^{-4} M) was applied to location A to confirm absence of preconditioning; this

is the control response. Second, we preconditioned the arteriolar network by applying SNP (10^{-4} M) to the remote location; this data is not shown. Third, fifteen minutes later, we tested whether preconditioning had been induced by applying L-arg again to the local exposure area.

2.3.7 Data Acquisition and Statistics

The in vitro release kinetics data was analyzed by averaging data points for each time point with standard deviation calculations. ANOVA one-way and Tukey post-hoc test was used to compare burst and cumulative BSA release after 1 hour and 14 days. These results were considered significant when $P<0.05$. For in vivo experiments, all diameter measurements were obtained online calibrated with a micrometer, using a video caliper system (Microvascular Research Institute, College Station, TX) and a software data acquisition system (Strawberry Tree; Workbench, Sunnyvale, CA). The diameter change is reported as the fractional change in diameter from baseline: ([(peak-baseline)/(max-min)], where the maximum and minimum diameter was obtained with 10^{-3} M adenosine and 10% oxygen while testing for tone. The diameter changes were evaluated with student's-t test for paired comparisons, alpha = 0.05 [119].

2.4 Results

2.4.1 BSA Release Kinetics

The release kinetics of various PLGA/PEG-g-CHN blended microspheres containing BSA is depicted in Figure 2.2. The loading of BSA was estimated for each

formulation after dividing the total weight of BSA added to the emulsion by the total weight of polymers. All formulations showed moderate initial “burst” releases; and the extent of “burst” increased as the weight percentage of PEG-g-CHN decreased (Table 2.1). Approximately 13.2% burst release was observed in the formulation containing 10% PEG-g-CHN, whereas a significantly larger 25.4% burst was seen in the formulation containing 0.5% PEG-g-CHN ($P < 0.05$). Additionally, there was a significant increase in burst release from the formulation containing 0.5% PEG-g-CHN compared with the one containing 5% PEG-g-CHN ($P < 0.05$). The formulation containing 1% PEG-g-CHN also showed a significantly larger burst release than its counterpart with 10% PEG-g-CHN ($P < 0.05$).

After 14 days, approximately 95.1% of the total BSA loading in the microspheres formulation containing 0.5% PEG-g-CHN was released; whereas, 85.5, 70.7, and 60.4% of proteins were released for the formulations containing 1, 5, and 10% PEG-g-CHN, respectively. The difference in 14 day BSA cumulative release in 0.5% was statistically significant when compared with 5% and 10% PEG-g-CHN formulations ($P < 0.05$). The results of this study were used as a guide to range-find the proper PEG-g-CHN content of the bFGF microspheres for further investigations.

2.4.2 FGF Release Kinetics

The concentration of selected release samples of bFGF was quantified using a receptor-based ELISA assay. The burst release seen at 2 hours was approximately 63.3 ng/mL. By day 5, the amount of bFGF detected by the ELISA assay was substantially less than that of detected at the 2 hour time point. The 7, 15, and 28 day

time points also showed bFGF release as 2.0, 3.6, and 0.16 ng/mL. A summary of the measured release data is featured in Figure 2.3.

2.4.3 In vitro verification of the bioactivity of released FGF

To verify the bioactivities of microsphere released bFGF, model dermal fibroblast cells were treated with PBS, 0.1% BSA solution, pristine bFGF, or releasate samples. Cells treated with releasate samples (Figure 2.4D) and bFGF (Figure 2.4C) were refractive in shape while the negative control (PBS) (Figure 2.4A) and cells treated by 0.1% BSA (Figure 2.4B) showed typical fibroblast morphology. This behavior was typical of similar sets of replicates.

2.4.4 Biological efficacy of encapsulated bFGF

In seven animals we tested the ability of PLGA microsphere-released bFGF to induce vasodilation, as compared to non-encapsulated bFGF (native protein), and PLGA/10% PEG-g-CHN microspheres containing only BSA, or PLGA/10% PEG-g-CHN microspheres without proteins. [Note that the microspheres formulated with only PLGA used here exhibited a characteristic high burst-release of protein, different from the slow sustained release of the PLGA/10% PEG-g-CHN microspheres that were tested over 7 days in the animal. This verified that vasoactive efficacy was not affected by encapsulation.] The average baseline diameter of the vessels tested was 9±3 μm, the maximal diameter was 14±2 μm and the minimal diameter was 4.5±1 μm. Using Protocol 1, native bFGF induced a peak local dilation of 0.4±0.05 (40%, n=3) by 30 seconds of exposure; in the same animals, PLGA microspheres with bFGF induced a

peak local dilation of 0.25±0.04 μm that required 2 minutes of continuous exposure. PLGA/10% PEG-g-CHN microspheres with bFGF and PLGA/10% PEG-g-CHN microspheres without any proteins were each applied for 2 minutes in four other animals. Neither significantly altered arteriolar diameter (PLGA/10% PEG-g-CHN with BSA, 0.04±0.04 μm; PLGA/10% PEG-g-CHN without proteins, 0.01±0.03 μm), yet native bFGF exposure for this group also showed vasodilation (0.42±0.06 μm). Thus, although the peak response required a longer exposure period for encapsulated bFGF vs. the native protein, a significant dilation was obtained with PLGA microspheres containing bFGF, which was not due to the microsphere formulation itself.

2.4.5 Effect of in vivo exposure to microspheres

Verification of animal wellness - On day 7, the adult animals treated with microspheres showed an average weight gain of 3±2 grams, as expected for this age of hamster. No animals showed any sign of illness. Thus, treatment did not compromise the overall health of the hamsters.

State of the Microcirculation - Upon initial dissection of the cheek pouch tissue, we visually confirmed the presence of the injected microspheres as spherical balls approximately 2-5 μm in diameter. They were scattered over approximately 1/3 of the tissue (diameter of dissected tissue is 2 cm), trapped in the superficial connective tissue and not washed away by the flowing superfusate solution (5 ml/min). Inflammatory states in general, will be associated with excess leucocytes rolling and adhering in the venules, and extravasation to the tissue. We noted the absence of extravasated leucocytes in each preparation (leucocytes are 11 μm in diameter, and thus by size

alone could not be missed due to the presence of microspheres). The cheek pouch vasculature instead had occasional leucocytes rolling in the venules, which is normal. The connective tissue layer was not friable indicating absence of inflammatory response (inflammatory states are usually accompanied by friability of the connective tissue). Finally, in inflamed tissues, microvascular flow is sluggish in some regions and brisk through preferential pathways. Flow in the arteriolar circulation was brisk throughout by visual observation; flow in the venular circulation was slower than in the arteriolar circulation, as expected, but not sluggish. There was no sign of disseminated intravascular coagulation (DIC), confirming that the formulation did not promote blood coagulation. We conclude that the formulations used were not pro-inflammatory, did not introduce gross microvascular changes, and were not thrombogenic. Microvascular responses were tested at locations within the scattered microspheres.

2.4.6 In vivo response with bFGF treatment

Arteriolar diameter was measured at the location depicted in Figure 2.1A, the entrance to the network. The baseline diameter was 9±3 μm, maximal diameter was 15±3 μm, and minimal diameter was 5±2 μm; there were no differences between juveniles vs. adults, nor between adults treated with the PLGA/10% PEG-g-CHN microspheres containing BSA only vs. PLGA/10% PEG-g-CHN microspheres with bFGF. Changes in diameter were compared for three experimental groups: juveniles, adults (±bFGF treatment), and historic laboratory control data (adult hamsters, source referenced in the figure legends). Our reasoning for including the juvenile group was to

obtain vasoactive responses in a group with actively growing tissue, for comparison to bFGF treatment, which potentially would induce angiogenesis.

Local responses were obtained using Protocol 1 and the results are depicted in Figure 2.5. KCl induced constriction was not affected by treatment, nor was it different in adults vs. juveniles. This confirmed that the contractile proteins within the vascular smooth muscle cell could function normally. However, endothelin induced constriction was enhanced by the presence of PLGA/10% PEG-g-CHN microspheres with encapsulated bFGF, not by PLGA/10% PEG-g-CHN (with BSA) microspheres alone; this effect was not mirrored by the juveniles. This suggested that a receptor linked pathway was enhanced by chronic bFGF treatment. SNP induced dilation was attenuated in both juveniles and bFGF treated adults. This suggests an attenuation of cGMP mediated dilation in actively growing tissue that is mimicked by chronic bFGF exposure. Dilation in response to ADO was unaffected by treatment and independent of age, consistent with an interpretation of no changes in cAMP mediated dilation with chronic bFGF exposure. Thus, prolonged exposure of bFGF via microspheres showed some similarity to juvenile responses with regard to dilation, but not for the constriction pathways, which was specifically related to endothelin and not due to the microsphere formulation.

Figure 2.6 shows the remote response results obtained using Protocol 2. These responses tested the ability of the arteriolar network to communicate individual stimuli to upstream and downstream locations to coordinate an orchestrated vasoactive response. Remote dilation in response to SNP or to LM609 were each attenuated in juveniles; however, only the responses to SNP were attenuated in adult animals treated

with bFGF microspheres, as compared to historic or MS-BSA controls. SNP-induced remote dilation requires gap junction signaling[4], and LM609-remote dilation consists of two parts: gap junction signaling and flow mediated dilation; a response requiring intact dilation to NO[2]. This provides multiple means for bFGF action by diminishing gap junctional communication and/or flow mediated dilation.

Microvascular preconditioning was achieved using Protocol 3 and the results of microvascular response to L-arg both Before and After preconditioning by SNP are depicted in Figure 2.6. Preconditioning confers a “protective” window of time to a blood vessel that protects from free radical injury during subsequent ischemic events or superoxide exposure. L-arg did not initially induce dilation (Before) and thus, the cheek pouch was not initially in the preconditioned state. The After response demonstrated that juveniles could be preconditioned, but to a significantly less extent than adults. Further, the presence of either PLGA/10% PEG-g-CHN microspheres with encapsulated BSA alone, or PLGA/10% PEG-g-CHN microspheres with bFGF appeared to have attenuated the preconditioning response, yet it was still significantly larger than in juveniles.

2.5 Discussion

In this investigation, protein encapsulation was achieved by taking advantages of polymer solubility characteristics through blending of PEG-g-CHN, an amphiphilic material, with PLGA, a hydrophobic material. Comparable PLGA/PEG-g-CHN blend microsphere formulations for encapsulation and sustained delivery of plasmid DNA

were previously reported by us [96]. In the current study, the PLGA/PEG-g-CHN blend allowed for electrostatic binding and thus, protection of protein, while achieving prolonged protein release through the interaction between the PEG-g-CHN/protein complexes embedded in PLGA microsphere matrices. The results of the BSA release kinetics experiment showed a moderate burst release for all microsphere formulations (Figure 2.2). The microspheres' capability for modulating BSA burst release was demonstrated by varying the PEG-g-CHN content, where a PLGA/0.5% PEG-g-CHN combination showed considerably higher amount of BSA release over a 14 day time-span as compared to its counterparts formulated from different PLGA/PEG-g-CHN combinations. Evidently, release of BSA from microspheres could be modulated by varying the amount of PEG-g-CHN.

The bioactivity of released bFGF proteins from a typical PLGA/PEG-g-CHN microspheres formulation was also demonstrated. BSA was used as a diluent to facilitate incorporation of bFGF into the microspheres. In the dermal fibroblast cells study, cells treated with released and bFGF stock solution demonstrated a refractive morphology, while cells treated with PBS or BSA solution were more spread out. Similar results were reported with NIH-3T3 cells and the addition of 10 ng/mL of bFGF to a 10% serum DMEM culture media [120]. Although the cell culture model in this study used a 0.5% serum DMEM for dermal fibroblast cells, the behavior of the cells was comparable and seemed to be independent of media serum concentration. Thus, the fibroblast cells appeared to be responding to the bFGF rather than the serum content of the media.

In addition to cell culture experiments, a standard, in vitro, protein quantification assay was used to investigate whether the released bFGF was bioactive. Nonetheless, the amounts of bFGF released from the microspheres formulation tested that were detected by the receptor based ELISA assay (see Figure 2.3), in general, appeared to be considerably lower than the total amount of bFGF added to the primary emulsion. This discrepancy could be attributed to the relative instability of the released bFGF in buffer solution. Heparin was used to dilute the lyophilized bFGF powder before the emulsion process to protect the protein from denaturation during mixing and the release experiments. Since the ELISA kit used for bFGF quantification was a receptor based assay, it could be inferred that only bFGF in its native conformation (i.e., both intact and not denatured) could be effectively detected and thus, producing signals indicating its presence on a receptor binding based technique. Due to a combination of initial burst and relatively brief exposure of the released bFGF in the buffer, the first sample collected after 2 hours of incubation was expected to contain a relatively high concentration of bFGF in its native conformation, consequently, producing a strong signal in the ELISA assay. Subsequent samples were collected after 1, 5, 7, 15 and 28 days, respectively; this increased time-span for sample collection resulted in a more prolonged incubation of bFGF released from microspheres in buffer, and inevitably, protein denaturation leading to weak signals produced in the ELISA assay. In addition, for logistical considerations the releasate samples were gathered and stored in freezers; and ELISA assays were performed collectively to determine the bFGF concentrations. Hypothetically, samples could be collected at much more frequent intervals (e.g., once every few hours) and assays should be performed instantaneously thereafter,

nonetheless, the prohibitive cost for performing ELISA assays in this fashion precluded this theoretical scheme. Nonetheless, the biological activities of the bFGF released were validated in cell culture models and more importantly, the goal of this study was to validate the efficacy of this type of microspheres preparation in vivo (i.e., hamster cheek pouches).

Biocompatibility of the individual materials that we utilized to prepare PLGA/PEG-g-CHN blended microspheres has previously been reported. PLGA alone does not induce cell death [121], but with in vivo implantation it could lead to inflammatory responses [122,123]. Chitosan, per se, is non-inflammatory in vivo [124] with evidence that it actually improves wound healing in normal and db/db mice [125]. PEG alone is likewise non-inflammatory in vivo that it may exert an anti-inflammatory effect [109,126]. Few laboratories reported using these three polymers in any combination and configuration as vehicles for delivering bioactive agents. In a prior study, we validated comparable PLGA/PEG-g-CHN blend microspheres formulation as a DNA delivery vehicle, and found no evidence of inflammation with chronic exposure in rat hind limb intramuscular injection models [96]. It was recently reported that cationic nanoparticles formulated from PLGA, PEG and chitosan for binding plasmid DNA were found likewise non-inflammatory [108]. In the present study, we confirm that the microspheres formulated from physically blending PLGA and PEG-g-CHN was non-inflammatory with chronic exposure to the hamster cheek pouch.

The hamster cheek pouch model is ideally suited for testing these formulations. The microspheres can be introduced without adverse effects to the animal. The tissue is well characterized for vascular architecture and responses, using intravital microscopy.

This enables us to directly examine both evidence of microvascular inflammation, to test how the treatment affects the ability of the vasculature to perform normally, and will be ideal for documentation of architectural changes with treatment in the future. Testing microvascular responses was performed for two key reasons. First, to determine whether we were introducing microvascular dysfunction, as would be associated with a proinflammatory state. The responses show we did not induce a proinflammatory state by either the microspheres alone, or by the chronic bFGF treatment. Second, to determine whether the vasoactive responses in bFGF treated animals mimicked those found in juvenile animals, where the vasculature is actively remodeling.

In this study, we elected to examine changes at 7 days after microspheres administration with the primary objective of evaluating the chronic inflammatory potential of the PLGA/PEG-g-CHN microspheres. There was no evidence that this formulation induced any major inflammatory response, which was consistent with our use of comparable formulation for DNA delivery in rat hind limb muscle injection [18]. It should be noted that significant angiogenic changes were not expected within this time frame, thus we separated biocompatibility testing (present study) from changes in microvascular architecture (anticipated with longer exposure). Consequently, the goal was to confirm that microvascular function was not compromised by the presence of these microspheres, and then to evaluate changes in response capability due to microspheres vs. bFGF treatment. Compared to adult controls, changes attributed to chronic exposure with bFGF included enhanced constriction in response to the presence of endothelin, and attenuated local/remote dilation through NO stimulation. bFGF has previously been shown to induce endothelin transcription [127], and recent

research has demonstrated a role of endothelin as the biological “counterpart” for NO [128]. Thus, evidence points to endothelin as providing negative feedback for NO. It is therefore expected that chronic bFGF exposure would elevate responses to endothelin, which would then attenuate response via NO, as we report here.

We compared the responses with chronic bFGF exposure to those of juvenile hamsters. These animals are in a state of vascular remodeling and we originally hypothesized that the vasoactive responses would be mimicked by bFGF exposure; but, this hypothesis has been disproved in this study. Juveniles displayed attenuated local and remote dilation responses caused by NO, and decreased flow mediated dilation (remote response to LM609, also mediated by NO) as compared to adult control data from our laboratory. Further, the microvascular responses in the PLGA/10% PEG-g-CHN microspheres with bFGF treated adults were not identical to responses in juveniles. This is a contrary finding, not supported by studies in rats; comparisons in hamsters were not found. For instance, juvenile vs. adult rats do not show a difference in acetylcholine (NO-mediated) dilation [129]. Further, the diminished remote dilation to SNP (or secondary dilation with LM609) is not likely due to decreased gap junction density because there is opposing evidence that myoendothelial gap junctions are in high density in juvenile vs. adult rats [130]. Importantly, the connexin isoforms responsible for these responses are not completely documented, thus the differences reported could be differences in connexin isoforms. At the moment, we cannot explain the juvenile data, other than to suggest a species differences between rats and hamsters, and/or connexin isoform difference for the responses.

Lastly, we tested a microvascular response associated with a pro-inflammatory state of early preconditioning. Microsphere treatment alone did not result in a preconditioned microcirculation. The ability of the microcirculation to demonstrate preconditioning was attenuated in both PLGA/10% PEG-g-CHN microspheres with only BSA and PLGA/10% PEG-g-CHN microspheres with bFGF exposed animals, and thus is likely due to the presence of the microsphere itself. The normal preconditioning response is tightly linked to oxidative stress, and is stimulated by either NO or reactive oxygen converging on the mitochondrial Katp channel activation [1]. We have shown in this tissue that preconditioning can be blocked by superoxide dismutase plus catalase. We speculate that attenuation of preconditioning with these microspheres is due to the presence of PEG, which has been reported to have an independent anti-inflammatory effect [109].

In all, the in vivo work supports that bFGF released from the microspheres is biologically active, does not induce an inflammatory response within the tissue, nor for the whole animal, and significantly alters key microvascular responses. Most important of these is increased vasoconstriction to endothelin, and attenuated vasodilation to NO, which is together consistent with the published effect of chronic bFGF exposure. bFGF exposure does not produce vasoactive responses identical to the juvenile hamster. Lastly, the attenuated preconditioning response with chronic exposure to the microspheres suggests that some component of the formulation (i.e., PEG) may confer an anti-inflammatory effect.

Table 2.1: PEG-g-CHN content and burst release of BSA from microspheres 2 hours after starting the release kinetics experiment [BSA release kinetics measured and analyzed by the author].

% PEG-g-CHN	% Burst Release of BSA
0.5	25.40
1	18.22
5	15.92
10	14.50

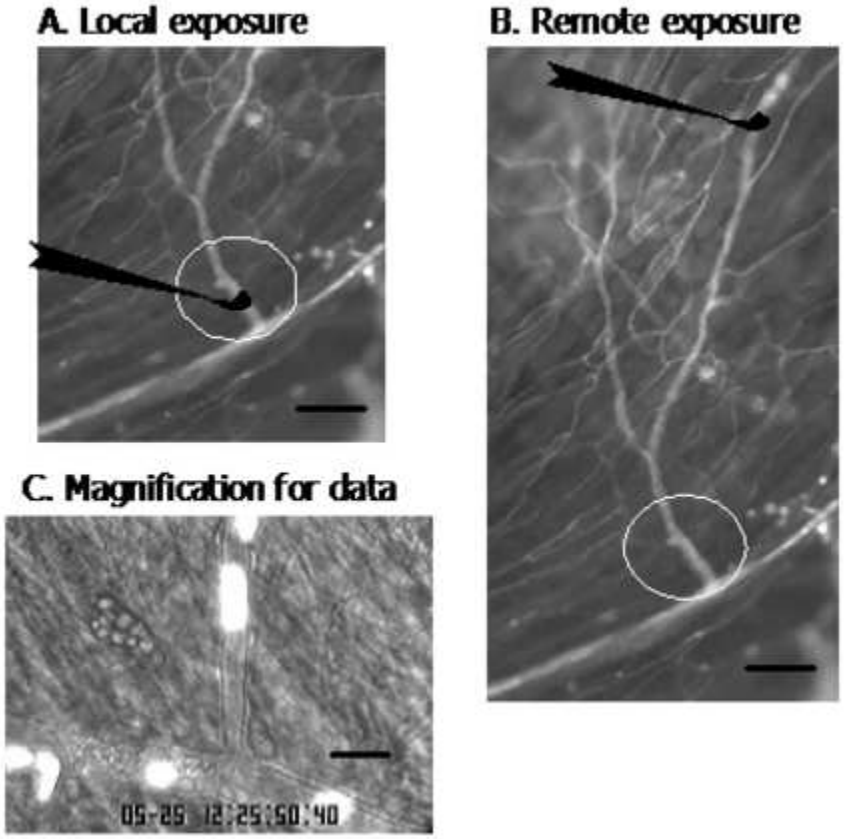

Figure 2.1: Shown are videomicrographs from the hamster cheek pouch. Fluorescence images A and B are taken at low power to show a typical arteriolar network (scale bar 100 µm). To highlight the vascular network, the vasculature was filled with fluorescein-isothiocyanate (FITC) conjugated to bovine serum albumin (BSA). The typical length of the network was 1000 µm. A combination of brightfield and fluorescence, image C, is taken at high power to show the typical magnification used for data analysis (scale bar 20 µm). This image shows very bright fluorescently labeled red blood cells that are used as flow markers; here they illustrate motion of individual red blood cells in the circulation (streaks occur when the cells are moving at high rates of velocity during image acquisition). Diameter changes were always noted within the white ring, the upstream region of the network. A. Local responses were obtained by applying the test agents to the upstream region of the network via micropipette (silhouette shown), and noting the diameter changes where the drug was applied (Protocol 1). B. Remote responses were obtained by applying the test agents to the downstream region of the network, and noting the diameter changes upstream (Protocol 2). Protocol 3 involves a combination of Local and Remote exposures (see text). [Images captured and analyzed by Molly Frame].

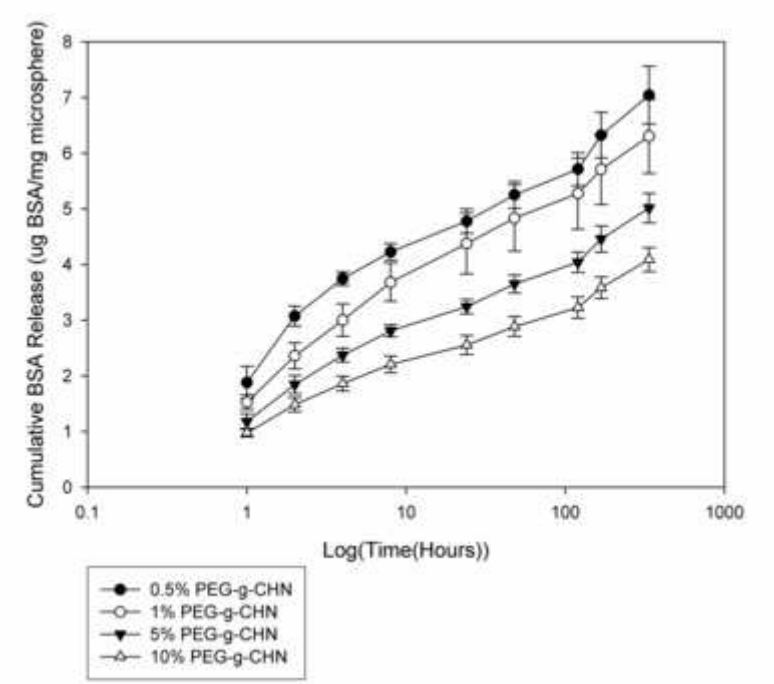

Figure 2.2: Measured cumulative release of BSA from different formulations of PLGA/PEG-g-CHN microspheres over 14 days. There were 4 formulations of microspheres with varying amounts of PEG-g-CHN: 0.5% (n=3), 1% (n=3), 5% (n=3), and 10% PEG-g-CHN/PLGA (n=3). All microsphere formulations received 3 mg of an aqueous BSA solution added to the primary emulsion process. The amount of BSA released was normalized to the average mass of microspheres used in each formulation and each data point represents the average and standard deviation of the normalized BSA release calculations [BSA release kinetics measurement and figure performed by the author].

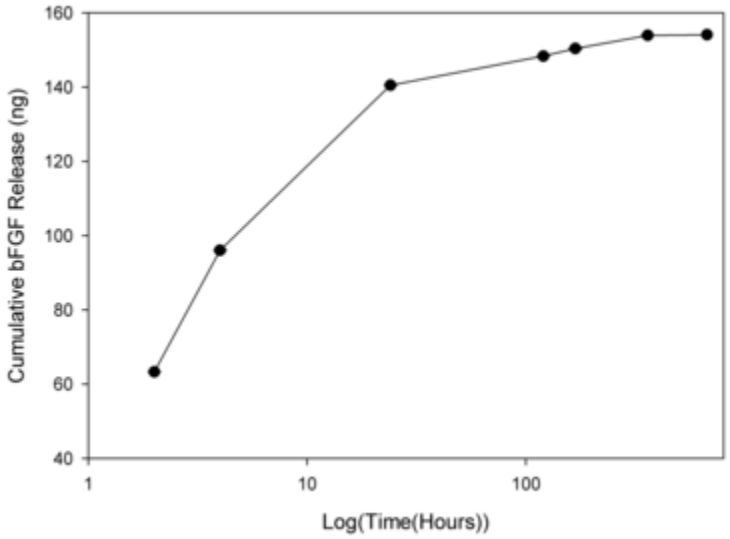

Figure 2.3: Measured cumulative release of bFGF from PLGA/5% PEG-g-CHN microspheres over 28 days, or 672 hours. This microsphere formulation also contained 100 µg bFGF, 100 µg heparin, and 3 mg BSA (from aqueous solution) added to the primary emulsion process. The amount of bFGF released was measured using a receptor-based ELISA kit and expressed as cumulative released bFGF per replicate [bFGF release kinetics and calculations performed by the author].

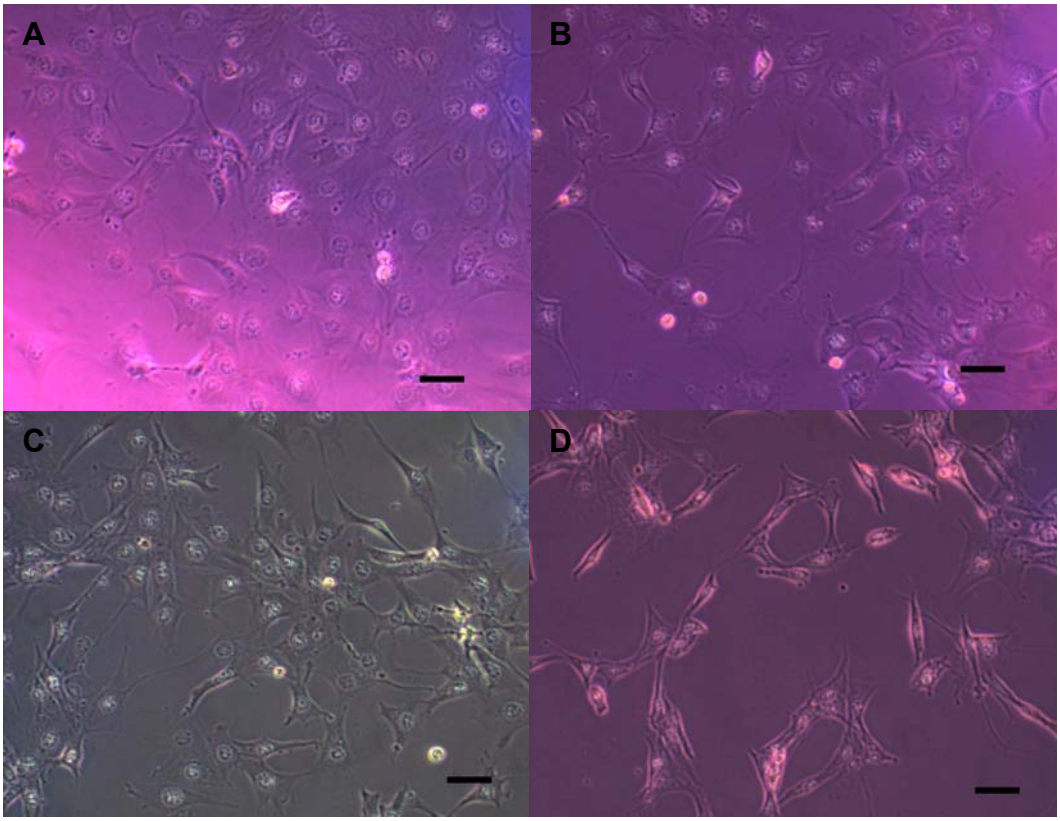

Figure 2.4: Murine dermal fibroblast cell (CRL-2017) morphology and in vitro verification of bFGF bioactivity. The fibroblast cells were incubated with A) PBS (n=3), B) 0.1% BSA solution (n=3), C) pristine bFGF (n=3), and D) released bFGF from microspheres (n=3) added to low-serum media for 48 hours. All images digitally captured at 20X magnification (scale bar = 50 μm) [Cell culture experiment and image capture performed by the author].

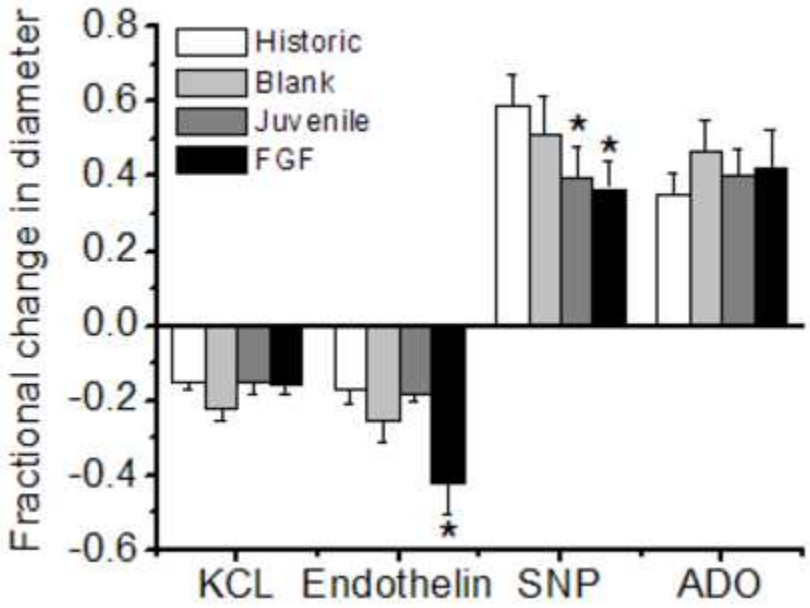

Figure 2.5: Local vasoconstriction or vasodilation, Protocol 1. Shown are fractional arteriolar diameter changes (mean±sem) at location A in response to drug application at location A (Local responses). KCl (20mM), endothelin (10^{-8} M), SNP (10^{-4} M), or adenosine (ADO, 10^{-4} M) were applied via micropipette using Protocol 1. Two adult groups were exposed to microspheres: PLGA/10% PEG-g-CHN containing only bovine serum album (Blank, n=4), PLGA/10% PEG-g-CHN containing bFGF (FGF, n=8); these were compared to untreated juveniles (n=6) and historic laboratory control data. Historic control data can be found for KCl, endothelin (unpublished), SNP, ADO [1]. *differs from historic controls. No other comparisons were significant [Measurements, except for historic controls, were performed by Molly Frame].

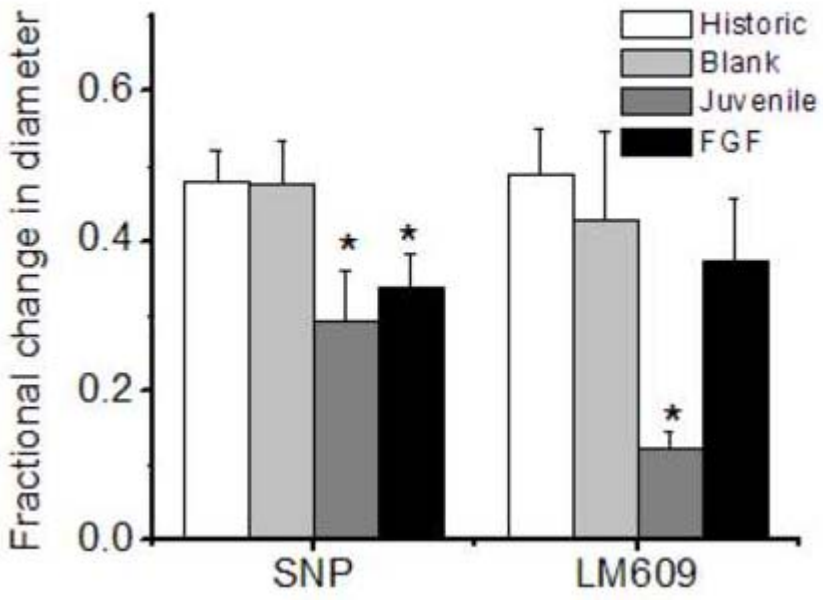

Figure 2.6: Remote vasoactive responses, Protocol 2. Shown are fractional arteriolar diameter changes (mean ± sem) at location A in response to drug application at location B (Remote responses). SNP (10^{-4} M) or LM609 (10 µg/ml) were applied to location B via micropipette using Protocol 2. Two adult groups were exposed to microspheres: PLGA/10% PEG-g-CHN containing only bovine serum album (Blank, n=4), PLGA/10% PEG-g-CHN containing bFGF (FGF, n=8); these were compared to untreated juveniles (n=6) and historic laboratory control data. Historic control data can be found for SNP [2] and for LM609 [2,3]. *differs from historic controls; Juvenile responses with LM609 differ from all others (no symbol). [Measurements, except for historic controls, were performed by Molly Frame].

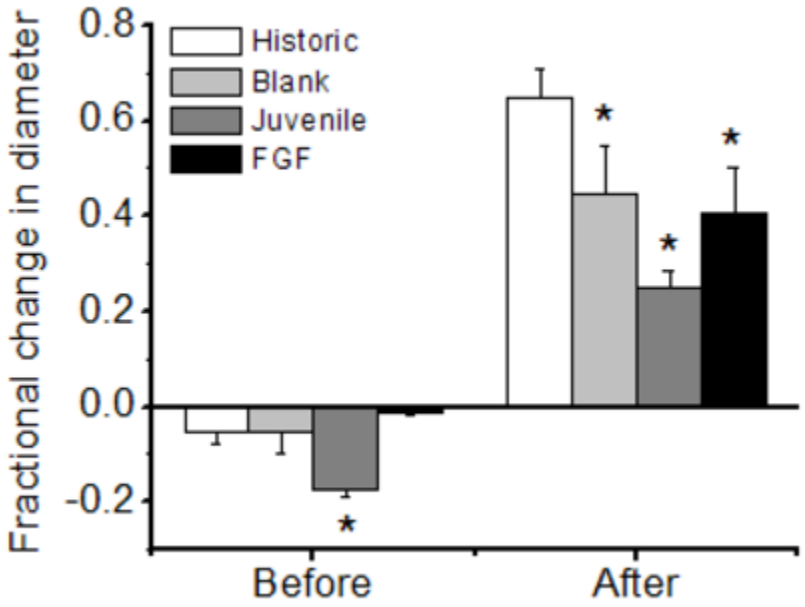

Figure 2.7: Microvascular preconditioning response, Protocol 3. Shown are fractional arteriolar diameter changes (mean ± sem) at the local exposure area (see Fig. 1A) in response to L-arg (10^{-4} M) application in this area Before and 15 min After SNP (10^{-4} M) application to the remote exposure area (Protocol 3; response to SNP not shown). Two adult groups were exposed to microspheres: PLGA/10% PEG-g-CHN containing only bovine serum album (Blank, n=4), PLGA/10% PEG-g-CHN containing bFGF (FGF, n=8); these were compared to untreated juveniles (n=6) and historic laboratory control data. Historic control data can be found for preconditioning[4]. *differs from historic controls; Juvenile responses After differ from all others (no symbol). [Measurements, except for historic controls, were performed by Molly Frame].

The results presented in Chapter 3 have been previously published (Falabella CA, Chen W. Digest Surg. 26(6):476-81. 2009). All tables and figures have been reproduced with written permission from S. Karger AG, Basel.

Chapter 3

Crosslinked hyaluronic acid films to reduce intra-abdominal post surgical adhesions in an experimental model

3.1 Summary

Intra-abdominal adhesions typically occur after surgically damaged tissues are situated in apposition, leading to fibrotic connections. The goal of this study was to demonstrate the in vivo efficacy of a crosslinked and insoluble hyaluronan (HA) film to reduce post surgical adhesion in a rat model. To measure in vitro adhesion resistance, porcine monocytes were deposited on the surface of films and their attachment was monitored by scanning electron microscopy. A rat cecum abrasion and abdominal insult model was utilized to demonstrate in vivo efficacy. Briefly, a HA film was deployed as a barrier between the damaged cecal and abdominal tissues surfaces for 21 days; control animals did not receive treatment. At the study conclusion, the rats were sacrificed and degree of adhesion was determined using a scale of 0-3, where 0 = no adhesion and 3 = severe fibrosis. HA films resisted monocyte adhesion in vitro. The in vivo study results demonstrated a significantly lower median adhesion score (1) with HA film treatment than the controls (3). Placement of HA films between injured tissues significantly decreases the severity of abdominal adhesions. Furthermore, the HA film's

resistance to monocyte adhesion could be contributory to lowering in vivo adhesion scores.

3.2 Introduction

Post-surgical adhesions caused by open abdominal procedures account for $1.33 billion per year in hospitalizations and revision surgeries in the US [31]. The cause of these adhesions is not well understood, but present knowledge and research suggests that a combination of prolonged inflammation and insufficient fibrinolysis result in fibrotic adhesions between damaged tissues inside the abdomen [131]. A generally accepted critical time period during which adhesions begin to form is 12 – 36 hours after a surgical procedure [43]. During the post-operative period, monocytes migrate from circulating blood to the wounded areas, transform into macrophages, and secrete cytokines to recruit fibroblasts that produce fibrous tissue “bridges” between tissue surfaces [132]. An overabundance of activated macrophages inside the abdominal cavity after surgery could increase the occurrence of adhesions [36,133]. Additionally, these macrophages and other polymorphonuclear leukocyte cells may also migrate into the initial fibrin connections between damaged tissues, further preventing fibrinolysis from occurring [34]. In an effort to reduce adhesion incidence, surgeons have changed their technique to accommodate a gentler handling of the sensitive tissues inside the abdominal cavity to reduce extensive serosal injury, provide adequate hemostasis [134,135], and even changing the type of surgical gloves used during surgery [136]. Despite these protocol changes, adhesions still occur in 50-76% of patients undergoing abdominal surgical procedure, and up to 93% of patients after multiple abdominal

procedures [137,138]. An effective adhesion prevention method would involve the interruption of fibrotic tissue bridging by physical separation of the damaged tissues, but also allow epivisceral healing to occur unimpeded [139].

A number of adhesion prevention devices have been researched and marketed by various companies in the US. These barriers can be divided into two groups: non-resorbable and resorbable. Preclude™ (Gore, Flagstaff, AZ) is a PTFE membrane that is typically utilized to repair abdominal wall weaknesses caused by hernias, but it has also been used to separate damaged tissues to prevent adhesions; however, the membrane must be surgically removed by follow-up surgeries. Resorbable barriers, in contrast, can be effective in adhesion prevention as they are designed to remain intact and in situ for up to 7 days post-op. Two resorbable films that have been approved for clinical use are Interceed™, fabricated from oxidized regenerated cellulose, and Seprafilm™, fabricated from carboxymethylcellulose/hyaluronic acid. Although these films have shown good efficacy in reducing the incidence of adhesions, they do not completely prevent the occurrence of adhesions. Another difficulty that arises with Interceed™ and Seprafilm™ is that they cannot be moved once applied to the hydrated tissue surface and the films also disintegrate easily when in contact with any wet surface including surgical gloves. Interceed™ also requires strict hemostatic conditions in the area of application to avoid complications [45]. Thus, there is a need for a film that will resist both negative interactions with blood and adhering to itself or any wet surfaces during application.

Solutions and materials made from hyaluronic acid (HA) have been researched extensively in the study of adhesion prevention. HA, a naturally derived polysaccharide,

has demonstrated excellent biocompatibility and low cytotoxicity in various studies and applications. One proposed method of hyaluronic acid application used either a spray coating [53] or as a irrigation solution [140]. When applied topically, HA solutions are thought to improve mesothelial wound healing and possibly limit monocyte/macrophage infiltration; decreasing the ability of these cells to attach to damaged tissue surfaces may also decrease the secretion of cytokines that recruit fibrotic tissue-forming cells[141]. However, the clearance of HA solution from the abdominal cavity is fairly rapid (about 12 hours) and the efficacy of these solutions has yet to be demonstrated in definitive large scale clinical trials [58,59]. Crosslinking of HA could be a strategy to enhance its stability and thus increase the residence time of HA inside the abdomen after deployment [56,65]. In some studies, solid HA films were formulated from either pure HA [142] or blending it with other biologically-derived materials [143]. Furthermore, some crosslinked HA films have demonstrated cell anti-adhesion in vitro [56]. Kim et al. proposed to use dihydrazide-crosslinked HA films for sustained delivery of a HA Synthase (HAS) gene that was postulated to prevent post-surgical adhesion by combining the physical HA barrier (as the primary mechanism) with continual enablement of cells to over-express HA (as the secondary mechanism) as the film is being enzymatically eroded over time [62]. The in vivo efficacy and degradation of the dihydrazide-crosslinked HA film has not yet been investigated in a post-surgical adhesion model. Thus, the primary goal of this study was to validate the anti-adhesion efficacy of such cross-linked hyaluronan films in a 21-day, rat cecum abrasion model for post-surgical adhesion.

3.3 Methods

3.3.1 Formulation of HA Film

HA films were prepared and crosslinked following our previously described methods [62]. Briefly, approximately 1.25 mL of a 1% aqueous hyaluronan solution (%w/v) was cast into a flat-bottom, 1 cm diameter circular mold; the solution was allowed to dry at 37° C for 5 days. The films formed were then immersed in 90% isopropanol for 1 hour followed by 80% isopropanol for another hour. Approximately 30 mg of adipic dihydrazide was added to the solution containing the film with agitation followed by the addition of 60 mg of ethyl-3[3-dimethyl amino] propyl carbodiimide (EDCI, Sigma-Aldrich, St. Louis, MO). Crosslinking was then initiated by the acidification of the reagent solution with 1N HCl. The crosslinked HA film was removed from the reagent solution after 24 hours and rinsed extensively in 80% isopropanol to remove residual crosslinking agents. Residual water in the film after crosslinking was removed first by dehydration in a series of 90-100% isopropanol solutions followed by an overnight incubation at 37° C. The dried, crosslinked film was stored in a desiccator before use (Figure 3.1).

3.3.2 Monocyte/Lymphocyte Attachment Study

Mononuclear cells (monocytes and lymphocytes) were isolated from heparinized swine whole blood by centrifugation with Histopaque®-1077 (Sigma-Aldrich, St. Louis, MO). These cells were deposited on HA films or growth coverslips (as controls) at a density of 35,000 cells/cm^2. They were cultured for five days in RPMI media (Invitrogen, Carlsbad, CA) with 10% fetal calf serum, followed by extensive rinsing and fixation with

2.5% glutaraldehyde buffer. After performing critical point drying, the morphology of cells attached was evaluated with SEM.

3.3.3 Post-Surgical Adhesion Animal Model

All animal experiments were performed using a protocol that was reviewed and approved by the Institutional Animal Care and Use Committee (Protocol number: 1473). The animals were housed and cared for by the Division of Laboratory Animal Research veterinary staff at SUNY Stony Brook.

Sprague-Dawley rats (250-300g) were anesthetized by isoflurane (5% for induction and 2.5% for maintenance). A mid-line laparotomy incision was performed on each rat similar to previously published studies using a rat model for post-surgical adhesion [144]. The cecum was then located and liberally abraded on one side using fine grit sandpaper until serosal bleeding was observed. A 1 cm^2 portion of the abdominal wall across from the damaged cecum surface was also removed. All wounded surfaces were dabbed with sterile gauze to remove any excess pooled blood before treatment. A single HA film was first rehydrated in sterile saline for 15 minutes prior to the surgical procedure. The film was applied to the damaged cecum surface and the film-covered cecum was then placed back inside the abdominal cavity approximating the damaged muscle surface (n=8). The incision was re-approximated and closed using 0-0 chromic gut sutures on the abdominal wall and 5-0 Prolene sutures for the skin layer. Control animals did not receive any HA film treatment or other barrier (n=11) and this data was shared by a parallel study aimed at evaluating the anti-adhesion efficacy of an in situ gelable hydrogel composed of modified chitosan and

dextran [145]. The animals were sacrificed after 21 days and the extent of adhesion was semi-quantitatively scored on a scale of 0-3 (0 = no adhesion, 1 = thin and filmy, 2 = significant and filmy, and 3 = severe with fibrosis) [53,144,146,147].

3.3.4 Data Analysis and Statistics

Surgical adhesion severity scores were compared using a Mann-Whitney Rank Sum Test with statistical difference determined by $p < 0.05$. The median scores of the control and film-treated animals were also determined and reported separately in the Results section.

3.4 Results

On SEM images, monocytes appeared to spread out and adhered very aggressively to the glass substrate surface (Figure 3.2A), in contrast, only very few monocytes were observed on cross-linked HA films with round morphology indicating no attachment (Figure 3.2B).

The tabulated scores of the control animals and HA film treated animals were summarized in Table 3.1. The mean adhesion score for the control group [145] was 2.09 while the HA film treated group had a mean score of 0.625 ($p<0.05$, Mann-Whitney Rank Sum Test). None of the HA film treated animals showed a score above 1 (Figure 3.3A); in contrast the control group had six out of eleven animals with score 3 (Figure 3.3B) while two having a score of 2. Seven out of 8 rats showed no traces of the HA film after 21 days; however, one animal retained (Figure 3.4) a residual portion of the

HA film which adhered lightly to the cecum surface, it could be easily removed from the cecum surface by gentle peeling without disrupting the tissue underneath.

3.5 Discussion

The occurrence of post-surgical adhesions following abdominal surgical procedures remains a difficult and sometimes persistent problem for both the patients and the medical care system. Studies suggest that the time window for adhesion formation occurs between 12 and 36 hours after surgery [43]; therefore an effective prophylactic treatment for adhesions would need to remain intact for several days before resorption. Crosslinked films composed of 1% hyaluronic acid reduced the average severity score of adhesions formed after a cecum and abdominal wall injury model in rats when compared to untreated control animals.

Historically, HA and HA-derivatives have demonstrated excellent biocompatibility and biodegradability in both animal [57,148,149] and clinical trials [150,151]. In this study, the implementation of a cross-linked HA film has shown promise in preventing post-surgical adhesion formation in the abdomen. The presence of remnants of the HA film at 21 days post-op in one animal could implicate the presence of intact film, at least initially, (i.e., during the crucial 12-36 hours) after surgery. The mode of adhesion prevention is likely due to the HA film forming a credible initial physical barrier between damaged tissues to resist cells migrating from the defect surfaces to “bridge” and subsequently evolved into fibrous tissue [35,152]. Furthermore, the intrinsic properties of hyaluronan could enable the HA film to serve as the equivalent of a lubricating surface to discourage significant cell attachment [56,153]. This conjecture was

demonstrated in vitro by the clear lack of attachment of monocytes on HA films. Monocytes are known to be involved in adhesion formation [132], therefore, the ability of HA to prevent cell attachment is a valuable attribute. Aside from abdominal adhesion applications, HA films, stabilized by other crosslinking methods, have been studied in other situations where adhesions could occur. For example, crosslinked HA films have been shown to moderate post-surgical tendon adhesions after flexor tendon repair by providing both a physical barrier and reduce the sliding friction between both injured tendon surfaces [60]. In addition to reducing adhesion occurrence, the HA films also offer surgeons more flexibility in handling because the HA film is first hydrated in saline prior to placement, unlike Seprafilm™ or Interceed™ which rapidly disintegrate upon contact with any hydrated surfaces. The wet HA films from this study could be easily repositioned after brief contact with the visceral surface if the surgeon finds it necessary to optimize the coverage area; also, the film resists adhering to itself when fully hydrated.

The method of crosslinking the HA films, in a solvent medium, presented in this study has not been used in a post-surgical adhesion model. In some previously published studies, HA and derivatives of HA were formulated by incorporating crosslinking reagents into the polymer solution during the casting procedure [60]. Although the combination crosslinking/casting procedure appears to simplify the production of HA films, it could also result in their retention of chemical residues leading to downstream cytotoxicity concerns after in vivo deployment. Other published studies utilize modified HA that crosslinks without the addition of other small molecule crosslinkers during the casting process. Yeo et al. developed a two-part, self-

crosslinking HA hydrogel composed of adipic dihydrazide and aldehyde-modified hyaluronic acid [61]. When blended, both HA components readily combine and crosslink to form a stable hydrogel either in situ or after casting the hydrogel in a film form. Potential drawbacks of this method include the time requirement and the cost of material processing and purification before they can be used in vivo. The HA films used in this study were crosslinked post-casting; the presence of exogenous chemicals for crosslinking (i.e., adipic dihydrazide and EDCI) could be removed by subsequent extractions with water/isopropanol co-solvent. In an independent investigation, the films prepared were extracted with water and the extracts were analyzed by High Performance Liquid Chromatography (HPLC), and we were not able to detect the presence of either adipic dihydrazide or EDCI (data not shown).

The retention of the HA film on the injured cecum surface over the course of 21 days has not been observed in this study and presents a possible limitation. Ideally, several intermediate time points would need to be incorporated to ensure that the reduction in severe adhesions with the HA film is due to the maintenance of a physical barrier during the critical 12-36 hour period and then for up to 7 days after surgery, and not other factors. Only 1 animal in this study showed a partially degraded HA film remnant on the cecum surface after 21 days, demonstrating that it is possible that a film could remain intact and in situ for at least several days after surgery. Another 5 animals showed very filmy and easily lysed adhesions of fatty tissue at the cecum or abdominal wall defect site at 21 days. It is possible that the film may be mostly degraded after the inflammatory and granulation tissue formation following injury. After the inflammation phase had passed and any blood/fibrin products had been cleared away, the healing

surfaces may have become less attractive to fibrotic tissue bridging even if they are brought into direct apposition. The presence of high, localized HA levels from the degrading film could be causing an increase in cellular infiltration and fibroblast proliferation during the early phase of wound healing. Prolonged elevation of HA in fetal wounds has often been a hypothesis for the decreased incidence of scar formation when compared with adult wounds [154]. Even if the HA from the degrading film may cause an increase in cellular activity, it appears that the barrier may have remained in tact to physically prevent the two injured surfaces from healing and adhering to each other.

In conclusion, we have formulated a biocompatible cross-linked, resorbable HA film that has great potential in preventing post-surgical adhesion following abdominal surgery. Adhesion scores for HA film treated animals were found to be significantly lower than the control group animals that did not receive any prophylactic treatment. In this preliminary study, we postulate that the intrinsic anti-adhesion property of HA is theoretically attributable to decreases of the ability of monocytes to attach to the film and thereby, possibly contributing to the inhibition of the formation of fibrotic bridging between visceral and abdominal wall. More in vivo studies are needed to elaborate on the presence or absence of monocytes/macrophages on implanted HA films placed over serosal injury. Furthermore, the HA film presented in this study could also offer a surgeon easier handling of an adhesion barrier both before and during placement inside the abdominal cavity.

Table 3.1: Adhesion severity scores for HA-treated and control animals.

Score	Control (n = 11)	HA Film (n = 8)
0	2	3
1	1	5
2	2	0
3	6	0

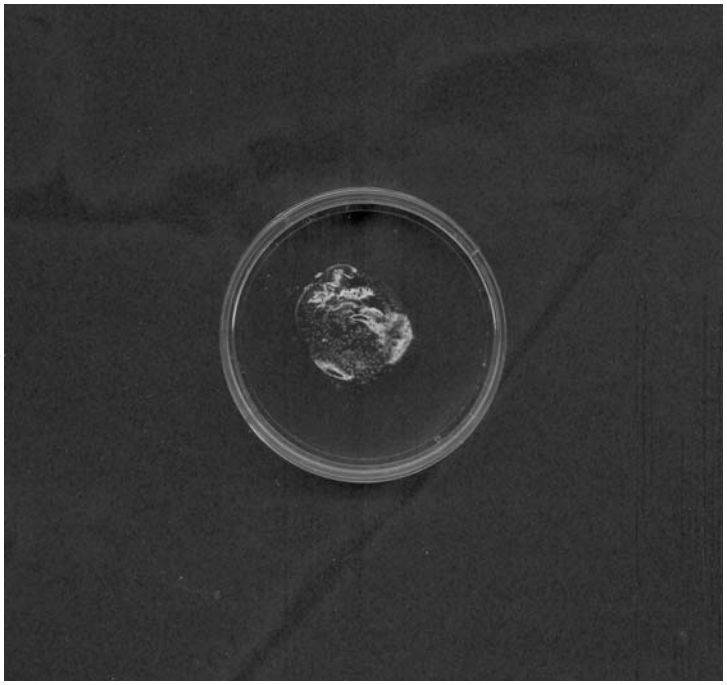

Figure 3.1: A crosslinked HA film.

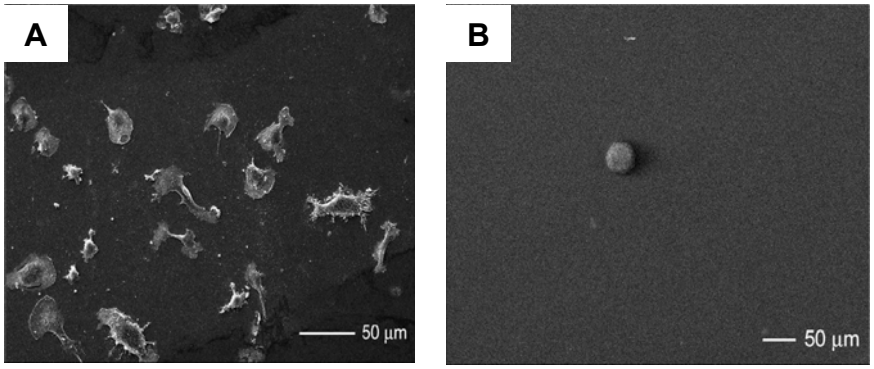

Figure 3.2: Porcine monocyte attachment comparison: (A) monocytes were spread out on the glass slide, but (B) monocytes seeded on the HA film appeared rounded. Scale bar = 50 µm.

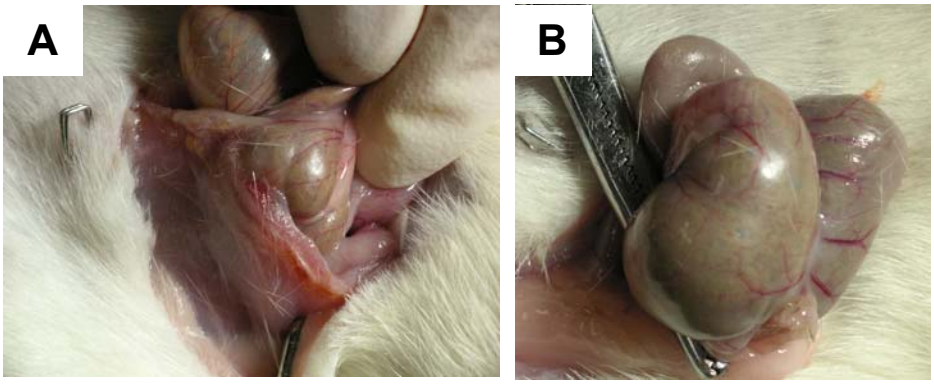

Figure 3.3: Examination of rat cecum and abdominal wall tissue 21 days after surgery. (A) Severe adhesion (score = 3) of the cecal surface to the abdominal wall in a control animal; (B) cecal surface of an animal treated with the HA film (score = 0).

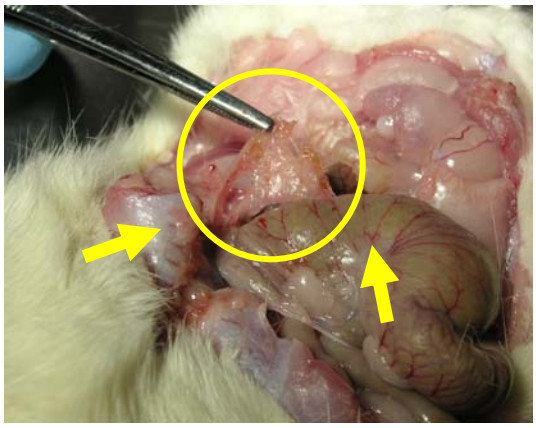

Figure 4: **HA film remnants found on the cecal surface of one rat after 21 days. The piece of film (circled) separated easily from the cecum without damaging the serosal tissue (arrows).**

The results presented in Chapter 4 have been previously published (Falabella CA, Melendez MM, Weng L, Chen W. J Surg Res. 159(2):772-778. 2010). All tables and figures have been reproduced with written permission from Elsevier.

Chapter 4

Crosslinked, oxidized dextran and N-carboxyethyl chitosan hydrogel to reduce intra-abdominal adhesions

4.1 Summary

The aim of this study was to compare the anti-adhesion efficacy of a biodegradable, in-situ, macromolecular cross-linking hydrogel made from oxidized dextran/N-carboxyethyl chitosan (Odex/CEC) with a commercially available carboxymethylcellulose/modified hyaluronan barrier film (Seprafilm) in a rat cecum abrasion model. The rat model utilized a cecal abrasion and abdominal wall insult surgical protocol. The 2% Odex/CEC hydrogel treatment was applied by syringe to coat both the cecal and the abdominal wall insults, while other animals were treated with Seprafilm applied to the cecal injury only. Control animals did not receive any treatment. Animals were sacrificed after post operative day 21 and adhesion severity was quantitatively graded using a whole number scale from 0 – 3. Histological analysis was also performed for animals receiving Odex/CEC hydrogel treatment and no treatment (control). Mean adhesion score was 2.09 ± 1.22 for control animals, 1.00 ± 1.00 for 2% Odex/CEC hydrogel animals, and 1.25 ± 1.22 for Seprafilm animals. Hydrogel treated animals showed significantly lower adhesion scores than control

animals ($p<0.05$), while Seprafilm demonstrated a marginally lower adhesion score ($p<0.1$) compared with the controls. Histological analysis of an Odex/CEC treated rat showed tissue repair and small fragments of hydrogel inside both healed abdominal and cecal surfaces. In conclusion, both Seprafilm and the 2% Odex/CEC hydrogel showed a significantly decreased adhesion score compared with the control. However, the hydrogel, compared with Seprafilm, offers ease of application and ability to conform to complex tissue geometries that could provide surgeons with another prophylactic treatment to prevent abdominal adhesions.

4.2 Introduction

In the previous chapter, crosslinked hyaluronan (HA) films were studied as an adhesion barrier to reduce intra-abdominal adhesions. The HA film was found to significantly reduce the adhesion severity score in rats compared to the untreated control animals. Additionally, the film itself was shown to reduce monocyte adhesion when cells were directly cultured on top of the films. The lubricating nature of these films also allowed the surgeon to manipulate the film when it was fully hydrated and could also allow the surgeon to reposition the film without tearing the film or damaging the injured/normal tissues. Even though the HA film demonstrated excellent adhesion reduction and handling during surgery, the film would not be easily adapted to laparoscopic procedures. Some surgeons have moved towards laparoscopy in recent years for some routine surgeries (e.g. gallbladder removal) because the surgical method allows for smaller incisions to heal, faster discharge of patients after surgery, less blood loss, a decrease in post-operative pain in patients, and reduced incidence of

tissue adhesion formation [155]. However, the rate of formation of adhesions after laparoscopy varies by type of procedure and the location of the procedure [156]. Thus, there is still a need to prevent adhesions after some abdominal or pelvic laparoscopic surgical procedures. In laparoscopic surgeries, instruments and materials to be inserted into the abdominal cavity must have a diameter smaller than the 10 mm trocars (or hollowed tubes with a seal) which create a temporary, sterile channel between the operating room and the abdominal cavity. The HA film is flexible when hydrated, but it has not been tested as to whether it can pass through a laparoscopic tool shaft and be successfully deployed. Another possible drawback is the ability of the HA film to conform to tight or complex geometries inside the abdomen. The film was able to be placed on top of the cecum inside the rat's abdomen; however, the cecum is a rather broad surface for application compared to other larger surface areas, such as the small intestine.

The topographical adaptability issue of a barrier film could be addressed by a fluidly applied, self-crosslinking hydrogel barrier capable of fully conforming to any complex geometries/folds inside the abdomen, serve as an effective barrier for several days, and also allow either endoscopic or laparotomy application. Several studies have introduced such hydrogel barriers with both synthetic and natural polymer components. A purely synthetic, poly(ethylene glycol)-based hydrogel (SprayGel, Confluent Surgical, Waltham, MA) is currently in clinical trials in the US. A possible drawback to the wide adoption of this treatment may be the additional need for an air supply set-up to propel the gel onto the wounded tissue in the surgical field. Self-crosslinking hyaluronan-based hydrogels have also reported good efficacy in both large bowel trauma models

[57,61] and pelvic surgical models [157,158]. However, consistency across different hyaluronan formulations has been elusive so far. Intergel (Ethicon, Somerville, NJ), consisting of a ferric hyaluronate-based, ionically crosslinked solution, initially showed promise in pelvic surgical clinical studies [159]; however, it was removed from the market after occurrences of severe complications [64]. Another possible setback to a hyaluronan-based hydrogel barrier is cost: medical-grade hyaluronan is expensive and could increase the price of the hydrogel above re-imbursement caps imposed by a third party.

Other natural polymers have also been modified to initiate gelation without the addition of third crosslinking agent. Chitosan is polymer that has been utilized in studies of drug delivery and tissue engineering. It is also considered to be biocompatible and it the main structure can be modified in numerous ways to enhance crosslinking activity. Self-crosslinking, chitosan with modified nitrogen and oxygen centers, such as N,O,-carboxymethyl chitosan (NOCC), have been studied as an adhesion reducer in a rat small intestine [67] and rabbit large intestine (cecum) [70] surgical model. In both animal studies, NOCC was added to the injured tissue and peritoneal cavity as a 1% gel and a 2% uncrosslinked solution, respectively. The results demonstrated statistical significance between cecal (large intestine) adhesion severity scores between the NOCC treated animals and the untreated controls. However, both groups of authors did not address whether the application of the 2% NOCC solution was necessary to prevent adhesions along side the 1% gel application. Yeo et al. investigated the biocompatibility of a UV-crosslinked, chitosan-based hydrogel inside the rabbit peritoneal cavity which could be used as a combination drug delivery vehicle and adhesion barrier [71]. The

animals received the chitosan solution on the cecum area and UV radiation was applied for approximately 5 minutes (1 min/mL chitosan solution). An additional treatment group of animals just receiving the un-crosslinked chitosan solution was also studied in parallel. The results of the study were less than desirable in terms of compatibility. Animals that received the UV-crosslinked chitosan gel and the un-crosslinked chitosan solution showed strong adhesions between and multiple nodules on the cecum and on the omentum (a section of the peritoneum) [71]. The nodules appeared to be granulomous and contain clusters of macrophage/lymphocyte cells surrounded by a thick, fibrotic capsule. Additionally, pieces of the chitosan gel were present inside some nodules. Strikingly, the control animals that received only UV radiation had a similar adhesion-negative reaction as the untreated control animals (no radiation or chitosan solution/gel). The results of this study suggest that the chitosan preparation used in the study would be unsuitable for intraperitoneal usage. It is possible that the modification of the chitosan polymers may play a larger role in biocompatibility and intra-abdominal tolerance than previously thought.

In a previously published study by Weng et al, a novel hydrogel formulation composed of partially oxidized dextran (Odex) and N-carboxyethyl chitosan (CEC) was developed [72]. There are two major advantages for usage of this system as an adhesion barrier: 1) both chitosan [160,161] and dextran [162] are FDA GRAS materials and have been widely investigated with demonstrated excellent biocompatibility; 2) Odex and CEC cross-link at physiological pH/temperature by electrostatic interaction, hydrogen bonding and eventually stabilization by Schiff base formation between aldehyde and amine groups located on the two molecules [72]. Specifically, the Odex

component serves as a macromolecular cross-linker to bind CEC to form a macromolecular network, thereby obviating the need for potentially cytotoxic small molecule cross-linking agents, which decreases toxicity concerns directly after application/during in situ degradation [163]. In vitro cytotoxicity studies have demonstrated that the Odex/CEC hydrogel formulation has excellent biocompatibility with dermal fibroblast cells in direct contact and encapsulated inside crosslinked hydrogel [75].

The purpose of this study was to evaluate the anti-adhesion efficacy of a 2% Odex/CEC hydrogel in a 21-day, rat cecum abrasion model. In parallel, the hydrogel was benchmarked against Seprafilm, a widely utilized anti-adhesion product. This comparison allowed us to assess the adhesion prevention quality of the Odex/CEC hydrogel against a current and proven standard of care used clinically.

4.3 Methods

4.3.1 Odex/CEC Hydrogel Synthesis

Synthesis of N-Carboxyethyl Chitosan (CEC)- The CEC for this protocol was synthesized Dr. Lihui Weng by a method previously described by our lab [72,73]. About 1 g of chitosan (deacetylation degree 85%, M_w = 750,000) was dissolved in 50 mL of water containing 1.88 mL acrylic acid under constant stirring at 50° C for 3 days. Afterwards, a 10N NaOH solution was added to the reaction mixture to increase the pH to 10-12. This step converted the CEC into its sodium salt. The mixture was then dialyzed extensively for 3 days until pure CEC was obtained by lyophilization.

Synthesis of Oxidized Dextran (Odex)- The Odex was synthesized by Dr. Lihui Weng using a method also previously described by our lab [72]. Approximately 3.28 g $NaIO_4$ (in aqueous solution) was added to an aqueous dextran (leuconostoc mesentereoides, M_w = 76,000) solution (1.25% w/v, 400 mL) and this mixture was stirred at ambient temperature for 24 hours. An equimolar of diethylene glycol was added to quench any un-reacted $NaIO_4$. The Odex solution was dialyzed exhaustively (MWCO 3500) for 3 days against water and pure Odex was obtained by lyophilization [72,73].

Formation of Hydrogel – The reaction between CEC and Odex was schematically depicted in Figure 4.1. Solutions of 2% Odex and 2% CEC were first prepared by dissolving 0.2 g of each polymer into 10 mL aliquots of distilled water; they were then sterilized by autoclave and stored at 4° C before use in the surgical model. For a typical hydrogel formulation, equal volumes of each polymer solution was loaded into two separate Luer-Lock syringes (Figure 4.2A), after engaging both syringes to a two-way connector, the syringe contents were mixed by pushing the plungers back-and-forth 10 to 15 times, totaling approximately 30-35 seconds (Figure 4.2B). Upon thorough mixing, the entire syringe contents were pushed into one of the syringes, the connector in conjunction with the empty syringe was disengaged, and the Odex/CEC hydrogel precursor was ejected and liberally deposited on the damaged tissue (Figure 4.2C). After 1 to 1.5 minutes, the macromolecular structure of the hydrogel has nearly reached completion of gelation, similar to previously reported studies (Figure 4.2D) [72,75].

4.3.2 Rat Cecum Abrasion Surgical Model

The animal experiments were carried out in accordance with a protocol approved by the Institutional Animal Care and Use Committee (Protocol number: 2007-1743). Housing and care for the animals was in accordance with the National Research Council guidelines (National Research Council. Guide for the Care and Use of Laboratory Animals. National Academy Press. Washington, DC. 1996).

Rats (Sprague-Dawley, weight: 350 to 450 g) were first anesthetized with inhaled isoflurane (5% for induction and 2.5% for maintenance) and a mid-line laparotomy incision was performed on each animal, similar to other published studies using the rat model [164]. The cecum was liberally abraded on one side with fine grit sandpaper until oozing of blood was observed from the serosa. Additionally, a portion of the posterior abdominal rectus muscle of approximately 1 cm^2 size was also excised and the wound surfaces were gently dabbed with sterile gauze to remove excess pooled blood. One milliliter of a 2% precursor solution of Odex and CEC was prepared by mixing 0.5 mL of each solution for 30-35 seconds by syringe (see Section 2.2 above) and liberally deposited onto the damaged cecal surface as well as the abdominal wall defect (n=9). The hydrogel was allowed to fully congeal (approximately 1 to 1.5 minutes) and the cecum was reintroduced inside the abdominal cavity, the damaged site on the cecum with the abdominal wall defect prior to closure. The incision was re-approximated and closed using 0-0 chromic gut sutures on the abdominal wall and 5-0 prolene sutures for the skin layer. For comparison, a group of animals was treated with a 1 x 1 inch square of Seprafilm (Genzyme Corporation, Cambridge, MA). This film was placed directly on the damaged cecal surface and the cecum was placed back into the abdominal cavity

similar to the hydrogel treated animals (n=8). Control animals did not receive hydrogel or Seprafilm intervention (n=11). The wound was re-approximated and closed using 0-0 chromic gut sutures on the abdominal wall and 5-0 prolene sutures for the skin layer. The animals were sacrificed after 21 days and the extent of adhesion was semi-quantitatively scored on a scale of 0-3 (0 = no adhesion, 1 = thin and filmy, 2 = significant and filmy, and 3 = severe with fibrosis) [53,144,146,147]. Animals with a score of 3 have adhesions that could not be separated by pulling with blunt forceps (Figure 4.3A).

The surgeries were performed by either the author (67% hydrogel, 37.5% Seprafilm) or Dr. Mark M. Melendez (33% hydrogel, 62.5% Seprafilm) from the Department of Surgery at SUNY Stony Brook.

4.3.3 Histological Sample Collection and Analysis

Samples of cecum and abdominal wall muscle were collected (by the author) from animals that either received no treatment (control) or animals that received the Odex/CEC hydrogel intervention. Tissues were dissected, rinsed in phosphate buffered saline (PBS), and preserved in 10% buffered formalin. The preserved tissues were embedded in paraffin, sectioned, and stained with hematoxylin and eosin stain (H&E) by the Pathology Department at Stony Brook University (Stony Brook, NY) which was utilized observe the gross morphology of the tissues. To highlight the location of the hydrogel, a modified Periodic Acid Schiff (PAS) and Toluidine Blue staining protocol was performed in our laboratory. PAS reaction is a useful indicator of the presence of carbohydrates in the tissue, including implanted chitin [165]. The sections were

deparaffinized and rehydrated to distilled water first. Then, the sections were placed in a solution of periodic acid for 5 minutes and afterwards rinsed in 4 changes of distilled water. After rinsing, the sections were then placed in Schiff's reagent for 10 minutes to develop color. The sections were rinsed in running tap water until the rinse water turned clear. In the next step, the rinsed sections were placed in a solution of 0.1% Toluidine Blue (aqueous) for 2 minutes to stain the cells, but not the hydrogel. The excess Toluidine Blue stain was rinsed from the sections with several changes of distilled water. The sections were then dehydrated in a series of alcohol bath, cleared in xylene, and mounted with xylene-based mounting media

4.3.4 Data Analysis and Statistics

Surgical adhesions severity scores were analyzed using a 1-sided, Wilcoxon Rank Sum Test with statistical difference determined by p-values less than 0.05. The mean and standard deviation of each group average score was also calculated and reported separately in the Results Section.

4.4 Results

The raw adhesion severity scores can be found in Table 4.1. The mean adhesion score for the control animals was 2.09 ± 1.22. Animals treated with Seprafilm and the 2% Odex/CEC hydrogel had adhesion scores of 1.25 ± 0.707 and 1.00 ± 1.00, respectively. The Odex/CEC hydrogel treatment had a significantly lower adhesion score ($p = 0.029$) than the control. Animals treated with Seprafilm also demonstrated a significantly lower adhesion score ($p = 0.056$). There was no statistical difference

between the two treatments, although the Odex/CEC hydrogel showed a slight trend towards a lower score than the Seprafilm ($p=0.214$).

Twenty-one days post intervention, modest amounts of hydrogel remnants (in small, individual fragments), mostly adjoining the cecum and abdominal wall, were recovered from six out of nine of animals treated with the Odex/CEC hydrogel (Figure 4.3B,C). Overall, these animals showed adhesion scores of 0 or 1. One hydrogel treated animal experienced severe adhesion of the cecum to the abdominal wall with Odex/CEC hydrogel remained under the adhesion edge on the wall defect; however, blunt dissection could not loosen the adhesions without causing tearing of the cecum. In four animals treated with Seprafilm (scores = 1), amber-colored pieces of degraded film were also observed.

Histological analysis of rats either no treatment (control) or Odex/CEC hydrogel were performed. The untreated specimen was consistent with a severe adhesion score of 3 (Figure 4.4A) with a strong, fibrous tissue layer formed between the cecum and abdominal wall surfaces. The Odex/CEC treated animal in this histological study had some visible remnants of hydrogel after 21 days. Views of the healed abdominal wall (Figure 4.4B) and cecum surface (Figure 4.4C) displayed wound repair as well as the active degradation of hydrogel pieces in an animal with an adhesion score of 1. The cecal and abdominal tissues were originally separated by blunt dissection after sacrifice to determine the adhesion score. Fused, multi-nucleated macrophages were also observed ingesting the residual hydrogel pieces within the re-epithelialized tissue (circled area, Figure 4.5B).

4.5 Discussion

Studies have shown that the window for efficacy of an adhesion barrier occurs between 12 and 36 hours after surgery [43,166]. The rats in this study were sacrificed 21 days after surgery to observe the adhesion severity. In many comparable rat cecum abrasion models, the typical post-operative sacrifice time range for a solid or hydrogel barrier is 7-14 days [48,167]. Since adhesions typically manifest within the first few days after surgery, it is between 5-7 days that the adhesion fibrosis becomes more organized, rigid, and vascular [33,35]. Any adhesions present in the abdominal cavity after 7 days could persist for several months due to the effects of remodeling inside the adhesion tissue [35].

Overall, the Odex/CEC hydrogel showed significantly less adhesion than control animals receiving no hydrogel intervention. Approximately seven out of nine hydrogel treated animals displayed adhesions with scores of 0 or 1, having no adhered tissue present in the abdomen or filmy adhesions that were easily lysed, respectively. Only one animal developed severe adhesions (score = 3) during the 21 days post treatment period. Possible causes of this outlier could be fracture of the hydrogel at or in proximity of the injured surfaces or insufficient coverage over the injured tissues. Hydrogel strength can be increased through modulation of various parameters such as the concentrations, molecular weight, or extent of molecular modification of the precursors, while also applying the hydrogel precursor mix across a larger surface area (insult areas and normal tissues), may further increase the efficacy of the barrier after surgery and decrease the incidence of severe adhesions. Although insufficient barrier coverage was suspected in the severe adhesion case, the persistence of hydrogel remnants were also observed in six out of nine Odex/CEC treated animals. Most of

these fragments were located on the surface of either the cecum, the abdominal wall adjoining the sites of tissue insult, or on top of any filmy adhesions observed (see Figure 4.4A, 4.4B). The presence of partially degraded hydrogel fragments did not appear to have affected the overall adhesion score. Degradation time, similar to gelation, could be modulated by controlling the concentration of Odex and CEC precursor solutions used (e.g., concentrations of less than 2% form less dense cross-links and a weaker overall hydrogel structure) [72]. Although the scope of this study was narrowed to a 2% polymer concentration and its effect on adhesion formation was compared with a clinically utilized adhesion barrier, it does not exclude future abdominal adhesion studies using different polymer formulations composed of different concentrations of Odex and CEC that could conceivably be more efficacious.

The histological result of residual Odex/CEC hydrogel in conjunction with the adjoining tissue at the insulted area after 21 days did not show cellular infiltration into the bulk of the material, suggesting the hydrogel may be degraded through surface erosion [75]. The noticeable absence of cellular infiltration suggested that the hydrogel served as an effective, occlusive barrier to prevent inflammatory cells and fibroblast cells from synthesizing aggressive tissue adhesions between the injured cecum and the abdominal wall. Moreover, as indications of wound healing, granulation tissue was observed at the site of injury with re-epithelialization occurring underneath the hydrogel thus restoring tissue integrity while also preserving the bowel's capacity of motion along the abdominal wall. However, some residual hydrogel fragments were recovered inside the granulation tissue on the cecum and abdominal wall. These hydrogel remnants appeared to be surrounded by macrophages with the noticeable presence of foreign

body giant cells; some with the material was apparently internalized by these cells, suggestive of finalizing biodegradation. Ingestion of hydrogel particulates by foreign body giant cells has also been reported in other biodegradable hydrogels containing dextran [168]. The presence of the multi-nucleated giant cells surrounding the hydrogel, or any foreign material introduced to the abdominal cavity during the surgery, is not unusual 21 days post-op [136,169,170]. Despite the presence of some residual inflammation around the hydrogel fragments in the histology samples, the extent of adhesion observed was very low (score = 1) and the tissues were easily separated without injuring the cecal tissue. Since the hydrogel did not appear to interfere with the expected immune response inside the abdomen, it can be further suggested that the main mechanism of adhesion-reduction of the hydrogel was through the maintenance of a physical barrier between the injured surfaces.

Similar to Odex/CEC hydrogel-treated animals, rats that were treated with Seprafilm also showed significantly less adhesions than the controls. Seven out of eight animals demonstrated thin, filmy adhesions (score = 1), and one animal developed dense adhesions of the small intestines (not the cecum) to the abdominal wall. The appearance of severe adhesions was previously documented in a small percentage of humans or animals when Seprafilm was applied as a prophylactic treatment for post-surgical adhesions. It was previously shown that the rate of severe adhesion for Seprafilm treated animals in a comparable model was 20% [48], which was within the range of the 12.5% (one out of eight animals) adhesion rate observed when the same film was applied in this study. Similar to the results derived from applying the Odex/CEC hydrogel in this study, the severe adhesion observed in the Seprafilm animal

could also be insufficient coverage of the film over the wounded surfaces. In this study, a 1 x 1 inch square of film was used to cover the cecum surface before placing it back into the abdominal cavity and proximal to the abdominal wall defect. It could thus be postulated that the efficacy of Seprafilm could be enhanced by introducing additional pieces to extend the coverage to undamaged tissue adjacent to the cecum or abdominal wall defects.

Although statistical analysis did not demonstrate any significant difference in the severity of adhesion scores between Seprafilm and the Odex/CEC hydrogel, the ability of the hydrogel to conform to complex geometries and folds within the abdomen is advantageous in both method of application and material durability during application. Seprafilm is applied to damaged tissues as a solid sheet thus limiting its application to open surgeries. Although Seprafilm has been reportedly demonstrated in laparoscopic surgeries, the brittle nature of the film makes rolling the film for insertion difficult and any moisture on the application tools will also cause the uncrosslinked film to fracture before proper placement [45,171]. Additionally, the film does not have the plasticity that a surgeon desires during an operation. In contrast, the Odex/CEC hydrogel, as a conformal tissue sealant, could be easily adapted in both conventional surgeries and laparoscopic procedures in either a syringe-borne configuration or through a laparoscopic trocar. It takes approximately 30 seconds for thorough mixing of the two components: a steady but rapid increase in both the viscosity and adhesiveness of the precursor mix ensures its localization. A surgeon has 30-45 seconds for deploying the precursor to the surgical field before the gelation point is reached. The gelation point observed with a 2% Odex/CEC hydrogel was slower but within the same range as our

recently published rheological data derived from a hydrogel composed of 2.5% Odex/CEC with a measured gelation point of 79 seconds [75]. Further in vivo studies on the biological responses of varying the Odex and CEC concentrations to expand the gelation point range may be needed. The Odex/CEC hydrogel may also eliminate the need to further irritate the surface of the bowel with additional drying methods before application beyond the removal of excess blood at the site.

In conclusion, we have introduced a novel application of an in situ gelable Odex/CEC hydrogel to reduce the incidence of abdominal adhesions in a rat cecum abrasion model. The hydrogel is easy to apply using a two syringe mixing system and has achieved comparable, overall efficacy in adhesion prevention as Seprafilm. Future studies using larger animal models of abdominal adhesion as well as laparoscopic application of the hydrogel are needed to further establish efficacy in humans prior to clinical evaluation.

Table 4.1: Adhesion severity scores for control and Odex/CEC hydrogel treated animals

Score	Control (n = 11)	Odex/CEC Hydrogel (n = 9)	Seprafilm™ (n = 8)
0	2	3	0
1	1	4	7
2	2	1	0
3	6	1	1

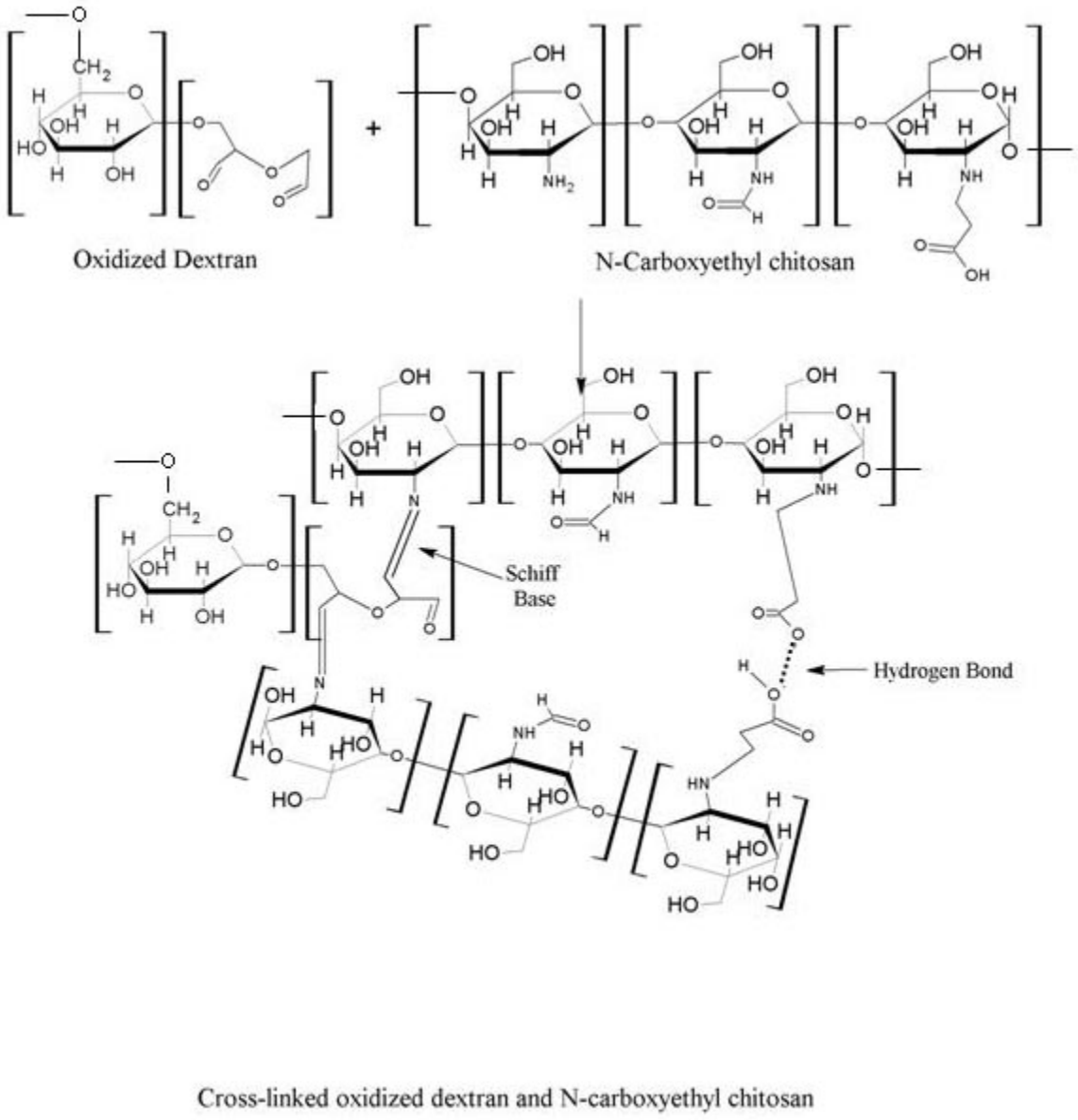

Figure 4.1: Schematic representation of the gelation process of Odex/CEC solutions

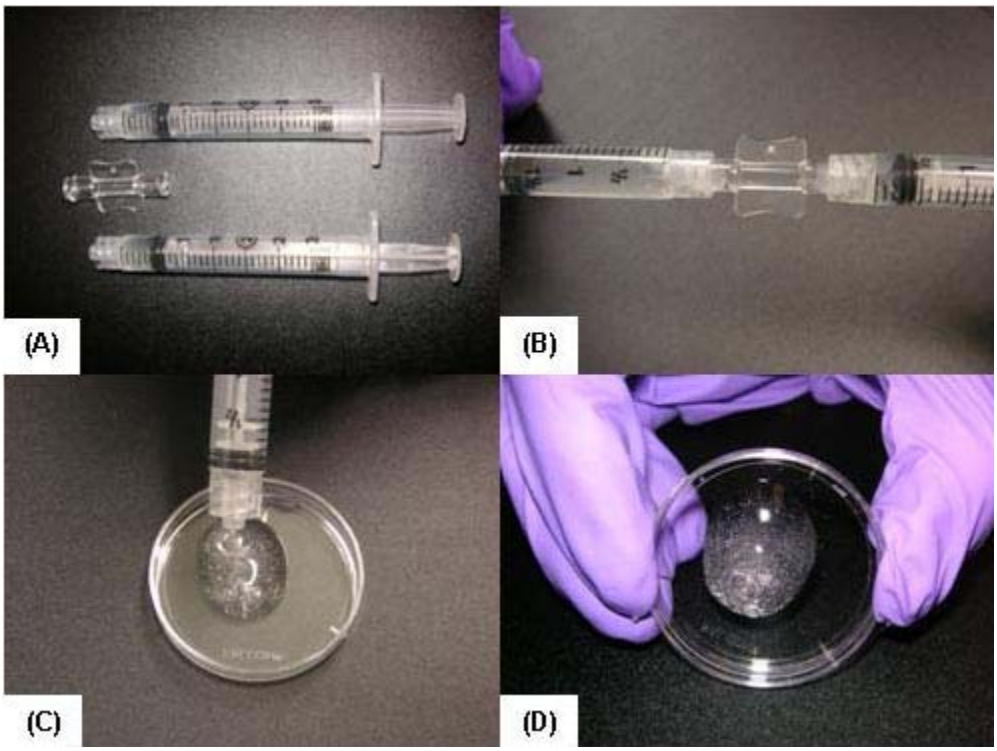

Figure 4.2: Formation of Odex/CEC hydrogel: (A) 2% solutions of Odex and CEC were loaded into separate syringes with the two-way Luer-lock adapter also pictured; (B) syringes were engaged using the adapter and mixed by pushing the syringe contents back and forth 10 to 15 times (about 30-35 seconds); (C) fluid application of the cross-linking hydrogel to an example Petri dish; (D) approximately 1-1.5 minutes after mixing, the hydrogel has congealed. Air bubbles were introduced into the hydrogel during mixing for ease of visualization of the final cross-linked product.

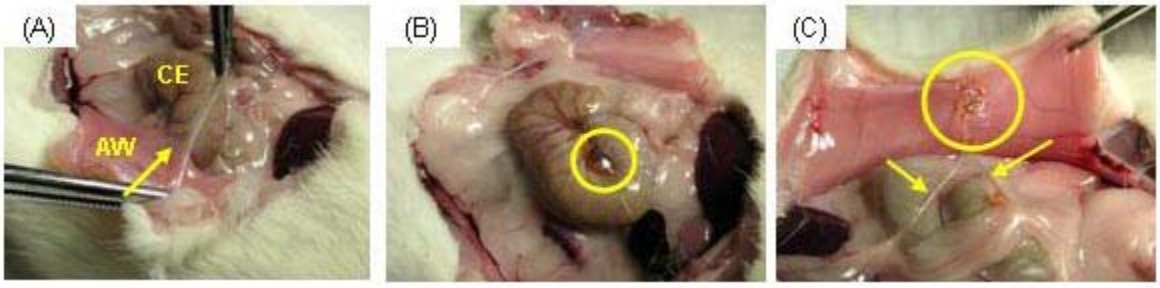

Figure 4.3: Examination of cecal and abdominal wall tissues from rats 21 days after surgery: (A) an example of a severe adhesion (score = 3) case: a control rat with adhesion of the cecum (CE) to the abdominal wall (AW). The arrow indicates the area where the adhesion is present. Odex/CEC hydrogel remnants were found on both the cecum (B) and abdominal wall (C) of one animal subject. This animal received an adhesion score of 1 due to some light, filmy adhesions of fat/omentum to the abdominal wall. The circled regions of (B) and (C) highlight the presence of the hydrogel pieces while the arrows in (C) point out the light adhesions that formed inside the rats abdomen after 21 days.

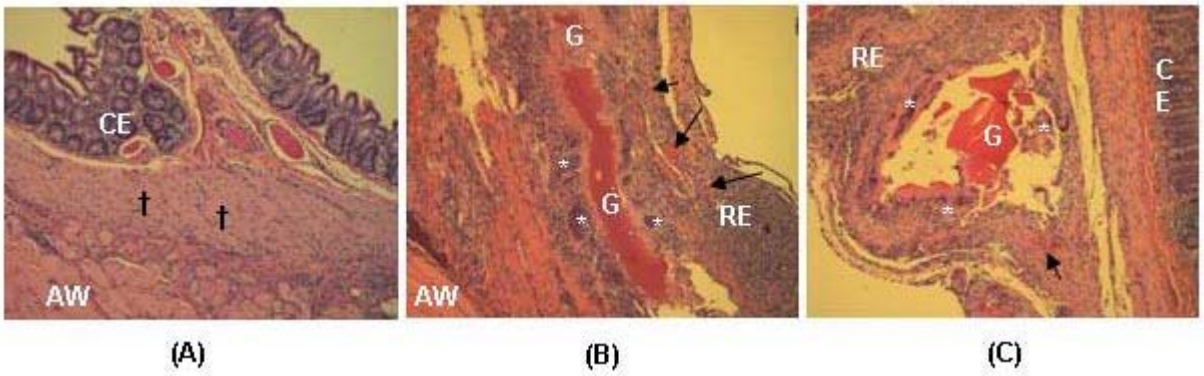

Figure 4.4: Photomicrographs of abdominal and cecum tissue excised 21 days after injury. (A) Cross-section of rat tissue from untreated, control animals with severe adhesions (†) between the abdominal wall (AW) and the cecum (CE) surface (score = 3). (B) Site of abdominal wall defect in a rat treated with the Odex/CEC hydrogel. Remnants of the hydrogel (G) are noted and some fragments are located inside the re-epithelialized (RE) defect site. (C) Site of cecum serosal abrasion from same rat as in (B). Fragments of residual hydrogel are located inside the RE tissue on the serosal surface. Asterisks (*) indicate fused, multi-nucleated giant cells surrounding hydrogel remnants inside the RE tissue. In both (B) and (C), arrows indicate the presence of blood vessels formed inside the RE tissue. Magnification 10x for all photomicrographs.

Chapter 5

Oxidized dextran/N-carboxyethyl chitosan microgels for drug delivery

5.1 Summary

The goal of research described in this chapter was to synthesize and characterize microgel particles made from self-crosslinking oxidized dextran (Odex) and N-carboxyethyl chitosan (CEC) and to measure their inflammatory potential with a macrophage cell line and in a murine subdermal implant model. The microgels were studied as a delivery vehicle for an inhibitor of inducible nitric oxide synthase (iNOS), guanidinoethyl disulfide (GED), or a model dye particle, Toluidine Blue O. The physical characteristics of the microgels were studied as overall morphology (scanning electron microscopy), particle size analysis, zeta potential, and GED/Toluidine Blue O release kinetics over 15 days. A macrophage cell line (RAW 264.7) was utilized to assess both the inflammatory potential of degraded polymer/released GED from microgels and the inflammatory potential of whole microgels with or without GED co-incubated with macrophage cells for up to 7 days. Assessment of inflammation utilized measurements of attached cell density, metabolic activity, nitrites, Tumor Necrosis Factor-alpha (TNF-α), and reactive oxygen species (ROS) production. The microgels were also subdermally implanted in mice for 3, 7, and 29 days. The effect of released GED and the overall biocompatibility of microgels without GED in the subdermal space were

assessed by examining the infiltration of inflammatory cells (macrophage, neutrophil) and quantifying fibrotic tissue formation (Collagen type I) around the implant area. Results of the study showed that the microgels exhibit a modest “burst” release of GED and Toluidine Blue O within the first 24 hours of the release study. Microgels loaded with GED did not show significant differences in physical parameters such as hydrodynamic radius or zeta potential. In the RAW 264.7 cell culture model, the released GED from microgels caused a significant increase in nitric oxide (NO) production compared with release samples from microgels without GED. Whole microgels were well tolerated by the same cell line and produced low amounts of nitrites similar to negative control cells. However, all microgel treated cells showed higher levels of TNF-α production relative to the negative control cells, signifying the macrophage cells still perceived the microgels as foreign bodies. Subdermally-implanted microgels produced a robust inflammatory response with leukocyte cell infiltration at short time points (Day 3). The presence of microgels with GED loaded produced significantly higher inflammatory cell infiltration scores than non-GED loaded microgels at Day 7. At Day 29, high dose GED microgels produced both significantly higher inflammatory cell infiltration scores compared to no GED and low dose GED microgels. Furthermore, the high dose GED microgels demonstrated lower Collagen type I content in the fibrous capsule surrounding the implant compared with the other two microgel treatments at the same time point. In contrast, low dose GED microgel implants produced the most Collagen type I in the surrounding fibrotic capsules and had a lower inflammatory cell infiltration score compared with the high dose GED and no GED microgels at Day 29.

5.2 Introduction

Damage caused by ROS typically occurs during an inflammatory process in which NO (from iNOS activity) and mitochondria-produced superoxide (O_2^-) combine to produce peroxynitrites, a highly reactive oxidative species capable of damaging tissues and cells [172]. Separately, NO and O_2^- do not produce significant damage to surrounding tissues [173]. The 2 main mechanisms for damage by peroxynitrites are the modification of intracellular molecules (e.g. DNA, lipids, proteins) directly by oxidation and nitration of proteins (i.e., modification of tyrosine residues into nitrotyrosine) [174]. The control of peroxynitrite formation is especially important in studies of neural stem cell (NSC) treatment for spinal cord injury and nerve regeneration. NSCs applied to the site of spinal cord injury between 0-5 days after injury have a low survival and differentiation rate because of damage caused by oxidation and the expression of inflammation-associated cytokines [175]. In studies so far, a key time period for NSC implantation falls between 7 and 14 days after injury, after which scar tissue forms at the injury site and the possibility of nerve regeneration is completely closed [176]. However, even with a specified timeline for successful implantation of NSCs, early reductions in peroxynitrite formation and inflammatory cytokines may allow the successful application of NSCs closely following injury. When scavengers of peroxynitrite were delivered in a polymer vehicle to the site of spinal cord injury, the survival and proliferation of donor stem cells and resident nerve cells were significantly increased [177]. In another example of tissue destruction produced by reactive nitrogen species, the formation of peroxynitrite inside the pancreas of a pre-diabetes type-I patient can damage insulin producing beta islet cells. As a result, the patient slowly looses the ability to produce insulin in response to increases in blood

glucose levels (e.g., after a meal is consumed). Although the formation of peroxynitrites in this disease is attributed to long-term autoimmune inflammation, studies have demonstrated that the inhibition of iNOS by pharmacological intervention significantly reduced the incidence of Type-I diabetes in lab animal models [178,179].

Methods of preventing cell and tissue damage arising from excess peroxynitrite formation have included direct scavenging of peroxynitrites or inhibition of iNOS (main NO producer after injury and during inflammation). In studies of spinal cord injury, peroxynitrite scavengers have shown much promise in preventing neuron cell death. Manganese (III) Tetrakis (4-Benzoic Acid) Porphyrin (MnTBAP) is a potent compound that has a strong affinity to scavenge and bind peroxynitrite [86,180]. When MnTBAP is applied directly to the spinal cord tissue after injury, a significant reduction in nitration and oxidation of proteins in the spinal cord tissue was measured [88]. However, MnTBAP does not appear to affect levels of O_2^- or NO produced by leukocytes, the pre-cursor molecules to peroxynitrite. Several studies of spinal cord injury and organ re-profusion related injury have indicated that NO is produced primarily by iNOS from activated macrophages [181].

Although the direct scavenging of peroxynitrite by MnTBAP has shown positive results in reducing peroxide-induced neuronal damage after injury, several researchers have also proposed utilizing inhibitors of iNOS as a prophylactic to stem the production of peroxynitrite by initially reducing NO production. In this way, if there is a shortage of NO during inflammation after injury, the O_2^- molecules will have fewer partners to produce peroxynitrites. Mercaptoethyl guanidines (MEGs), including N^G-nitro-l-arginine methyl ester (L-NAME) and guanidinoethyl disulfide (GED), are small molecule drugs

that reduce NO through the competitive inhibition of L-arginine, a substrate for the iNOS enzyme. In several recent studies, a number of MEGs were found to also act as scavengers of peroxynitrites in addition to their actions as iNOS inhibitors [86,87,92,179]. Although MEGs have been shown to reduce iNOS activity, they also target other nitric oxide synthases that are not large contributors to peroxide-mediated cell damage. For example, endothelial NOS (eNOS) is important in the regulation of blood pressure in healthy individuals and the inhibition of eNOS can cause hypertension if a nonspecific NOS inhibitor is administered systemically [91]. Of the drugs mentioned, GED is 4 times more specific in targeting iNOS over other NOS molecules [91]. In this study, GED was chosen both because of its strong specificity towards inhibiting iNOS and its peroxynitrite-scavenging ability [83,91]. However, GED, like other MEGs, does have vascular side-effects when it is systemically or orally administered at high doses [182]. Thus, the localized application of GED through a polymeric delivery vehicle would further enhance the utilization of the drug in the treatment of inflammation-induced peroxynitrite tissue damage while also circumventing the hypertension problem that occurs with traditional delivery methods.

In previous studies, a self-crosslinking hydrogel composed of oxidized dextran and N-carboxyethyl chitosan has been physically characterized using viscometry [72] and utilized as a wound dressing in an experimental mouse full-thickness dermal defect model [75]. Chapter 4 demonstrated that crosslinked Odex and CEC is well tolerated in the abdominal cavity on cecal (large intestine) wounds/abdominal wall muscle defects in rats and reduces post-surgical adhesions compared with untreated control animals [183]. In all of the models, tissue healing occurred with acute, chronic inflammatory

response, which was caused by macrophage cell-mediated degradation of the hydrogel surface. The hydrogel's self-crosslinking is especially advantageous because it does not require the addition of a separate cross-linking initiator to the polymer solution. Any un-reacted initiators retained inside the crosslinked hydrogel could cause complications by irritating the surrounding tissue if they diffuse out of the hydrogel bulk at a later time. Additionally, water soluble drugs can be easily incorporated in the hydrogel matrix by adding it directly to either Odex or CEC component of the hydrogel before mixing them. The aldehyde (-CHO) and amine ($–NH_2$) side groups on Odex and CEC molecules, respectively, could also be explored as binding sites for small molecule drugs to modulate local drug release. To our knowledge, the Odex/CEC hydrogel system has not been utilized as a drug delivery vehicle in previously published literature. The drug that was chosen for this study, GED, has 4 -NH_2 groups attached to its terminal ends. The NH_2 groups present an opportunity for the drug to attach to the -CHO presenting Odex molecules and thus serve as a mechanism to modulate the release of the drug over time. We also hypothesized that the GED included in the crosslinking hydrogel would affect the Schiff base formation between Odex and CEC as well as become bound to crosslinked polymer structure.

In this study, we synthesized microgels (i.e. microspheres formulated from hydrogel) using solutions of Odex and CEC by a suspension emulsion method. The Odex and CEC solutions are mixed thoroughly outside of the emulsion first to initiate the crosslinking reaction between the two polymers. Next, the mixture is added to the continuous phase consisting of mineral oil and the aqueous polymer phase is dispersed into individual droplets. These droplets of Odex/CEC mixture continue self-crosslinking

while they are stirred inside the emulsion, resulting in the formation of solid microgel particles. The microgels are isolated from the emulsion using sequential washes of acetone and isopropanol and air dried as a final step. The microgel drug delivery vehicle has a few advantages over a bulk hydrogel drug delivery system. Due to their small size, microgels have a larger surface area to volume ratio than hydrogels, which allows for more contact of the microgels to water and more opportunity for the drug to release evenly over the microgel surface. Also, given their sizes, microgels can be easily reconstituted in a saline solution and injected into the area where they are needed to deliver their therapeutic payload. This attribute gives the microgels more versatility in their applications.

After preparing any microparticulate drug delivery system, it is necessary to perform initial *in vitro* tests to examine the inflammatory and cytotoxic potential of microparticles with and without encapsulated drug. Transformed macrophage and primary macrophage cell lines have been utilized to screen particulate matter in previous studies [184-186]. Macrophage cells are important foremost in the production of NO during the inflammation phase following injury. In this study, a murine macrophage cell line, RAW 264.7 (TIB-71, ATCC, Manassas, VA), was utilized to study the inflammatory potential/cytotoxicity of degraded Odex/CEC microgels and whole microgels. RAW 264.7 cells are potent producers of inflammation indicators such as TNF-a and interleukin 1 beta (IL-1β) when they are activated and thus demonstrate a method to measure inflammation response to foreign materials [187] or endotoxins [188-190]. These cells also produce high levels of reactive oxygen species (ROS) and NO through the L-arginine pathway when they are activated. Previous publications have

used RAW 264.7 cells to evaluate particles from orthopedic implant wear [188,191-193], silica [194,195], and metallic particles [196,197]. These cells are utilized in ASTM protocol F1903-10 as mediators to test the biocompatibility of particle compounds before performing *in vivo* tests [185]. This project will measure NO, ROS, and TNF-α production by RAW 264.7 cells to evaluate the inflammatory potential of released GED from the microgels as well as direct contact with whole microgel particles with or without GED encapsulated.

Short-term, subdermal implantation of biomaterials has also been used to assess biocompatibility (to measure the tissue and immune system response due to the close proximity of the material to the surrounding tissue) [198] and the localized effect of anti-inflammatory drugs on fibrotic tissue encapsulation [199]. In this study, we designed our *in vivo* experiment to measure the inflammatory response and fibrotic tissue formation around implanted Odex/CEC microgels with or without GED encapsulated. We hypothesized that by increasing GED content in the microgels, a corresponding decrease in inflammatory cell infiltration and fibrosis surrounding the implanted microgels would be observed. In the early stages of implantation, the material displaces the space between the loose connective tissue under the dermis layer and dorsal muscle layer and inevitably causes some blood vessel rupture and bleeding [200,201]. Leukocytes (e.g. neutrophils and monocytes) arrive at the implant area from the compromised blood vessels and the tissue surrounding the wound bed [16,202]. The main function of these cells is to clear damaged tissue, identify foreign bodies, and produce cytokine signals to promote inflammation [203]. When leukocyte cells encounter a foreign body (similar to the microgels in this project), they attach to the

material surface and attempt to phagocytize the material [203,204]. As the macrophages, present in the early inflammatory process, are interacting with the foreign body, they also produce signals including NO, TNF-α, IL-1β, and IL-6 that signal mesenchymal cells (e.g. fibroblasts) to migrate and proliferate in the wound bed [200,204]. As the inflammatory phase draws towards an end, a down regulation of TNF- α, IL-1, IL-6 is caused by the production of IL-10 (an anti-inflammatory cytokine) by both mesenchymal cells and other macrophage cells inside the wound [205]. The mesenchymal cells produce Collagen type III and later re-arrange to form stronger, more organized Collagen type I fibers [206]. The collagen fiber capsule formed around the implant mainly serves to separate the foreign material from the rest of the body and further contact with the immune system [199,203]. In healthy wounds, a certain level of NO is required as a chemical messenger to regulate the influx of neutrophilic cell types during the inflammation period [207] and to signal fibroblast cells to produce collagens to close the wound [208,209]. If the production of NO is diminished during the inflammatory period, wound fibrosis is diminished. Several iNOS inhibitors, including GED and L-NAME, have demonstrated the ability to disrupt collagen III deposition and collagen I (produced from re-arranged collagen III fibers) organization in healing skin [85,210,211]. A recently published study in our lab utilized oxidized hyaluronan and gelatin microspheres to deliver GED to a full thickness dermal wound in mice [212]. The results of the study indicated that released GED from these microspheres *in situ* reduced both inflammatory cell infiltration and fibroblast cell migration into the wound bed up to 7 days after injury. However, this study did not address the effects of GED loaded microspheres on wound fibrosis and Collagen I or III deposition.

5.3 Methods

5.3.1 Microgel Synthesis Using a Water-in-Oil Emulsion Method

To synthesize microgels, 0.08 g of Odex and CEC were dissolved overnight in separate 10 mL aliquots of distilled water overnight at room temperature. The Odex and CEC polymers utilized in this chapter were synthesized by both Dr. Lihui Weng and the author (see Chapter 4). To prepare the oil phase of the emulsion, a mixture of 80 mL of light mineral oil (Sigma Aldrich, St. Louis, MO) with 1 mL of SPAN 80 (Sigma Aldrich, St. Louis, MO) was placed in -20°C for 2 hours to pre-cool. At the end of this period, the oil/SPAN 80 mixture was placed on ice and mixed at 500 rpm for 5 minutes with a rotary mixer fitted with a 3-cm propeller. Each solution of 0.8% Odex and 0.8% CEC was loaded into separate syringes and the syringes were placed on ice briefly. After the oil/SPAN 80 was mixed for 5 minutes, the speed of stirring was increased to 1100 rpm. The Odex and CEC filled syringes were engaged to a two way connector and the syringe contents were mixed by pushing the plungers back-and-forth 10-15 times, totaling approximately 30-35 seconds. Upon thorough mixing, the entire syringe contents were pushed into one of the syringes, the connector in conjunction with the empty syringe was disengaged, and the Odex/CEC mixture was ejected into the oil/SPAN 80 phase under constant stirring. The emulsion was allowed to stir on ice for 1 hour. After 1 hour, the emulsion vessel was placed in a 48°C water bath and the stirring speed was decreased to 800 rpm for 1 hour. The speed of mixing was further reduced to 500 rpm to be mixed at 48°C overnight.

Incorporation of dye/drug molecules – The above protocol was modified slightly for the incorporation of either guanidinoethyl disulfide (GED), a drug, or Toluidine Blue O ($C_{15}H_{16}ClN_3S$, Electron Microscopy Services, Hatfield, PA). Toluidine Blue O was

chosen as a model payload molecule to test release kinetics of the Odex/CEC microgels. Both Toluidine Blue O and GED have similar molecular weights (305.8 and 360.5 g/mol, respectively) and solubility in water (3.8 and 2.7 g/100 mL, respectively), but Toluidine Blue O only has 1 amine group compared with GED's 4 amine groups. The dye also allows the qualitative evaluation of the elution of payload over time by monitoring color change of the release medium over time.

The drug or dye was added to the aqueous Odex solution prior to crosslinking because it is less viscous than the CEC solution, ensuring that the drug is incorporated homogenously into one polymer phase before mixing. To accommodate the addition of a payload molecule, an Odex solution was prepared by adding 0.08 g of Odex to 9 mL of distilled water instead of 10 mL. For microsphere batches containing 10 mg of dye or drug ("high dose" microgels, 63 μg drug or dye/mg microgel), a 1 mL solution of 10 mg/mL of dye or drug was added to the 9 mL of Odex solution already loaded into a syringe. The dye or drug solution was incorporated into the Odex solution by tapping the syringe several times. Microgels containing 1 mg of dye or drug received a 1 mL solution of 1 mg/mL of dye or drug ("low dose" microgels, 6.3 μg drug or dye/mg microgel) added to 9 mL of Odex solution. The dye/drug containing Odex was then mixed with 10 mL of CEC solution using the protocol described previously.

Microsphere recovery – Microspheres were recovered using a series of isopropanol and acetone washes to dissolve and remove the residual oil remaining from the emulsion. Briefly, after overnight stirring, 80 mL of pure isopropanol was added to the emulsion and the mixture was aliquoted equally into 4 separate 50 mL centrifuge tubes. The mixtures were centrifuged at 2500 rpm for 10 minutes at room temperature

(Allegra X-15R, Beckman Coulter, Brea, CA). The supernatant was aspirated from each tube leaving a “pellet” of microgels. The microgels were further consolidated into a single centrifuge tube by suspending each microgel pellet in 5 mL of pure isopropanol and transferring by pipette to a single vial. A volume of 20 mL of pure acetone was added to the microgel/isopropanol suspension (isopropanol:acetone, 1:1). The microgels were centrifuged again at 2500 rpm for 10 minutes. Afterwards, the supernatant was aspirated and 30 mL of pure acetone was used to wash the microgel pellet. The microgels were centrifuged again and the pure acetone washes were repeated thrice with the same volume of solvent. At the last acetone wash, the microgels were suspended in 5 mL of acetone and aliquoted out into 2 mL Eppendorf tubes, and centrifuged at 2500 rpm for 10 minutes using a bench-top centrifuge (Microfuge 22R, Beckman Coulter, Brea, CA). After the final centrifugation step, the acetone was aspirated out and the microgel pellets were allowed to air dry for 36 hours in a laminar flow hood. The microgel pellet tubes were labeled with lot numbers assigned by the author and placed in a dark, dry container at room temperature until needed.

5.3.2 Physical Characterization of the Microgels

SEM study of microgel morphology - To assess the morphology of the microgels, 1 mg samples of microgels (containing GED or no GED) samples were placed in 1 mL of pure isopropanol and the sample vials were placed in a sonicator bath (FS30H, Fisher Scientific, Pittsburgh, PA) briefly (30 seconds) to suspend. About 0.2 mL of each microgel suspension was added drop-wise to a 1 x 1 cm aluminum stub. The solvent

was allowed to fully evaporate before processing the samples for SEM imaging. The microgels and stub were then sputter-coated with gold and placed inside the scanning electron microscope (LEO1550 with Robinson Backscatter Detection, Carl Zeiss International, Peabody, MA) specimen chamber. Images were captured digitally.

Particle size analysis - Particle size analysis was performed on blank microgels (no GED loading) and microgels loaded with GED. Microgels loaded with Toluidine Blue O were not included in the size analysis. Equivalent diameter values were determined using dynamic light scattering (DLS) (ZetaPlus, Brookhaven Instruments, Brookhaven NY). The detailed protocol for DLS is located in Appendix A. Briefly, each batch of microgel was resuspended in PBS and sonicated to disperse any aggregated particles. The resuspended microgels were then transferred to a disposable, polystyrene cuvette and the cuvette was placed in the zetasizer instrument. Particle size analysis was initiated by the provided software and algorithm (ZetaPlus Particle Sizing Software v.4.10, Brookhaven Instruments, Brookhaven NY). Sizing was performed on 3 different batches of each GED loading. Average and standard deviation of effective diameter were used in statistical analysis.

Zeta potential analysis - Zeta potential analysis was performed using the same instrument (ZetaPlus) as described in the particle sizing protocol. Toluidine Blue O containing microgels were excluded from zeta analysis because dye eluted from the microgels could damage the plate electrodes. The zeta potential measurements were determined by utilizing phase analysis light scattering (PALS) technique and Smoluchowski Equation, calculated internally by the installed software package (PALS Zeta Potential Analyzer v.3.57, Brookhaven Instruments Corp., Brookhaven NY). The

detailed protocol for preparing the microgel samples for zeta potential analysis can be found in Appendix A. Briefly, samples for zeta analysis were prepared in a less turbid suspension than their particle size analysis counterparts. The diluted suspensions of microgels were added to disposable, polystyrene cuvettes and the zeta electrode unit was inserted inside the cuvette. Each sample was analyzed for 30 cycles a total of 5 times. The samples were rested for 30 seconds between runs to prevent the samples from overheating. The zeta potential values from each run set were averaged and standard deviation was calculated.

5.3.3 Release Kinetics of GED and Toluidine Blue O from Microgels

Release kinetics and sample collection – The goal of this protocol was to measure the release of Toluidine Blue O and GED over time in an aqueous solution formulated with physiological pH and ion concentration. The PBS as a release medium has been well documented in literature and is often the first measure of drug release kinetics from drug delivery devices [213]. For both Toluidine Blue O and GED loaded microgels, approximately 15 mg of each formulation (n=3 each dye/drug loading) was placed in 2 mL cryovials and re-suspended in 1.5 mL of PBS (pH = 7.4). The vials were then mixed by rotation end over end in a 37°C warming oven. Samples of the release medium were taken at 1, 4, 8, and 24 hours first, followed by sampling every 2 days for a total of 9 days for GED microgels and 42 days for Toluidine Blue O microgels. At each time point, the vials were removed from the warming oven and each vial was centrifuged at 2500 rpm for 10 minutes at room temperature. An aliquot of 1.2 mL was extracted from the supernatant in each vial, placed in separate sample tubes, and

stored at -20°C (GED) or room temperature (Toluidine Blue O). Fresh PBS (1.2 mL) was added back to each microgel-containing vial to return the release medium vial volume to 1.5 mL. The microgel vials were then placed back inside the warming oven and rotated until the next sample time point.

Quantification of GED release – Released GED was quantified using high performance liquid chromatography (HPLC) techniques by Mr. Yuqun Hong in the Department of Surgery at Stony Brook University Hospital (column: Superco 5μ C18 RP, 250 x 4.6 mm; mobile phase: 40 mM KH_2PO_4, 3% acetonitrile, pH=3; flow rate: 1 mL/min; temperature: 25° C; UV-Vis detector: Agilent HP G1314A; detection wavelength: 245 nm). Release samples were first filtered to eliminate any microgel or microgel degradation products that could damage the HPLC column during measurement. The amount of GED released from the microgels was expressed as fraction of GED released compared to the total amount of GED loaded:

$$F = \frac{M_{\mathrm{Released}}}{M_{Loaded}} \qquad (2)$$

where $M_{Released}$ is the cumulative measured GED released (μg GED/mg microgel) and M_{Loaded} (μg GED/mg microgel) is the theoretical loading of GED per microgel sample. $M_{Released}$ is calculated by multiplying the measured concentration of GED from the HPLC measurement (μg GED/mL PBS) by total volume of supernatant (1.5 mL) and dividing the amount of GED released by the total weight of the microgel sample. M_{Loaded} is calculated by dividing the total amount of GED loaded in one microgel batch (either 1 or 10 mg) by the total polymer weight (160 mg). The cumulative amounts were plotted versus time in hours.

Quantification of Toluidine Blue O release – Toluidine Blue O release was quantified using a visible light spectrophotometer (Infinite M200, Tecan, Mannedorf, Switzerland) and a detection wavelength of 691 nm. A standard curve of Toluidine Blue O in PBS was performed and the resulting equation from the curve was used to calculate the amount of dye released at each time point. Dye release over time was calculated using F, similar to the GED release calculations described previously (Equation 2).

Toluidine Blue O total loading – To measure total Toluidine Blue O loading in the microgels, the amount of Toluidine Blue O lost during the recovery period was measured using visible light spectrophotometry. The mixture of mineral oil, residual water, and isopropanol in the recovery solutions creates an absorption spectrum different from pure water and it was necessary to produce similar diluents for a calibration curve. Mixtures of 4 mL of light mineral oil/SPAN 80 (oil:span, 80:1), 1 mL aqueous Toluidine Blue O (0 - 0.08 mg/mL), and 5 mL of pure isopropanol were produced. The resulting standard solutions had dye concentrations ranging from 0 to 0.014 mg/mL after accounting for dilution by mineral oil/SPAN 80 and isopropanol. Approximately 0.1 mL samples of the primary wash solutions from microgel batches (1 or 10 mg dye initially loaded) were placed in a 96-well plate and an equal amount of pure isopropanol was added to dilute each sample. Total amount of dye was calculated from the standard curve equation and correcting for total volume of wash solution.

5.3.4 Macrophage Cell Culture

Macrophage cells, RAW 264.7, were purchased from American type cell culture (TIB-71, ATCC, Manassas, VA). Cells were cultured in Dulbecco's modified essential media (DMEM) (Invitrogen, Camarillo, CA) supplemented with 10% heat inactivated fetal bovine serum (Atlantic Biosciences, Atlanta, GA) and 1% penicillin/streptomycin (Gibco, Invitrogen, Camarillo, CA). The media was changed every 2 days. Cells that were destined for experiments were not given fresh media 24 hours before re-plating.

5.3.5 Biocompatibility and Inflammation Potential of Release Samples from Microgels

The microgel release samples were obtained from either microgels that were initially loaded with a high dose of GED (63 µg GED/mg microgel) or no GED. The goal of this experiment was to determine whether the released GED or any degraded by-products of the Odex/CEC microgels may induce any cytotoxicity or inflammatory reaction in macrophage cell culture. The release samples were prepared and collected using a similar method as described in Section 3.2.7, except that the release media used in this study was cell culture media (DMEM without fetal bovine serum) instead of PBS. Prior to adding the release media to the microgel samples (n=3, each formulation), the microgels were first disinfected by soaking in 100% isopropanol for 1 hour. The microgels were then centrifuged at 2000 rpm to pellet and the isopropanol was aspirated out of each sample under sterile conditions. Any residual isopropanol remaining in the microgel pellets was extracted under vacuum. The average sample weight for GED loaded microgels and no GED loaded microgels was 19.2 mg and 18.5

mg, respectively. The release time points used in this experiment were 1, 2, 4, 8 h first, then 1, 3, 5, 7, 10, and 12 days thereafter. Release samples were placed in sterile sample tubes and stored at -20°C until use.

RAW 264.7 cells were plated in 96-well plates at a density of 9.5 x 10^4 cells per well in DMEM supplemented with 10% FBS and 1% penicillin/streptomycin. The plated cells were allowed to acclimate to the new plates overnight at 37°C with 5% CO_2 before any microgel releasate samples were added. The next day, the macrophage cells were treated with release samples from high dose GED and no GED microgels. The media from each well was aspirated out, approximately 0.1 mL of release samples were added to each well (n=3 for each release sample), and the cell plates were placed back inside the cell culture incubator. The cells were exposed to the release samples for 24 hours before performing the

5.3.6 Biocompatibility of Whole Microgel Particles With and Without GED Loaded

RAW 264.7 cells were plated in 48 well plates at a density of 2.5 x 10^4 cells per well in DMEM supplemented with 10% FBS and 1% penicillin/streptomycin. For ROS measurements, macrophage cells were cultured in phenol-red free DMEM (Gibco, Invitrogen, Camarillo, CA) and supplemented with similar concentrations of heat inactivated serum and antibiotics. The cells were allowed to acclimate to the multi-well plates for 24 hours at 37°C with 5% CO_2 before adding any microgels to the cultures.

After the plating procedure, microgels destined for cell culture were first weighed (9.8 mg per microgel formulation or 75 µg microgel per well). The amount of microgels used per well was determined from literature investigating inflammation potential of

microparticles with RAW 264.7 macrophage cells. According to published studies, inflammation-causing particulates at concentrations 50 to 300 μg/mL produced robust levels of inflammatory cytokines (e.g. TNF-α, IL-6, IL-8) within 24 hours of exposure [189,214,215]. In this protocol, we decided to use a concentration of 300 μg/mL of microgels per well. The microgels were disinfected by soaking in 100% isopropanol for 1 hour. Afterwards, the isopropanol was aspirated out of each vial under a sterile hood and a piece of aluminum foil was placed over the vial opening. A small hole was punctured in the foil and the residual isopropanol was evaporated from microgels under vacuum. When the microgels were thoroughly dried (24 hours after disinfection), the vials were removed from the vacuum vessel and then sealed with the original vial lid under sterile conditions. Before the microgels were added to the cells, the cell culture media was removed from each well and replaced with 0.15 mL of fresh DMEM. The microgels were suspended in DMEM at a concentration of approximately 0.75 mg microgels/mL DMEM and 0.1 mL aliquots of the suspension were added to each well. Negative control cells received 0.1 mL of fresh DMEM in each well instead of microgel suspension. The cell plates were then placed back inside the cell culture incubator. Time points for measuring nitrite production, TNF-α production, metabolic activity, cell density, and ROS production occurred at baseline (Day 0) and at 1, 3, and 7 days after microgel treatment. Cells were fed with 0.25 mL of fresh DMEM on Day 3 and Day 5 (not a data collection time point).

5.3.7 Microgel Co-Incubation with Endotoxin Stimulation

Lipopolysaccharide (LPS) has been utilized as an inducer of inflammation in RAW 264.7 cells. The objective of this experiment was to measure inflammatory response of LPS-activated RAW 264.7 cells after they are treated with microgels containing GED (2 doses) or no GED. This experiment was performed in parallel with the protocol in Section 5.3.6, except that 1 μg of LPS (E.coli B5:55, Sigma Aldrich, St. Louis, MO) was added to each well containing either no microgels or microgels with 0, 6.3, or 63 μg GED/mg microgel. Microgels used in this experiment set were the same microgels that were used in the previous protocol. Time points for measuring nitrite production, TNF-α, metabolic activity, iNOS detection, adhered cell density, and ROS production occurred at baseline (Day 0) and at 1, 3, and 7 days after microgel and LPS treatment. Cells were fed with 0.25 mL fresh DMEM with LPS on Day 3 and 5 (not a measurement time point).

5.3.8 Adhered Cell Density.

Following treatment of macrophage cells to microgel release samples or whole microgels, the adhered cell density was measured by staining methanol-fixed macrophage cells with a 0.5% crystal violet solution and then measuring the amount of dye contained inside the fixed cells after the stain is extracted using detergents [185,188,216,217]. The measured optical density of each treatment sample was compared with the measurements obtained from the negative control cells. Briefly, the media from each well was removed completely and stored in sample tubes for nitrite determination. The cells were rinsed twice with cold PBS, fixed with a 70% aqueous

methanol solution (ice-cold), and the plates were placed on ice for 20 minutes. After the fixation process, the methanol solution was aspirated from each well and replaced with 100 µL of 0.5% crystal violet solution for 10 minutes at room temperature. When the staining process was completed, the dye solution was removed and the wells were rinsed with tap water until all unbound dye was washed away. The crystal violet was then extracted from the stained cells using a 1% solution of sodium dodecyl sulfate (SDS) in distilled water. To increase the dye extraction rate, the plate was placed on an orbital shaker at room temperature for 1.5 hours. After the dye was completely extracted from the adhered cells, 0.1 mL aliquots of each extraction supernatant were loaded into a 96 well plate. The optical density of each solution was measured using a visible light plate spectrophotometer set at 570 nm. The optical density readings from each microgel release sample treatment were compared to the readings obtained from the negative control cells.

5.3.9 Nitrite Measurement

Nitrite concentration was determined by Greiss reaction (Molecular Probes, Eugene, OR). Sulfanilic acid (Reagent A) is quantitatively converted to a diazonium salt by reaction with nitrite in acid solution. This salt is then coupled to N-(1-naphthyl)ethylenediamine (Reagent B), forming an azo dye that can be quantified with a spectrophotometer based on its optical density at 548 nm. Media from each cell culture well (baseline and 24 hours) were collected before determining adhered cell density and stored in sample tubes (-20°C). At the time of analysis, the samples were defrosted at room temperature and 0.15 mL of each sample was combined with 0.02 mL of Greiss

reagent (50:50, Reagent A:Reagent B) and 0.130 mL of distilled water was added to each sample in a 96-well plate. The assay was incubated at room temperature in the dark for 30 minutes. The optical density of each sample was measured using a visible light spectrophotometer set at 548 nm. A calibration curve of nitrite (0 – 200 mM) was also produced in parallel to the unknown samples using DMEM as a dilution agent.

5.3.10 TNF-α ELISA

Cell culture supernatant from each well was collected and frozen at -20°C before the ELISA assay protocol (TNF-α Mouse ELISA Kit, Invitrogen, Camarillo, CA). At the time of this assay, the supernatants were defrosted on ice and then briefly vortexed. Approximately 0.05 mL of each sample (n=3 for each treatment per time point) was added to the wells of the assay plate along with 0.05 mL of the supplied diluents solution from the kit. The samples were prepared and treated with the supplied antibodies and wash solutions per the manufacturer's instructions. The optical density readings were measured using a visible light spectrophotometer (EL 800, BioTek, Winoosk, VT) using a 405 nm wavelength. The optical densities of the microgel treated samples were normalized to cell density and averaged for each treatment group.

5.3.11 Metabolic Activity in Macrophage Cells

The MTS assay (CellTiter 96 Aqueous One Solution Cell Proliferation Assay, Promega, Madison, WI) measures mitochondrial activity (i.e. oxidative metabolism) of cells in culture by measuring the reduction of a tetrazolium salt to formazan producing a color change in the cell culture supernatant. The depth of this color change is indicative

of the amount of reduction reaction: the greater the oxidative metabolic activity in cells, the darker the solution becomes. Macrophage cells that are activated by inflammation-inducing substances have an increased oxidative metabolism compared to inactive cells [218]. The goal of this protocol was to measure the metabolic activity of macrophage cells after co-incubation with whole microgels (with and without GED) as a measure of microgel inflammatory potential. To perform this assay, the cell media was removed and replaced with 0.25 mL of fresh media without additional microspheres. Approximately 0.0125 mL of MTS reagent was added to each well and the plates were incubated for 1 hour in the cell culture incubator at 37°C. At the end of one hour, 0.1 mL of each well supernatant was transferred to an empty 96-well plate and the optical density of each sample was read at 490 nm using a spectrophotometer (Tecan M200, Tecan Mannedorf, Switzerland).

5.3.12 Reactive Oxygen Species (ROS) Determination

This assay measures levels of ROS in the form of hydrogen peroxide that is produced by macrophages inside the cytoplasm when the cells are challenged with bacterial endotoxins or a foreign body. The production of ROS is detected by the oxidation of 2',7'-dichlorofluorescin diacetate (DCFH-DA) to dichlorofluorescein (DCF) and the oxidized molecule is detected by fluorescence spectrophotometry [219]. Cells in this portion of the study were cultured in phenol-red free DMEM with 10% heat inactivated fetal bovine serum. At the start of the assay, the media was removed from all the wells and replaced with fresh phenol-red free DMEM containing 15 mM DCFH-DA (Sigma Aldrich, St. Louis, MO) and the cells were returned to the cell culture

incubator for 15 minutes. After 15 minutes, the DCFH-DA solution was removed and the wells were rinsed with PBS to remove any un-reacted DCFH-DA. An aliquot of 0.2 mL of 0.1% Triton-X100 (in PBS) was added to each well and the cells were incubated at room temperature for 7 minutes. The Triton-X100 is added in order to lyse the macrophage cells and release the DCF into solution. Approximately 0.1 mL of each well's content was added into an empty 96 well plate. The fluorescence of each sample was read at ex 504/em 530 nm (gain=50) by a fluorescent plate reader (Infinite M200,Tecan, Mannedorf, Switzerland). The results were averaged for each treatment group (n=3) and reported as percent of control readings.

5.3.13 Subdermal Implantation of Microgel Particles Containing GED and Measure of Inflammatory Reaction and Fibrotic Encapsulation

Animal Care and Welfare - Mice used in this protocol were wild-type, CD-1 males (weight: 20 - 30 grams) that were 6-7 weeks of age at the time of the procedure. The animal experiments were carried out in accordance with a protocol approved by the Institutional Animal Care and Use Committee (Protocol number: 2007-1722). Housing and care for the animals was in accordance with the National Research Council guidelines (National Research Council. Guide for the Care and Use of Laboratory Animals. National Academy Press. Washington. DC. 1996).

Sterilization of microgels – Approximately 10 mg of each microgel formulation (0, 6.3, and 63 µg GED/mg microgel) and 10 mg of poly(lactic-co-glycolic acid) (PLGA 50:50) were measured into sample vials and disinfected by soaking in 1 mL of pure isopropanol for 1 hour. After 1 hour, the vials were centrifuged at 2500 rpm for 10

minutes to pellet the microgels and PLGA microspheres and the supernatant was aspirated under a sterile hood. Any residual isopropanol was removed by placing the samples under vacuum overnight. The dry microgels and PLGA microspheres were then stored at room temperature until the implantation time. The zeta potential and effective diameter values of each microparticle treatment (from Section 5.3.2) are found in Table 5.1.

Subdermal implantation – Mice were first anesthetized with inhaled isoflurane (5% for induction and 2.5% for maintenance). The fur and skin between the shoulder blades was cleaned thoroughly with 70% isopropanol. Each Odex/CEC microgel sample (n=3, each GED loading) was re-constituted with 0.2 mL of saline prior to implantation. The microgel suspension was loaded into 1 mL syringes with 25 gauge needles and placed vertically with the shielded needle pointing down. The microgels were injected under the dorsal skin between the shoulders of the animal. PLGA microsphere samples (n=3) were prepared in the same manner as the microgels. Control animals (n=3) received 0.2 mL of saline only. Odex/CEC microgels and PLGA microspheres that remained in the syringes after implantation were flushed out with isopropanol, dried, and weighed (Table 5.2). The residual microgel/microsphere weights were subtracted from the starting sample weight to determine the approximate amount of particles implanted. The implant area was marked on the animal's fur using permanent ink markers and the animal was then returned to its cage. The implants remained for 3, 7, or 29 days after placement. Saline control animals were only sacrificed at Day 29. For animals in the Day 29 implant group, the site of implantation was re-colored every 7 days with permanent ink until the sacrifice time point.

5.3.14 Subdermal Implant Collection

Tissue sample collection – At 3, 7, or 29 days after implantation, the mice were sacrificed by inhaled carbon dioxide. The time points for sacrifice and tissue evaluation were chosen based on an evaluation of the literature available for wound healing studies and subdermal implantation for biocompatibility testing. Day 3 represents an early time point following implantation where the process of inflammation has reached its peak of activity [220]. At this time point, the predominant cell type in the implant area would be polymorphonuclear leukocytes (PMN) cells, such as neutrophils and macrophages. Measuring the density of PMN cells in the implant site would yield information about the tolerability of the microgels in the subdermal space and whether released GED has an effect on these cell populations. Day 7 represents the later portion of the normal inflammatory reaction. In the late inflammatory period, the cell population inside a wound shifts from predominantly neutrophils to mostly macrophages. The later time point at Day 29 represents the remodeling phase of wound repair in which collagens are re-arranged into thick, fibrils and scar tissue begins to form. In terms of subdermally implanted biomaterials, the re-arrangement of collagen fibrils occurs in the form of a fibrous capsule that segregates the material from the body's immune system. The thickness of the collagen capsule surrounding the implanted material is largely dependant on the severity and length of the inflammatory period caused by the foreign body reaction [203].

At each sacrifice time point, the site of implant was determined by the permanent ink markings on the animals' fur. The tissue was excised under the pen markings (skin and dorsal muscle), rinsed briefly in distilled water, and placed in 10% buffered formalin

to fix. Within 24 hours, the saline and microgel implant samples were embedded in paraffin (embedding and sectioning performed by McClain Laboratories, Smithtown, NY). Microspheres made from PLGA could not be processed for paraffin embedding because this polymer is readily soluble in xylene (a required solvent for paraffin processing). Instead, PLGA microsphere samples were embedded in optimal cutting temperature (OCT) compound for cryosectioning (OCT embedding and sectioning was also performed by McClain Laboratories).

5.3.15 Histological Evaluation of Inflammation and Microgel Localization Inside the Tissue

Inflammatory cell infiltration (macrophages and neutrophils) was determined using a semi-quantitative grading system described previously by De Jong et al. [221]:

1 = Minimal inflammatory response with 1 or more small conglomerates of macrophage or neutrophil cells present or a few single cells present;

2 = Moderate inflammatory response, several small conglomerates or single macrophage or neutrophil cells are regularly present;

3 = Marked inflammatory response, several large conglomerates of macrophage or neutrophil cells present;

4 = Severe inflammatory response, large confluent areas of macrophages or neutrophils present.

H&E staining for the inflammatory cell infiltration study was performed by McClain Laboratories as part of their standard embedding and sectioning service. All H&E stained sections were examined with 10x magnification and a minimum of 5 images were captured throughout each section. The inflammation scores were collected for Day 3, 7, and 29. The resulting scores were reported as median values.

Microgel localization inside and surrounding the microgel implant area was determined using a standard Masson's Trichrome Staining protocol (see Appendix B for complete details). Tissue sections of 5 μm thickness were stained using this method and images were captured using a 20x objective.

5.3.16 Picrosirius Staining to Evaluate Capsule Fibrosis

Although Masson's Trichrome staining can identify collagens in tissue, it does not differentiate between types of collagen or whether the collagens present are in the cytoplasm of fibroblasts or assembled into mature fibrils. The picrosirius red staining protocol utilizes a birefringent stain that allows the identification of Collagen type I and III fibrils under polarizing light microscopy. The staining method used in this study was modified from a previously published protocol [222] and performed by the author (see Appendix B for full details). After re-hydrating, the sections were placed in a solution of 0.1% Sirius red (Direct Red 80, Sigma Aldrich, St. Louis, MO) dissolved in an aqueous 0.1% saturated picric acid.

Polarizing microscopy was performed by the author using a Nikon inverted light microscope. Images were captured using the attached camera system (Retiga EXi Fast 1394, Quantitative Imaging Corp., Surrey, British Columbia) and image capture software

(Qcapture v.2.71.0.0, Quantitative Imaging Corp., Surrey, British Columbia). Collagen type I fiber content was measured in the cyst capsule directly surrounding each implant by digitally capturing 1 image at 2x magnification and measuring the intensity of the coloring using ImageJ (ver. 1.43o, National Institutes of Health, http://rsbweb.nih.gov/ij/). Collagen type I was quantified by first splitting the color image of the birefringence into separate RGB channels. The green channel was utilized to measure intensity of the red/yellow fibers that indicate the presence of Collagen type I. The implant area was traced using the polygon select tool to denote the area over which the collagen measurements will take place. The threshold was then adjusted to mask off the grey-to-white collagen fibers displayed in the image. Output readings were adjusted to display both area fraction (Collagen type I vs. total implant area) and area in pixels squared. The resulting normalized measurements were averaged for each animal and then averaged with other animals within each treatment group.

5.3.17 Data Analysis and Statistics

Particle diameter, zeta potential, and GED/Toluidine Blue O release kinetics results were expressed as mean ± standard deviation. Statistical analysis was performed for all tests using the One-Way ANOVA (power = 0.800, $p<0.05$ for significance) with Tukey HSD post-hoc test using a statistical program package (SPSS v. 14.0.0, LEAD Technologies Inc., Charlotte, NC).

Results of *in vitro* tests including cell density, metabolic activity, nitrite production, ROS, and TNF-α production were calculated as mean ± standard deviation. The averaged results within each test group were statistically compared using the One-Way

ANOVA (power = 0.800, $p<0.05$ for significance) with Tukey HSD post-hoc tests also using SPSS software.

Where a graded scale was used, the Kruskal-Wallis One-Way Analysis of Variance on Ranks was performed ($p<0.05$) followed by a Dunn's post-hoc test. A Mann-Whitney Rank Sum test was used to evaluate graded scale scores when only 2 treatment groups are compared ($p<0.05$). Student's t-test was utilized to compare the amount of Collagen I in 29 day implant tissue sections ($p<0.05$).

5.4 Results

5.4.1 In vitro characterization of Odex/CEC microgels

Microgels from all GED loadings demonstrated a smooth, spherical topology (Figure 5.1). The range of diameters microgels in the SEM images appears to fall between 3600 and 260 nm. There also appear to be some much smaller particles (>130 nm) that were compressed against the surface of some of the larger microgel particles; otherwise, these particles appear only sporadically in the image. Dynamic light scattering analysis showed the mean effective diameters for microgels loaded with 0 μg GED/mg microgel (no GED microgels), 6.3 μg GED/mg microgel (low dose GED microgels), and 63 μg GED/mg microgel (high dose GED microgels) were 1954.1 ± 150.8, 2080.0 ± 373.4, and 1988.8 ± 370.1 nm, respectively (Figure 5.2). No significant difference was detected in average, effective diameters between GED loadings in microgel particles ($p=0.888$).

The zeta potential measurements for each GED loading are located in Table 5.3. There were no significant differences ($p=0.748$) in zeta potential measurements

between drug loadings in the microgels: -22.2 ± 0.4, -21.3 ± 2.3, and -20.9 ± 2.7 mV for no GED, low dose GED, and high dose GED microgels, respectively. However, some significant differences in zeta potential measurements were detected between batches of GED-loaded microgels (Table 5.4). Both microgels containing low dose and high dose GED loaded initially showed some significant differences between lots ($p<0.001$, both drug loadings). There was no significant difference detected between no GED microgel batches ($p=0.331$).

5.4.2 GED Release Kinetics

The high dose GED microgels demonstrated a burst release of 12.5±0.48% at the 1 hour time point (Figure 5.3). At 24 hours after the study began, approximately 32.1 ± 1.3% total of the GED was released from the high dose GED microgels. GED continued to release, but at lower levels than the 24 hour time point, until the 9 day time point, which showed a cumulative release of 36.9 ± 1.4% of loaded GED. After this point, the amount of GED released plateaus and does not release significant amounts of drug. The release of GED from the low dose GED (6.3 μg GED/mg microgel) particles could not be measured by HPLC because the amount of GED was below the detection threshold of 1 μg/mL.

5.4.3 Toluidine Blue O release kinetics and total dye loading

The release of Toluidine Blue O from microgels demonstrated modest burst releases (1 hour after experiment start) of 10.5 ± 0.24% and 5.2 ± 0.78% for microgels loaded with high dose Toluidine Blue O (63 μg dye/mg microgel) and low dose Toluidine

Blue O (6.3 μg dye/mg microgel), respectively (Figure 5.4). After 24 hours, the total accumulated release of dye was 30.6 ± 0.68% and 9.0 ± 0.76% for microgels loaded with high dose and low dose Toluidine Blue O, respectively. At 9 days, the cumulative fraction of dye released from high dose microgels was up to 55%, which was significantly higher than the cumulative release of GED with similar loading. Microgels loaded with the high dose of Toluidine Blue O initially demonstrated dye release past the 24 hour time point and eventually reached a slower rate of release after 15 days in release buffer. There was a significant difference between the accumulated amounts of dye at Day 63 versus Day 15 in the high dose Toluidine Blue O microgel samples ($p < 0.05$). Samples with a low dose of Toluidine Blue O did not show any significant increases in dye release after Day 5 ($p > 0.9$). Both microgel formulations showed some blue dye was retained inside the polymer matrix after 15 days. Microgels with the highest concentration of Toluidine Blue O appeared to be darker blue in color than microgels with the lowest concentration at this later time point. The release kinetics experiment was allowed to be continued past the reported 15 days with total release media changes every 2 days.

Wash solutions from microgels loaded with Toluidine Blue O were light blue in color, signifying loss of the dye into the isopropanol/light mineral oil mixture during the first wash. The loss of the dye into the first wash solution is not unexpected, as Toluidine Blue O is soluble in many types of alcohols, including isopropanol. Toluidine Blue O containing microspheres were found to have an 88.9% loading rate for microgels loaded with 10 mg dye and 83.2% for microgels loaded with low dose of dye.

5.4.4 Microgel Release Samples Co-Incubated with Macrophage Cells

Overall cell density – As demonstrated in Section 5.4.2, microgels loaded with GED exhibit burst release in the first time point (1 hr) followed by a more modest release of GED after 24 hours. A dose response could be observed with cells that were exposed to GED released from microgels. Macrophage cells treated with the earliest time samples (1, 4, and 8 hr) showed a significant decrease in overall cell density (54% of negative control cell readings) (Figure 5.5B). Cells that were treated with releasate samples from microgels without GED did not show any significant differences in relative cell density after exposure to any of the samples (Figure 5.5A). However, the cell density of treated macrophage cells was nonetheless increased over the negative control cells at the same time point. Unfortunately, a few groups had to be excluded from the statistical analysis because the sample sizes were too small (n=2), including 8 hour and 3, 5, and 7 days. These samples had optical densities that were in excess of the measurement limits of the spectrophotometer.

Nitrite Production – Cells that received release samples from no GED microgels did not show any difference in nitrite production ($0.8 < p < 1.0$) between any of the release sample time points (Figure 5.6A). Cells exposed to early time point GED release samples (1 and 2 hrs) produced significantly higher ($p<0.01$) amounts of nitrites compared to later time point (8 hrs and later) (Figure 5.6B). After the 8 hour release sample, there were no significant differences in nitrites produced in macrophage cells exposed to release samples from the 24 hour collection time point to the 12 day GED release sample. Normalized levels of nitrites produced from exposure to later GED

release samples showed magnitudes similar to nitrite levels from release samples of microgels without GED.

5.4.5 Whole microgels co-cultured with macrophage cells

Overall cell density – The complete summary of relative cell density of microgel treated cells (both with LPS and without LPS activation) is found in Figure 5.7. Microgel treated cells displayed a decrease in cell density at Day 1 for all GED doses. Macrophages treated with high-dose GED microgels (63 μg GED/mg microgel) at this same time point demonstrated significantly higher cell density than macrophages treated with microgels with no GED loaded ($p=0.002$). Microgels without GED loaded had the lowest cell density compared with low or high dose GED microgels and the negative control cells. At Day 3, low dose and high dose GED microgel treated cells had significantly lower cell density than the negative control cells or the microgels without GED loaded. However, at Day 7, all microgel treated cells showed significantly higher cell density than the negative control cells.

At Day 1, cells treated with only LPS showed significantly higher cell density than all other treatment groups ($p<0.001$). Visual inspection of LPS-only treated cells before stain extraction showed an increase in cell density. Similarly, macrophages treated with high-dose GED microgels plus LPS showed significantly increased cell density compared with cells receiving only microgels without GED loading ($p = 0.002$). However, there was no statistical difference between cells exposed to low dose GED microgels and the no GED microgels with LPS stimulation. At Day 3, all LPS treated cells (with and without microgels) showed significantly decreased cell density compared

with the Day 1 results. The morphology of these cells showed increased cell spreading and surface area compared with their non-LPS treated cell counterparts. Cells that were not exposed to LPS with or without microgels did not demonstrate extensive cell spreading and these cells remained small and rounded with occasional elongation. At Day 7, LPS treated cells maintained a spread morphology. Overall, at this time point, the relative cell density of all LPS treated cells had fewer attached cells than their non-LPS treated counterparts. However, the cell density for the LPS treated cells across all microgel treatments was still slightly higher than the results measured at Day 3.

Nitrite production – Macrophage cells exposed to only microgels showed very low levels of nitrite production Day 3 and Day 7 that were similar in magnitude to negative control cells (Figure 5.8A). There was an increase of nitrite detected in high dose GED microgels at the Day 3 time point compared with the other microgel treatments and negative control cells, but no statistical significance was determined. However, at Day 7, there were no significant differences between any treatment group and the measured levels were similar in magnitude to the Day 1 nitrite levels. There were significant decreases between the negative control cells and cells treated with no GED or low dose GED microgels.

Cells treated with both microgels and LPS showed significantly higher nitrite production levels at Day 3 and Day 7 time points than cells treated with microgels alone (Figure 5.8B). However, LPS treated control cells and all microgel treatments with LPS produced similar nitrite levels as the non-LPS treated cells at Day 1. At Day 3, cells treated with high dose GED microgels plus LPS showed significantly lower nitrite production than cells treated with LPS and microgels containing no GED and a low dose

GED. The nitrite levels in cells treated with no GED and low dose GED microgels in the presence of LPS were also significantly lower than in cells treated with LPS alone. At Day 7, nitrite levels were decreased in LPS treated control cells and cells receiving no GED microgels and low dose GED microgels plus LPS compared with Day 3 results. However, at Day 7, cells treated with LPS plus high dose GED microgels showed a significant increase in nitrite production from Day 3. The high dose GED microgels also had significantly higher nitrite levels than the other LPS-treated cells with either low dose GED or no GED microgels co-incubated for 7 days.

TNF-α production – Macrophages exposed to all microgels treatments produced significantly higher levels of TNF-α compared to negative control macrophages at Days 1 and 3 (Figure 5.9A). At Day 3, there is there is significantly higher TNF-α production in macrophages exposed to high dose GED microgels compared with the other microgel treatments. However, at Day 7, the levels of TNF-α in these cells is significantly decreased compared with earlier time points. Within the Day 7 time point, the no GED microgel and high dose GED microgel treatments showed significantly increased levels of TNF-α production compared with the control cells.

When the cells were exposed to LPS stimulation and microgels, the levels of TNF-α were increased across all treatment groups (including LPS-treated control) from Day 1 to Day 3 (Figure 5.9B). The levels of TNF-α remained elevated at Day 7, but slightly decreased in magnitude compared with Day 3 measurements. At Day 1, all microgel treatment groups, except for high dose GED microgels, had significantly higher levels of TNF-α in their cell culture media compared with the LPS treated control cells ($p < 0.01$). At Day 3, the no GED microgel and low dose GED microgel groups could not

be incorporated into the statistical analysis because the sample size was too low (n=2 instead of 3). LPS controls at Day 3 had significantly increased TNF-α production compared to the high dose GED microgels ($p = 0.01$). The no GED microgels and low dose GED microgels which also had a similar trend of increased TNF-α production levels as the LPS treated control cells. By Day 7, the levels of TNF-α production are slightly decreased across the control and microgel treatment groups. Also, the LPS treated control cells produced less TNF-α than all the microgel treatment groups. The microgels without GED produced the highest level of TNF-α compared with the other treatment groups ($p < 0.01$) at Day 7.

Metabolic Activity Assay - In general, cells treated with microgels alone, the MTS assay showed some changes in metabolic activity over 7 days (Figure 5.10A). A significant increase in metabolic activity was seen in high dose GED microgels on Day 3 compared with the negative control cells and the other microgel treatments. At the same time point, there were no significant differences seen between the negative control cells, no GED microgels, and low dose GED microgel treatments. Day 7 results showed a significant decrease in metabolic activity in microgel treated cells compared to the negative control cells. At Day 7, all microgel treatment groups showed decreased levels compared with Day 1, but the control cells had a significantly elevated level of metabolic activity compared with the Day 1 time point and Day 7 microgel treatments.

Macrophage cells that were treated with LPS showed a significant increase in metabolic activity from Day 1 to Day 3 (Figure 5.10B). At Day 3, macrophages treated with low dose GED microgels showed a trend of a slight increase in metabolic activity compared with other treatment groups and LPS treated control cells. At Day 7, all

treatment groups showed a trend of decreasing metabolic activity compared with Day 3; however, the levels remained higher than Day 1 measurements. There were no significant differences between microgel treatment groups at any of the time points.

Reactive Oxygen Species - The data from this experiment followed similar trends seen in the metabolic activity assay. There were some more significant differences between negative control and microgel treated cells at some of the time points in the ROS data (Figure 5.11A). At Day 1, the microgels without GED showed a significant increase compared with the negative control cells, but there was no significant increase above both of the GED loaded microgel treatments. Day 3 showed a significant increase in ROS produced in high dose GED microgels. At the same time point, both the no GED microgels and low dose GED microgels also had ROS levels that were only slightly increased over the control cells. On Day 7, the ROS levels of all microgel treated cells were significantly lower than the control cells. Among the microgel treatment groups, high dose GED microgels had significantly higher ROS production than the other two microgel treatments (low dose GED and no GED).

LPS treated cells (with and without microgels) showed progressively higher levels of ROS from Day 1 to Day 7 (Figure 5.11B). The high dose GED microgels showed similar ROS levels as the control cells at all time points. In fact, there was no statistical significance between the high dose GED microgels and the LPS-treated controls. At all time points, low dose GED microgels produced significantly more ROS than the LPS-treated controls.

5.4.6 Subdermal implant of microgels containing GED

Overall observations - Microgels stained bright red with the Masson's protocol and greatly aided in pinpointing the location of both microgels and macrophages containing microgels within the cyst capsule at all time points (Figure 5.12). However, some bright blue particles/spheres could also be seen inside the cyst capsule and surrounded by leukocytes (Figure 5.12C). One hypothesis as to the origin of these blue particles was that they were impurities from the raw dextran material before oxidation or un-crosslinked Odex aggregates. To test this hypothesis, separate slides of dried Odex, CEC, and crosslinked Odex/CEC solutions were stained using Masson's method. Crosslinked Odex and CEC at a 0.8% concentration stained bright red (data not shown) from the Biebrich scarlet fuchsin step. The dried Odex stained bright blue (data not shown), similar to the color shown in the blue particles in the tissue sections. Dried CEC did not show any staining from the Masson's method.

Animals at all time points and with all treatments did not experience pili muscle (in epidermal layer)/dorsal muscle layer degradation or hair loss at the site of implantation. Also, Masson's trichrome staining did not reveal any blood vessel formation inside the implant area at any time point. Some blood vessel formation outside the cyst capsule was noted on Day 29 samples.

Day 3: All animals treated with Odex/CEC microgels showed a raised subdermal lump at time of sacrifice. The median inflammatory cell scores for the microgel implants were 4, 3, and 3 for no GED, low dose, and high dose GED microgels, respectively (Table 5.5, reported scores for all time points). H&E staining also revealed areas of dark, blue/black stain accumulation usually found inside the cyst lumen, not the cyst

capsule wall. Specifically, these accumulations of dye were usually observed in areas directly adjacent to microgel aggregates or in ribbon-like formations traversing areas of microgel aggregates. Further treatment of the sections with DAPI stain showed strong binding of the fluorescent dye to similar areas, suggesting these areas are accumulations of nucleic acids from groups of cells that ruptured during the initial inflammatory period.

Animals treated with PLGA microspheres did not show any palpable lump at the site of implantation. During examination of H&E stained PLGA implant samples, only 1 of 2 animals had microspheres present in the cyst wall and lumen. At this time point, the median inflammatory score was 3. This score could not be calculated into the statistical comparison with the microgel treatment inflammatory cell scores because the N for this group was too low.

Day 7: Animals that received Odex/CEC microgels (with no GED, low dose GED, and high dose GED) had palpable lumps under their skin in the area of implantation. Masson's trichrome staining highlighted the cytoplasm of the fibroblasts in light blue, indicating the presence of soluble collagen pre-cursors; however, this staining method is not sensitive enough to discern between smaller, soluble collagens and thicker, fibrillar collagens that are seen in fibrous capsules in a foreign body reaction that can occur weeks after implantation of a biomaterial. At 7 days, there was an absence of organized collagen in the cyst capsule surrounding any of the implants when the tissue sections were stained with picrosirius red and viewed with polarized light microscopy. Instead, the microsphere implants were surrounded by a macrophage-dense ring that sequestered the implant. Fibroblasts were also present in all cyst capsules and

dispersed between the microgel-swollen, macrophage cells. The macrophage cells within the cystic capsules also appear to have phagocytized many microgels (4+ per cell, on average) within a single cell body (Figure 5.13). The median inflammatory cell infiltration scores for No GED, low dose GED, and high dose GED microgels were 2, 4, and 4, respectively. The inflammatory cell infiltration scores from each treatment group indicated that there was a significantly higher infiltration in microgels that contain either low or high dose GED relative to the no GED microgel treatments. However, no significant difference in inflammatory cell infiltration was seen between the low and high dose GED microgels at this time point.

PLGA microsphere implanted mice did not have a discernable lump under their skin that would indicate the presence of those microspheres. PLGA microspheres were observed in all 3 treated animals at this time point. The microspheres were found in very thin, elongated collections (Figure 5.14). Additionally, the microspheres did not appear to be surrounded by a multiple layer of macrophages and fibroblast cells like the Odex/CEC microgel treated animals (Figure 5.12). The median inflammation score for the PLGA microsphere implanted animals was a 2. In statistical analysis, these microspheres had a significantly lower score than both low and high dose GED microgels ($p < 0.05$). No statistical differences were observed between PLGA microspheres and no GED microgel inflammation scores.

Day 29: Implanted animals at this time point showed different degrees of cellular infiltration and new tissue formation within the implant area of Odex/CEC microgel implanted animals. Animals that received either the microgel vehicle alone or high dose GED microgels showed palpable lumps under the skin. In animals treated with low

dose GED microgels, there was no palpable lump under the skin where the implant would have been located. In only two out of three mice, the implant appeared to be smaller in area with the low dose GED microgel treated animals compared with both the no GED and high dose GED microgel treated animals. In these cases, the tissue from the low dose treated animals was excised directly under the indelible pen-marked area on the animal's fur where there had been a lump in the previous weeks. The inflammatory cell infiltration scores for no GED, low dose GED, and high dose GED microgels were 2, 2, and 3, respectively. At the 7 Day time point, there appeared to be no difference in the median score of infiltrated inflammatory cells or fibroblast cells between the low and high dose GED microgels. Animals that received high dose GED microgels showed more inflammatory cells presence inside the capsule surrounding the implant compared with the no GED microgels ($p < 0.001$). Low dose GED microgel treated animal inflammatory cell scores could not be included in the statistical analysis because only 2 animals showed evidence of the implanted microgels after 29 days. Using polarized light microscopy and picrosirius red staining, animals that received high dose GED microgels had significantly lower amounts of Collagen Type I inside/surrounding implant area than animals receiving the microgel vehicle alone ($p = 0.026$) (Figure 5.15). The total area fraction of Collagen I was 11.62 ± 1.48% and 4.45 ± 2.47% for microgels without GED loaded and high dose GED microgels, respectively (Figure 5.16). The area fraction of Collagen I for low dose GED microgels could not be incorporated into the statistical analysis also because the sample size was too small (n=2). However, the total area fraction of Collagen I at the implant sites had an average of 17.61% area of fibrosis. This showed a trend of greater fibrosis in the implant site

and capsule compared with the high dose GED microgels and microgel vehicle without GED.

Similar to Day 7, PLGA microspheres were observed subcutaneously in 2 out of 3 animals for this later time point. The microspheres were collected in elongated capsules with some elongated, fibroblast-like cells located between groups of microspheres. In one of the treated animals, a single foreign body giant cell was observed (Figure 5.14B). The median inflammatory cell infiltration score was 2 for both animals.

5.5 Discussion

In the previous chapter, the efficacy of a self-crosslinking hydrogel composed of Odex and CEC was tested in a prophylactic treatment for post surgical adhesions in the abdominal area of rats. The hydrogel demonstrated significant reductions in adhesion severity and allowed the damaged bowel/abdominal wall surfaces to heal with minimal inflammatory reaction. In this present study, the synthesis of microgel particles composed of 0.8% Odex and 0.8% CEC was demonstrated using a water-in-oil emulsion method and the physical characteristics (i.e. morphology, mean particle diameter and zeta potential) of the microgels were measured. We also evaluated the inflammation and cytotoxic potential of microgels with or without GED, an iNOS inhibitor, encapsulated. To examine these two conditions, we measured levels of nitrites, TNF-α, and ROS produced by a macrophage cell line that were exposed to whole microspheres. These measured products have been previously utilized in similar

literature studying the inflammatory potentials of micro- and nano-particles using murine macrophage cell lines [188,197]. In the final phase of this study, we investigated the *in vivo* biocompatibility and inflammatory potential of microgels with GED and without GED in a murine subdermal model by evaluating the infiltration of inflammatory cells into and the formation of fibrotic tissue surrounding the implanted microgels.

The characterization of the Odex/CEC microgels as drug release vehicles was performed by measuring the *in vitro* release of GED in buffer at physiological temperature and pH 7.4. High dose GED microgels exhibited a moderate burst release of drug after 1 hour and nearly 1/3rd of the total payload after 24 hours. Significant release of GED continues after the first day, but after 9 days, the cumulative release reached a plateau during which very insignificant amounts of drug were released. A therapeutic application that would take advantage the moderate burst release characteristics of the microgels involved the early suppression of acute inflammation to reduce later scar tissue formation. In spinal cord injuries, the acute inflammation phase is most strong in the 3-12 hours following nerve tissue damage [181]. During this time, iNOS is up-regulated by tissue macrophages and peroxynitrites are formed in large quantities by the combination of NO and O_2^- in the vicinity of the damaged tissue. Early scavenging of peroxynitrites within the first 24 hours following injury was shown to reduce damage of existing nerve cells and increase the survival of neuronal stem cells also implanted at the site [88,177]. GED may further augment the preservation of both nerve cells and implanted therapeutic cells by reducing the amount of NO produced by iNOS, thereby reducing the formation of peroxynitrite. The reduction of peroxynitrite formation would also reduce the amount of scar tissue formation surrounding the

damaged spinal cord that follows the acute inflammatory phase [175]. Any scar tissue formation at the site of injury would reduce the ability of damaged nerve cells to regenerate and reduce the ability of any implanted stem cells from differentiating into competent nerve cells. The application of GED microgels would have to occur within the first 12 and 24 hours after injury to help reduce the damage caused by acute inflammation. At this point, few studies have examined the application of peroxynitrite scavengers and/or iNOS inhibitors applied at later time points (24 hours plus) after wounding.

Another portion of the physical characterization study of the microgels was designed to investigate the effect of GED incorporation on the zeta potential and particle diameter of the microgels. Macrophage cells have demonstrated sensitivity to different types of charged surfaces [223] and particle size/morphology [204,223,224], and these properties affect the cell's ability to attach to or internalize the materials. Zeta potential is not a direct measurement of the actual surface charge of the particles, but rather the measurement of the particle's surface interaction with the dispersion media and the propensity of the particles to aggregate in a physiological buffer solution [225]. In some published studies, the drug loading in polymer microspheres can cause differences in zeta potential by the presence of drug located on the surfaces when compared with just the vehicle [226,227]. Prior et al. observed a significant difference in zeta potential between PLGA 50:50 microspheres loaded with gentamicin sulfate (-86.2 mV) versus microspheres without the drug (-41.0 mV) [226]. While observing phagocytosis of microspheres by murine macrophages *in vitro*, the research group recorded a significant increase in macrophage-microsphere uptake with gentamicin sulfate-loaded

microspheres compared to the PLGA 50:50 vehicles by themselves [226]. They suggested that the difference in zeta potential was caused by the presence of the drug on the surface of the microspheres. All Odex/CEC microgel batches containing a low or a high dose GED showed no significant differences in measured zeta potential. This outcome suggested that that there was not an abundance of GED on the microgel surfaces that the GED is dispersed throughout the microgel bulk instead.

Particle size can also be influenced by drug loading and the interaction of the drug with the polymer structure [228]. Molecules of GED have a total of 4 amine groups on their terminal ends. The Odex and CEC monomers crosslink by forming Schiff-base linkages between the two molecules, which is caused by the amine side groups of the CEC interacting with the aldehyde residues on the Odex molecules [72,212]. Previously published research from our laboratory studied the effect of GED concentration on oxidized hyaluronan and gelatin microsphere diameters [212]. The crosslinking method of these two polymers was also believed to be the formation of Schiff-base-linkages. Their study found that as GED concentration increased in the polymer phase, the diameter of their microspheres decreased. The proposed mechanism for the diameter changes was a decrease in polymer phase viscosity due to GED interfering with the Schiff-base linkages between the two polymers. In this study, we also hypothesized that the CEC/Odex microgels would show similar differences in diameter based on GED loading. However, this material behavior was not measured in any of the microgel batches and this signified that the crosslinking was not affected by the inclusion of GED. The microgel diameters were instead influenced solely by the emulsion process.

Control of microgel diameters was dependent on a two key parameters in the formation of the suspension emulsion: polymer phase viscosity and continuous phase (oil/surfactant) temperature. In our microgel formulation, we utilized very dilute solutions of CEC and Odex (0.8%) which produced a final solution with low viscosity. The continuous phase both produced a shear force to break up the initial polymer solution into droplets and aided in preventing the polymer droplets from coalescing/aggregating [99]. The low viscosity allowed for the formation of smaller droplets by the continuous phase compared to a polymer solution with a higher viscosity (1-2% Odex/CEC). Another consequence of utilizing a low viscosity polymer phase was the increase in crosslinking time. Along with polymer phase viscosity, continuous phase temperature was also important in increasing the crosslinking time and maintaining the spherical shape of the microgels. Low temperature maintained in the first hour of processing helped to increase the crosslinking time and decrease the water loss from the polymer droplets. If the water was removed from the droplets too quickly at the beginning of the emulsion, the result would have been non-spherical and non-uniform microgels. The water was later removed by heating the emulsion one hour after the initial droplet formation and crosslinking occurred. Another result of water loss was the intensifying of crosslinking between the Odex and CEC in each microgel droplet. The end result of the synthesis is the production of micron-sized, hard microgels.

Although an Odex/CEC hydrogel was found to be biocompatible as a wound covering [75] and adhesion barrier [183], it was necessary to understand how compatible the same material would be in microgel form. Inflammatory response to an implanted material is caused by several factors including surface chemistry, water

content, and density of polymer strands. Foreign body reaction to a material can also be influenced by the size of the implant. Implanted biomaterials that exceed 20 μm in diameter cannot be phagocytized by macrophages or neutrophils [229]. To degrade these larger pieces of the material, macrophage and neutrophil cells will secrete lysosomic enzymes on the material surface in an attempt to create smaller fragments of material that would be more easily endocytosed [203,220]. When materials of a smaller size (<10 μm) are implanted, phagocytes are able to separate and engulf the particles more readily than the same cells attempting to break down the surface of a larger piece of the biomaterial [16]. In both cases, the macrophages secrete several cytokines and signaling molecules in reaction to the biomaterial that helps direct the inflammation response; however, the degree and length of the inflammatory reaction is dependent on the size of the implanted material [220]. Additionally, the incorporation of a drug into the microgels can also affect their inflammatory response compared to the microgel vehicle alone [230]. It was also necessary to measure the reaction of macrophage cells to released GED without exposure to microgel particles directly. Several studies have indicated that released drugs from microparticle systems can cause significant inflammation and cytotoxicity after implantation compared with unloaded microparticles [231-233]. In this chapter, we chose a macrophage cell line (RAW 264.7) to perform these two protocols since they are a type of phagocytic cell and they are widely utilized in particulate screening studies [185].

In the first test of *in vitro* biocompatibility, GED released from microgels containing a high dose (63 μg GED/mg microgel) appeared to produce elevated NO levels with release samples from the first few time points. Conversely, cells exposed to

release samples from microgels without GED showed levels of NO similar to the negative control cells. Chitosan-based materials and material extracts have been shown to decrease NO production in RAW 264.7 cells [234]. Additionally, cell density was decreased with the same early time point GED release samples. Although it is possible for some types of ultrafine particles (12-120 nm in diameter) to produce cell necrosis *in vitro* [235], macrophage cells exposed to release samples from non-GED loaded microgels did not show a decrease in attached cell density relative to the control. In fact, the density of cells treated with these samples showed increased density (up to 120% of control) with 24 hours of exposure. The decrease in cell density with GED release sample treated macrophage cells could be best explained by the "burst" release of a higher amount of GED from the microgels during the early release time points, which was measured in PBS in Section 5.3.3. GED is cytotoxic to cells at concentrations above 0.1 mg/mL (results not shown). Furthermore, it was also likely that the combination of fine, microgel degradation products and released GED could be augmenting a mild inflammatory reaction, observed as an increase in NO, in these macrophage cells. Even though the early time point release samples from GED microgels reduced cell viability and significantly increased NO levels, the later release sample time points had viability and NO levels close to the negative control cells. This effect was reported in a previously published study by Yamaguchi and Anderson where they observed localized inflammation occurred when they applied a PLGA microsphere vehicle loaded with naltrexone subcutaneously in rats [230]. The microsphere vehicle itself was found to be well tolerated in the subcutaneous space, but when the microsphere was loaded with drug, the combination produced a strong inflammatory

reaction far above what was seen with the vehicle alone. A similar effect was likely produced *in vitro* using release samples from GED loaded microgels versus release samples from non-GED loaded microgels.

When whole microgels were added to macrophage cell culture, interesting differences between nitrite and TNF-α production was observed. Across all microgel formulations, the levels of nitrites produced were similar to the negative control cells, and at least 1/10th of the nitrite levels produced by LPS treated cells. At the same time, TNF-α production levels at early time points were significantly increased relative to the negative control cells. At Day 7, TNF-α production decreased to levels comparative to the negative control cells. Early time point behavior indicated that the RAW 264.7 cells did not perceive any of the microgel treatments as invading pathogens, but rather recognized them as a foreign body and secreted TNF-α far above control cell levels. In visual observation, cells treated with the microgels did not show any spreading or elongation/branching that is typical of macrophage cells in an activated state [236,237]. Similar observations were recorded in previously published studies where RAW 264.7 cells were challenged with silica microparticles [187]. Cardona et al observed other biomaterials, such as polyurethane and Dacron, produce high levels of TNF-α in human macrophage cells when co-cultured [238]. The cells exposed to silica microparticles produced more than twice as much TNF-α as the negative control cells, but the NO levels of silica treated cells was exactly at the level of the negative control cells [187]. Another indicator of an activated, inflammatory macrophage cell is a marked increase in oxidative metabolism [218]. The metabolic activity of the microgel treated cells remained similar in magnitude to the negative control cells at each time point,

suggesting that the cells were not fully activated like their LPS-treated counterparts, but only slightly more activated with the microgel treatments [187,229]. Any activation of the cells above the negative controls between Day 1 and 3 time points could be attributed instead to the increase in metabolism the cells experience during phagocytosis of the particles.

Macrophage interaction with some materials, from bulk materials to particulate matter, can also elicit some elements of an inflammatory response in the absence of endotoxins or bacterial infection [239,240]. According to the literature, a macrophage cell can have multiple activation states and these different states have differences in cytokine production and gene expression. The two states of activation that will be discussed are classical and alternative. Classical activation is produced by exposing macrophages to bacterial or endotoxin challenge, such as LPS [241,242]. The signs of classical activation include a change in cell morphology (e.g. spreading and branching), increases in NO, TNF-α, IL-1, IL-6, and ROS production [241-243]. Classically activated macrophages also produce matrix metalloproteinases that help to disassemble damaged collagen fibers in the wound bed shortly after repair is initiated [244]. In a wound, classically activated macrophages are present early stages of inflammation during healing. Over time, these macrophages receive cytokine signals from fibroblast cells and even other macrophage cells to decrease their production of NO, TNF-α, IL-1, IL-6, and ROS [245]. The macrophage cells convert into an alternatively activated state and begin to produce new types of cytokines, including IL-10 and transforming growth factor beta-1 (TGF-β1) [246]. Also, collagen deposition, which occurs in late inflammation/early remodeling stage of healing [247], is controlled

by TGF-β1, which is secreted by alternatively activated macrophages. Changes between activation states have been noted in other biomaterial studies and have also been shown to occur within a similar time frame as this study [248]. In this project, macrophages treated with microgels likely changed their activation state from classically activated to an alternatively activated state, as evidenced by a significant drop in TNF-α production after 7 days of co-culture.

In the final set of *in vitro* cell culture experiments, RAW 264.7 cells were exposed to both the gram-negative bacterial product LPS, which causes inflammation in these cells [242], and microgels with encapsulated GED to observe whether the released drug reduces TNF-α, nitrite, and ROS production in these activated cells. Microgels without GED were also tested in parallel in this portion of the study. All three products are abundantly produced in this macrophage cell line upon incubation with LPS. Little response of the RAW 264.7 cells to LPS was seen in the first 24 hours; however, it typically takes between 48 and 72 hours for these macrophage cells to become fully activated with LPS exposure and produce high levels of NO, TNF-a, and ROS [185]. At Day 3, the levels of TNF-α increased significantly across all treatment groups when LPS was added to the culture medium. Several studies also reported increases in TNF-α with silica particles [187], Dacron [238], and polytetrafluoroethylene (PTFE) [188] added to macrophage/monocyte culture in the presence of LPS-induced inflammation. Since one function of TNF-α is the recruitment of macrophage cells during inflammation, a significant increase TNF-α would increase the number of these cells to the implant area and further lead to an increase in peroxide damage to the surrounding tissue [238]. By themselves, the materials induced the cells to produce this cytokine above the negative

control cell levels. The induced inflammation state (caused first by LPS) in the cultured cells was utilized to observe whether the particles would further augment the inflammatory response and TNF-α release. Our results showed that there was a significant decrease in TNF-α production with the high dose GED microgels and no difference in production with the other microgel treatments from the positive control levels. At the later time point, however, the no GED and low dose microgels had significantly increased TNF-α level over the positive control. The high dose microgels did not have significantly higher TNF-α level over the positive control at this later time point, which suggested that these microgels were not augmenting the inflammatory reaction, unlike their low dose and no GED counterparts. The NO levels produced by cells by Day 3 demonstrated that all microgel treatments exerted some anti-inflammatory effects. The levels of NO were significantly decreased compared to the positive control at this time point, with the high dose microgels producing the most dramatic decrease. The higher dose microgels released a large “burst” of GED during the first 3 days that suppressed iNOS function and NO production. However, at Day 7, the effects of all microgel treatments appeared to have an additive effect on NO production in a dose-dependent manner. To a similar note, the ROS levels of microgel treated cells appeared to significantly increase with activated cells at Day 3 and Day 7. This cellular behavior would suggest that application of these microgels with a low dose of GED in a condition where inflammation already existed, such as during a mild infection or early post-injury tissue, would enhance the inflammation response.

After studying the microgels using *in vitro* cell culture models and finding them to be satisfactorily biocompatible, the microgels were subdermally implanted in mice to

test for inflammatory potential and fibrotic tissue formation surrounding the implants utilizing the same 3 GED doses. Animals at Days 3 and 7 displayed a strong immune response with Odex/CEC microgels (0, 6.3, and 63 μg GED/mg microgel). The predominant cell type inside the implant area at these early time points was leukocyte-derived (e.g., macrophages, neutrophils). Studies have reported that implanted microspheres/microparticles produced from positively charged polymers, such as dextran, can augment wound healing [249,250] and enhance connective tissue response in subdermal implant sites [251]. At Day 7, the no GED microgel treatments showed a robust infiltration of inflammatory cells inside the implant area. The attraction of macrophages into the implant area could be attributed to the charged microgel surface [251,252]. Once attached, the macrophages would proceed to phagocytize the microgels and produce more cytokines to recruit additional monocytes from the circulating blood into the wound/implant area. While microgels without GED demonstrated a vigorous inflammatory cell infiltration at the implant site, microgels containing either a low or high dose of GED had significantly higher inflammatory cell infiltration scores at the same time point. The increase in inflammatory cell infiltration in GED microgel treated animals may be attributed to the presence of necrotic cells that were produced by the initial burst release of the drug from the microgels after implantation (Days 3 and 7). In this case, the high number of newly infiltrated cells would remain inside the implant area and phagocytize the cell debris. At Day 29, microgels with high dose GED maintained a significantly higher cell infiltration score compared with the other microgel formulations. These results suggest that a high dose of GED is increasing the inflammatory cell infiltration and not decreasing it, as it was

originally hypothesized. Furthermore the data from the GED-containing microgels suggest that the NO produced by macrophages at the implant site is important to prevent further leukocyte (i.e. neutrophil and monocytes) infiltration from the peripheral blood supply and lengthen the inflammatory period [179]. Liu et al. reported that physiological levels of NO produced during inflammation reduces the expression of leukocyte-binding receptors on the endothelial surface of blood vessels located near the area of tissue damage [253]. When NO production was decreased by using a NOS inhibitor (L-NAME), the researchers observed a significant increase in neutrophil infiltration into the damaged tissue and significant increases in the gene expression of P-selectin and intracellular adhesion molecule-1 in blood vessel endothelium, which bind leukocytes passing through the blood vessel [253]. Other studies demonstrated that the total ablation of macrophages in the wound bed in the early portion of healing does not affect neutrophil infiltration into the wound area and the presence of neutrophils in the wound at later time points [207,254]. In addition to decreasing NO production by macrophages, GED may also act as a scavenger for peroxynitrites, the molecular product of combining super oxides (O_2^-) and NO [255]. The traditional role for peroxynitrite in the wound healing process has been defending the wound bed from bacterial infiltration and proliferation shortly after wounding [172]. Other studies have suggested that peroxynitrites may also have a role in thwarting leukocyte infiltration into the wound bed during later stages of the inflammatory period and subsequent removal of peroxynitrites by using scavenger molecules also resulted in a significant influx of neutrophils into the wound bed [255]. In our study, it is likely that the GED acted to decrease NO production through both the competitive inhibition of iNOS and the

scavenging of any peroxynitrites inside the implant area, leading to an increased influx and persistence of leukocyte-derived cells and further inflammation.

At the early implant time points (Days 3 and 7), there was an abundance of amorphous, basophilic, stained material (black) located inside the microgel implant area. This phenomenon was not observed in the tissue samples from PLGA microsphere treated animals at both time points. The darkly stained material appeared to ooze between areas of inflammatory cells and aggregated microgels. The results of hematoxylin and eosin staining suggested that the dark material was strongly basophilic, much like cell nuclei, which also stain a dark, blue/black color with the same stain. Counterstaining the same tissue sections with DAPI demonstrated that the dark material also had an affinity for the fluorescent dye and that the darkly stained areas are most likely pooled DNA that was spilled from necrotic neutrophils and macrophages [256]. Large scale apoptosis is not unusual when even a biocompatible material is implanted inside the body [220]. Typically, when a macrophage or neutrophil encounters a piece of material that is too large to be phagocytized, the cells will transport their lysosomal contents (including digestion enzymes and an acidic solution) along with O_2^- outside of its cytoplasm to attack the material surface directly [170]; however, if too many neutrophils/macrophages exocytose their lysosomal contents, they cause localized, strong toxicity at the material surface that can cause necrosis of cells in the vicinity [201]. In this case, aggregates of microgels formed in the subdermal space after implantation would also have a similar effect on neutrophils and macrophages. The presence of any pooled DNA is not detected at Day 29. Although there were no time points checked between Day 7 and 29 in this experiment, the tissue samples from

the later time point suggest that the implant site reached the resolution of the acute inflammatory stage. Macrophages at the end of the acute inflammatory phase cleared away any necrotic cell debris to prepare the implant area for the chronic, steady-state phase of biomaterial interaction. The resolution of the acute inflammatory stage is necessary before the assembly of fibrillar Collagen I can be performed by transformed fibroblast cells that surround the microgels [257].

The effect of GED dose on fibrotic encapsulation of the microgel implants was most noticeable on Day 29. Microgels containing the lowest dose of GED showed the most aggressive particle clearance from the implant area versus the high dose GED microgels and the microgels without GED. With the same low dose GED microgels, there was also a trend of higher fibrosis inside and surrounding the capsule area. Macrophage cells that had engulfed multiple microgel particles remained nestled in a network of Collagen I and III fibers inside the subdermal capsule. It is likely that these macrophage cells will remain trapped in the capsule/implant area, not migrate towards nearby blood vessels, and deliver the microgels to the lymph nodes [258]. The low dose of GED appeared to have caused a more prominent, pro-fibrotic reaction inside the implant area compared with the other microgel treatments. There are reported connections between the suppression of NO produced by macrophages in early stage of inflammation that could affect collagen deposition by fibroblasts at later points in the healing process [85,208]. In previous studies, the pro-fibrotic reaction to iNOS inhibitors was investigated for systemically applied iNOS inhibitors added before or after experimentally inflicted damage. Dharmani et al. utilized a tendon crush model in rats to determine how the iNOS inhibitor L-NAME would affect the healing process if applied

systemically directly after the crush injury was initiated [259]. L-NAME was administered only once, but the effect on healing outcome at the later time points was profound. Their findings demonstrated that a systemic dose of 5 mg/kg produced a strong initial increase in neutrophils at the early time point (3 days) after crush injury, but they also observed the persistence of chronic inflammation (4 weeks after injury) resulting in collagen fiber adhesions to form between tendons [259]. As discussed in a previous paragraph, the production of NO during the wound healing process by macrophages may help conduct the normal wound healing process by scavenging peroxynitrites to reduce tissue damage [260], signal fibroblast cells to deposit Collagen III in the wound bed [260], and block excess neutrophils from entering the wound site when the acute inflammation phase is nearing its end. The low dose GED microgel released a small, but significant, burst of GED during the first few days of implantation. This burst of drug then caused a similar effect as seen in the Dharmani study, albeit in a localized manner.

In contrast to the low dose GED microgels, high dose GED microgels demonstrated significantly lower fibrotic tissue formation around the implant area compared with the no GED and low dose GED microgels at Day 29. The decreased fibrosis surrounding the high dose GED implants is likely due to a prolonged inflammatory period that was also perpetuated by an influx of leukocytes in the absence of the inhibitory signal from NO. An explanation for this observed behavior is the high dose GED microgels were releasing the drug for a longer period of time than the low dose GED microgels, thus increasing the duration of leukocyte infiltration and presence inside the implant area. During inflammation, matrix metalloproteinases (MMP) are also

produced by macrophage cells during classical activation to aid in breaking down damaged collagen structure within the wound area [244]. The presence of MMPs produced by the macrophage cells also hinder the formation of new fibrillar collagens around the implant area during the inflammatory period [261]. At Day 29, the histological analysis showed the presence of collagen-producing fibroblasts in the capsule surrounding the implant (Masson's trichrome staining), but the picrosirius red staining did not show a large accumulation of fibrillar Collagen I in the same vicinity. The inflammatory cell infiltration score was also lower for the high dose GED microgel treated animals at Day 29 compared to Day 7. Typically, as inflammation tapers off, alternatively activated macrophages begin to dominate the wound bed and promote fibrotic tissue formation by fibroblasts [247]. Despite a decreased inflammatory cell infiltration score at Day 29, the fibroblasts in the high dose GED microgel implant capsule would not have had enough time to produce a fibrous capsule similar to those observed surrounding the low dose and no GED microgel treatments [199].

When the Odex/CEC microgels were compared to PLGA microspheres at the same time points, the no GED microgels demonstrated similar inflammatory cell infiltration scores as the PLGA microspheres at Day 7 and 29. PLGA has widely demonstrated good biocompatibility in both a microsphere form [258,262] and also in a bulk scaffold material [263]. This result confers that the Odex/CEC microgel vehicle by itself has a similar *in vivo* biocompatibility as PLGA in particulate form during the mid inflammation (Day 7) and early reorganization (Day 29) phases following implantation. However, the median scores deviate at Day 3 with the microgel vehicle showing a higher inflammatory cell infiltration score than the PLGA microspheres. This result

suggested that the charged dextran and chitosan polymers in the microgels were more attractive to inflammatory cells than the PLGA microspheres and there was a larger observed infiltration of these cells as a result.

In summary, we have successfully synthesized Odex/CEC microgel particles to be used as a delivery vehicle for GED. The microgels (with and without encapsulated GED) demonstrated good overall biocompatibility when co-cultured with macrophage cells. However, when the high-dose GED microgels were co-incubated with LPS-activated macrophages, the inflammation reaction was augmented. Lastly, the *in vivo* subdermal implantation of the microgels demonstrated some dose-dependent differences in inflammation cell infiltration and fibrotic tissue encapsulation. The results of this study suggest that the Odex/CEC microgels could be further studied in a model of oxidative damage prevention, such as spinal cord injury. Examination of the fibrotic capsule surrounding GED-loaded microgel implants demonstrated that the high dose of GED microgels produce an anti-fibrotic function that could be utilized in the clinic to reduce undesirable scar tissue formation.

Table 5.1: Physical characteristics of Odex/CEC microgel batches and PLGA microsphere batch used for subdermal implant

Microparticle Composition	GED Loaded per batch (mg)	Zeta Potential (mV)	Effective Diameter (nm)
0.8% Odex/CEC	0	-22.46 ± 3.29	1528.1 ± 297.8
0.8% Odex/CEC	1	-19.7 ± 3.88	1649.6 ± 232.6
0.8% Odex/CEC	10	-17.09 ± 4.06	1480.4 ± 230.6
PLGA (50:50)	0	-4.32 ± 2.03	---

Table 5.2: Weights of implanted microspheres per time point and percent initial weight loaded. Averages are reported with ± standard deviation, except for Day 3 PLGA microspheres where the standard deviation was not calculated due because the number of replicates was too low (n=2).

Composition	GED Loading (mg)	n	Time (Days)	Average Initial Weight (mg)	Total MS Weight Implanted (mg)	% Initial Weight Loaded
0.8% Odex/CEC	0	3	3	10.3 ± 0.10	8.47 ± 0.51	82.20
		3	7	10.6 ± 0.38	8.23 ± 0.50	77.64
		3	29	10.4 ± 0.21	7.47 ± 0.60	71.83
0.8% Odex/CEC	1	3	3	10.2 ± 0.15	9.23 ± 0.47	90.49
		3	7	10.5 ± 0.10	9.23 ± 0.35	87.90
		3	29	10.3 ± 0	7.33 ± 0.25	71.17
0.8% Odex/CEC	10	3	3	10.2 ± 0.12	9.77 ± 0.30	95.78
		3	7	10.5 ± 0	9.3 ± 0.40	88.57
		3	29	10.6 ± 0.17	9.97 ± 0.8	94.06
PLGA (50:50)	0	2	3	10.7	4.35	40.65
		3	7	10.3 ± 0	6.03 ± 0.64	58.54
		3	29	10.5 ± 0.21	4.40 ± 0.95	41.90

Table 5.3: Average zeta potential measurements for each GED loading

Initial GED Loading (mg)	N	Average Zeta Potential ± SD (mV)
0	3	-22.20 ± 0.40
1	3	-21.38 ± 2.38
10	4	-20.90 ± 2.70

Table 5.4: Zeta potential measurements for all batches within GED loaded batches and statistical power between each batch.

Initial GED Loading (mg)	Zeta Potential ± SD (mV)	P-value
0	-21.73 ± 1.87	0.331
	-22.39 ± 3.81	
	-22.46 ± 3.29	
1	-19.71 ± 3.88	<0.001
	-20.33 ± 3.47	
	-24.11 ± 1.94	
10	-22.82 ± 3.24	<0.001
	-22.77 ± 3.53	
	-17.09 ± 4.06	
	-20.93 ± 2.24	

Table 5.5: Inflammatory cell infiltration scores for subdermally implanted Odex/CEC microgels and PLGA (50:50) microspheres

Time Point (Days)	Treatment	N	Median Inflammation Score
3	No GED MGs	3	4
	Low Dose GED MGs	3	3
	High Dose GED MGs	3	3
	PLGA (50:50) MS	2	3
7	No GED MGs	3	2
	Low Dose GED MGs	3	4
	High Dose GED MGs	3	4
	PLGA (50:50) MS	3	2
29	No GED MGs	3	2
	Low Dose GED MGs	2	2
	High Dose GED MGs	3	3
	PLGA MS (50:50)	2	2

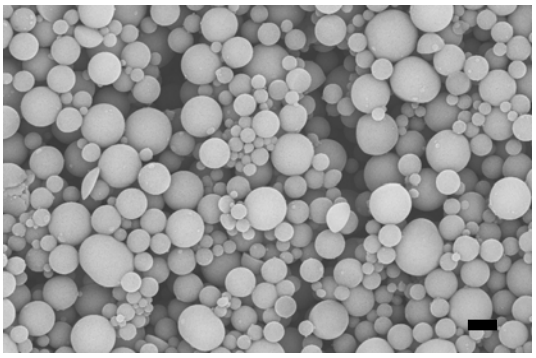

Figure 5.1: Scanning electron microscope image of microgels composed of Odex/CEC without GED loaded (scale bar = 2 μm).

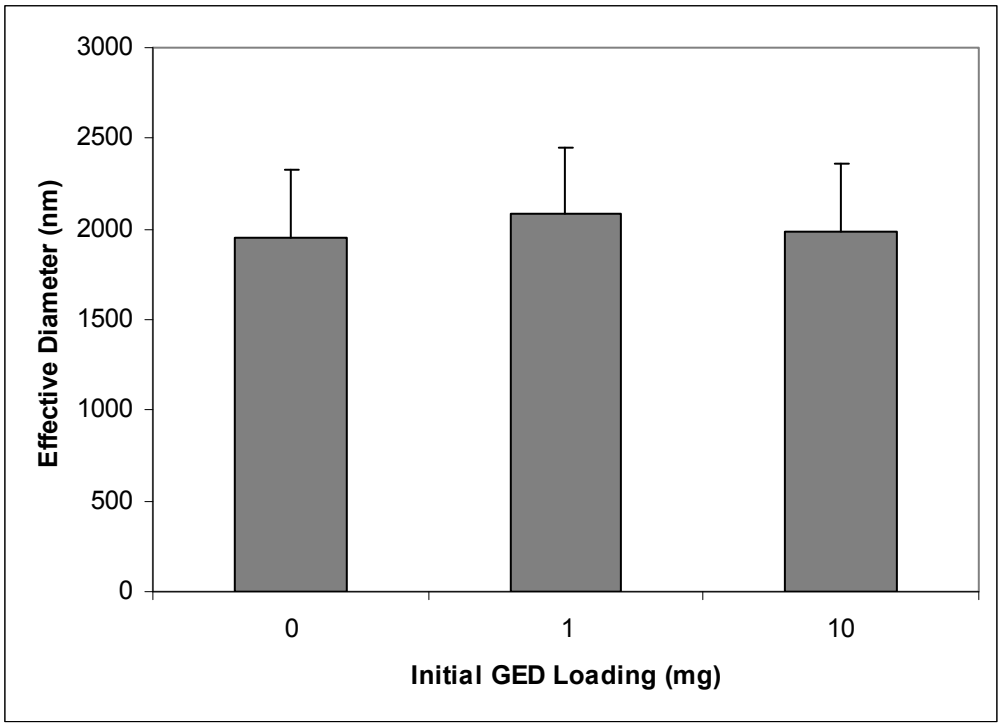

Figure 5.2: Results of dynamic light scattering analysis of microgel diameter by initial GED loading. No significant difference was detected in diameter measurements between GED loadings (One-Way ANOVA, p=0.888).

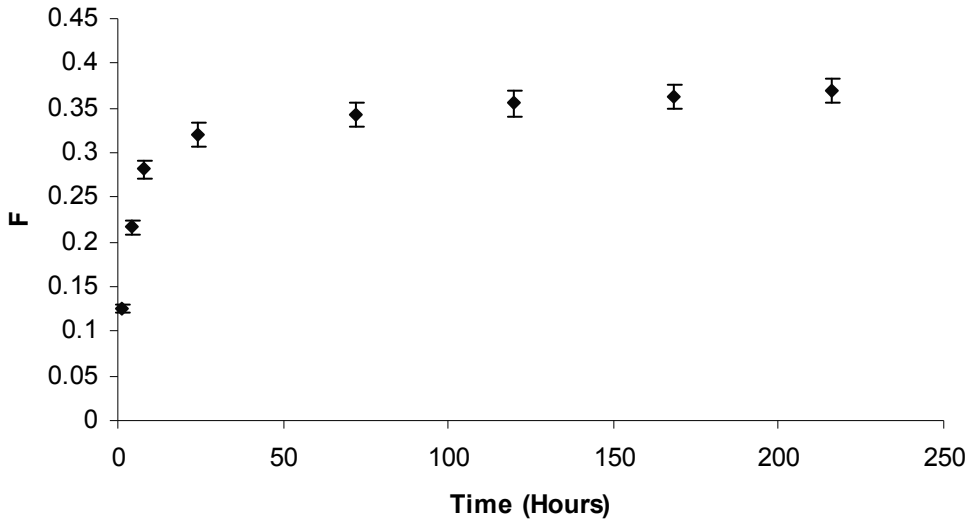

Figure 5.3: Cumulative GED released from microgels over 9 days (or 216 hours), where F is the cumulative GED released (mg) divided by total GED loaded (n=3). The data represented in this figure comes from release kinetics of microgels loaded with 63 µg GED/mg microgel only. Error bars represent standard deviation.

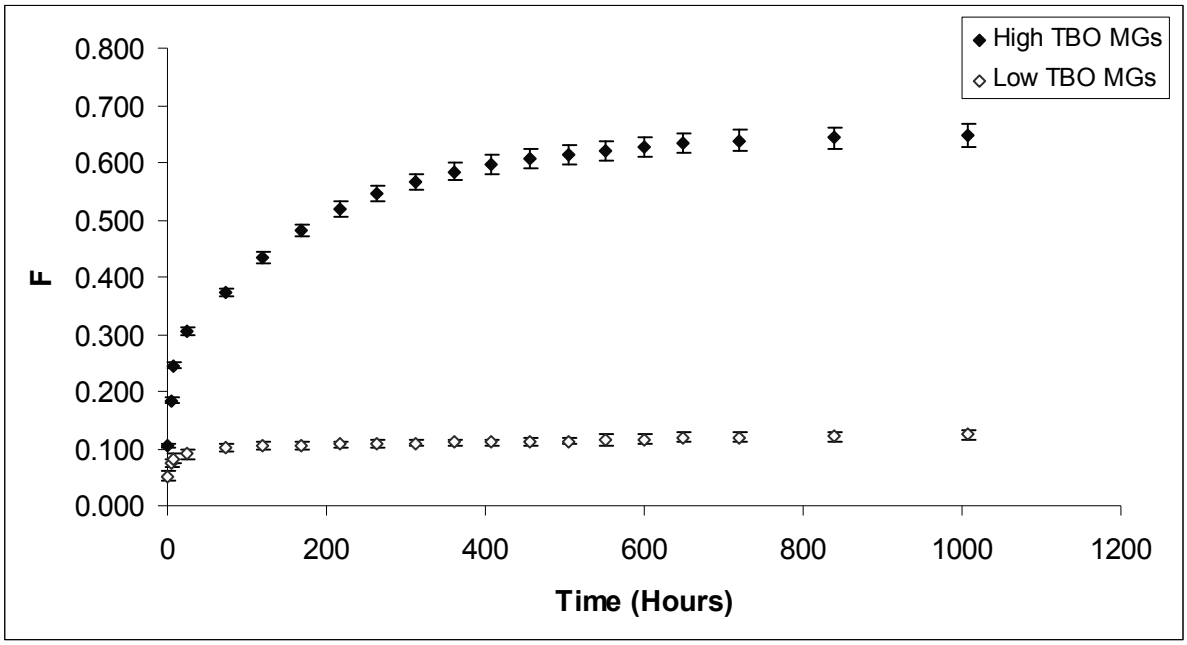

Figure 5.4: Cumulative release of Toluidine blue O (TBO) released from microgels over 42 days (or 1008 hours), where F is the cumulative TBO released (mg) divided by actual TBO loaded (n=3, each TBO loading). Error bars represent standard deviation. (High TBO MGs = 63 µg Toluidine Blue O/mg microgel, and Low TBO MGs = 6.3 µg Toluidine Blue O/mg microgel)

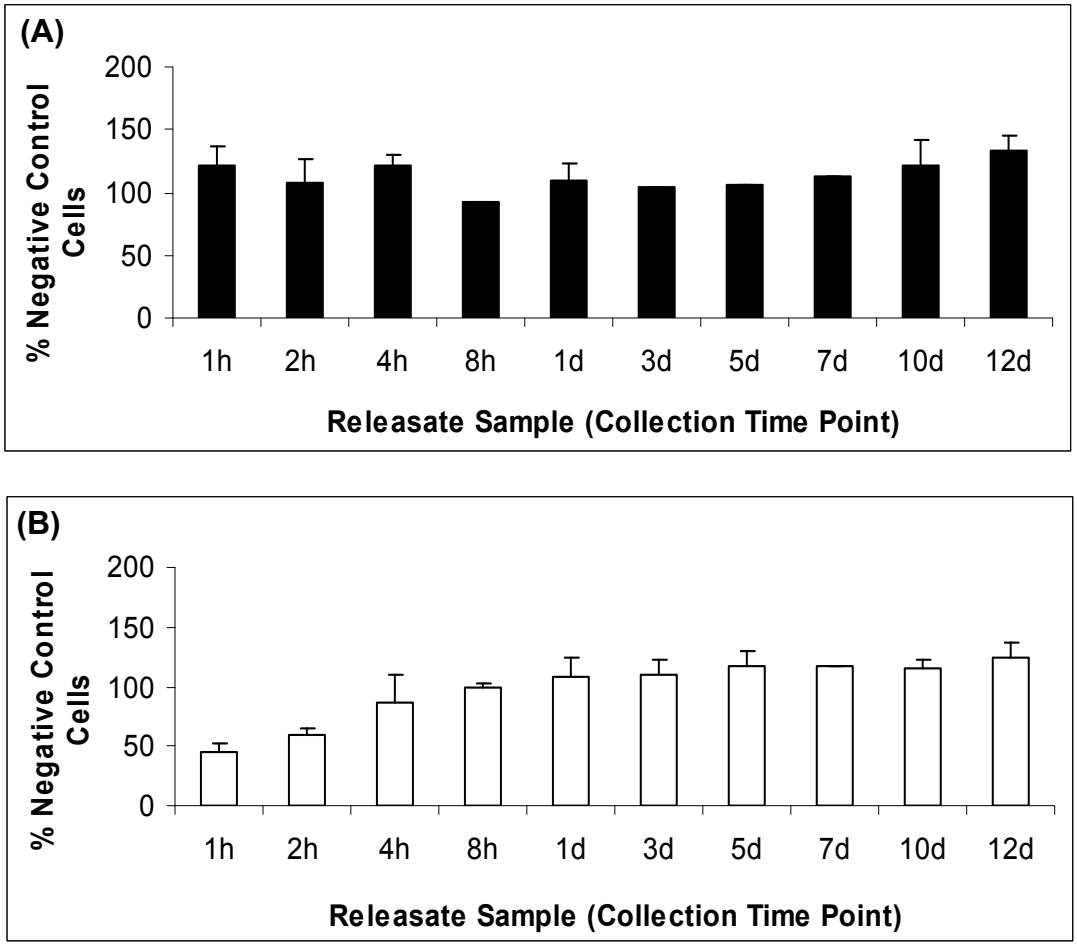

Figure 5.5: Relative cell density measured by crystal violet staining. Cell density was calculated from the ratio of the measured absorbance of each treatment and the measured absorbance of the control cells after 24 hours. Macrophage cells were exposed to either release samples from microgels (A) without GED, or microgels (B) with GED. The horizontal axis refers to the time point in the microgel release study was obtained. Samples in (A) without error bars represent samples with sample size too small for statistical analysis (n=2). For all other samples, n=3. Error bars represent mean ± standard deviation.

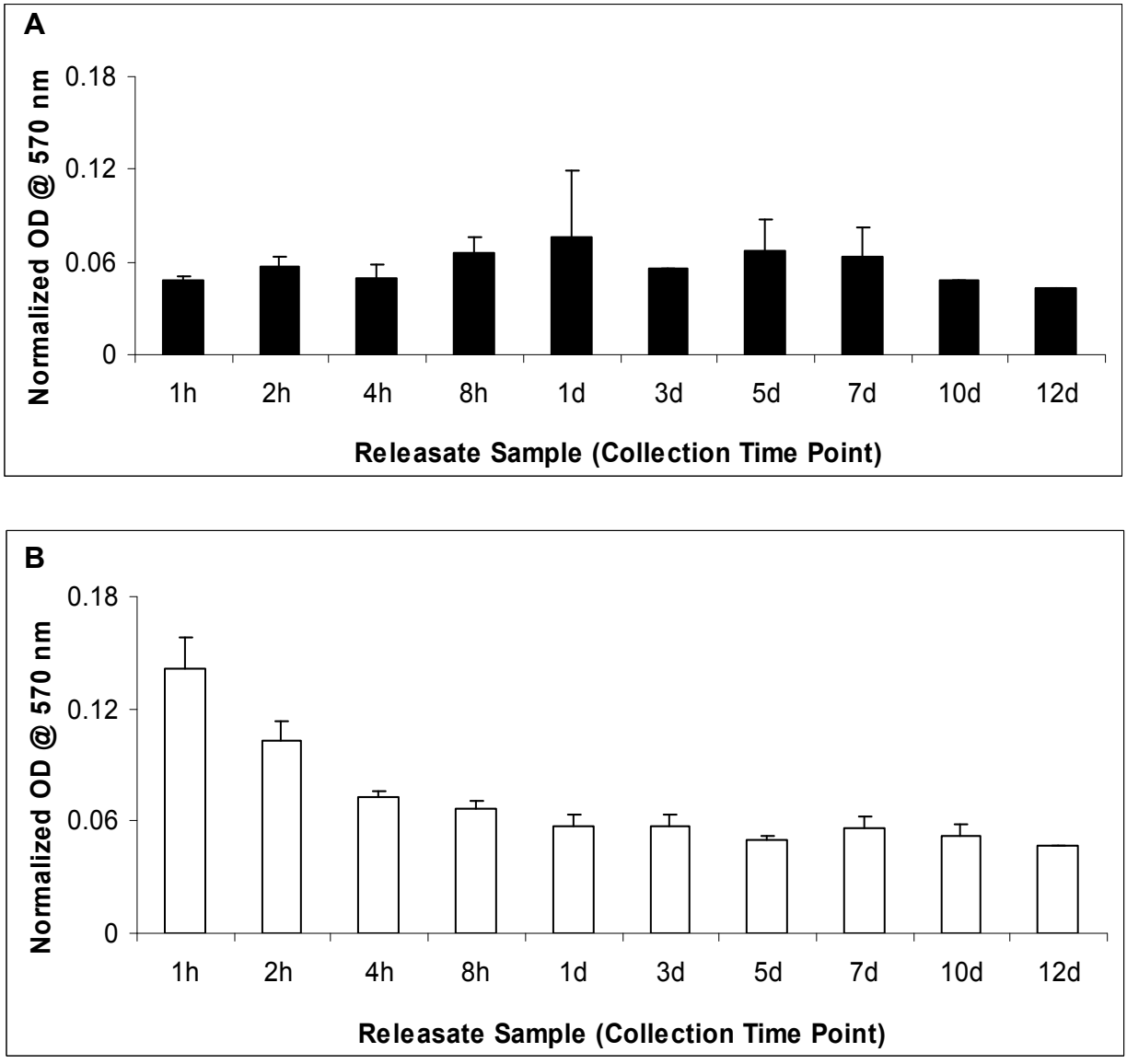

Figure 5.6: Nitrites released by macrophage cells after exposure to microgel release samples containing either (A) no GED, or (B) high dose GED (63 µg GED/mg microgel). The spectrophotometer data was normalized to the crystal violet staining results of cell density (see Figure 5.5). There was no statistical difference between treatments of release samples from non-GED microgels (A). However, microgel release samples from GED containing microgels (B) demonstrated statistically increased nitrites produced by cells treated with 1 and 2 hour release samples compared with other treatments. Error bars represent the mean ± standard deviation of each release sample treatment (n=3).

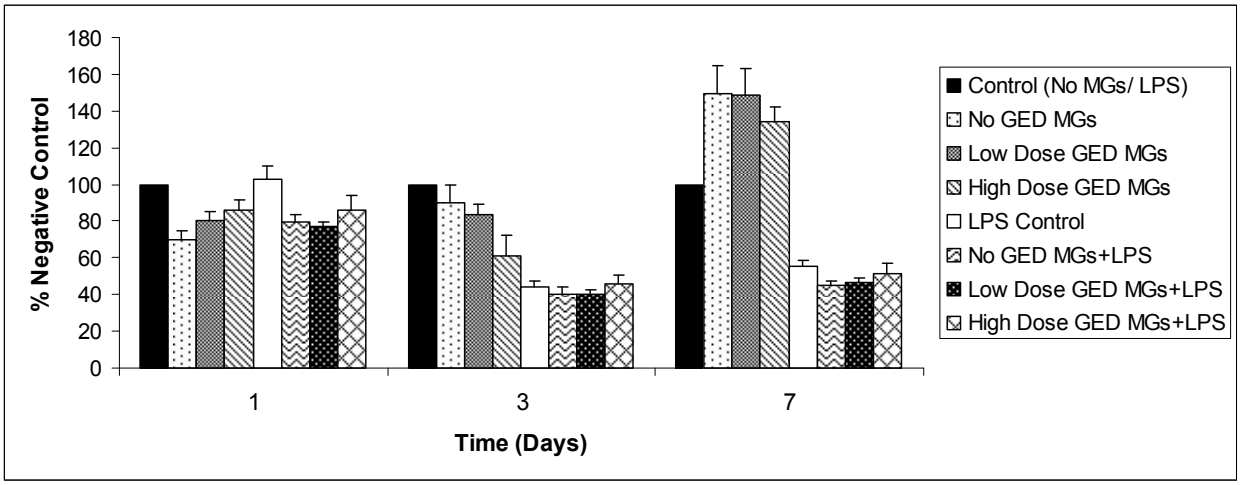

Figure 5.7: Relative cell density of macrophage cells that were treated with microgels and/or media containing no LPS, or LPS (1 µg). The LPS control treated cells only received media with LPS. The resulting optical density of the re-solubilized crystal violet dye was compared with the negative control cells at each time point (n=5). (No GED MGs = 0 µg GED/mg MGs; Low dose MGs = 6.3 µg GED/mg MG; High dose GED MGs = 63 µg GED/mg MGs)

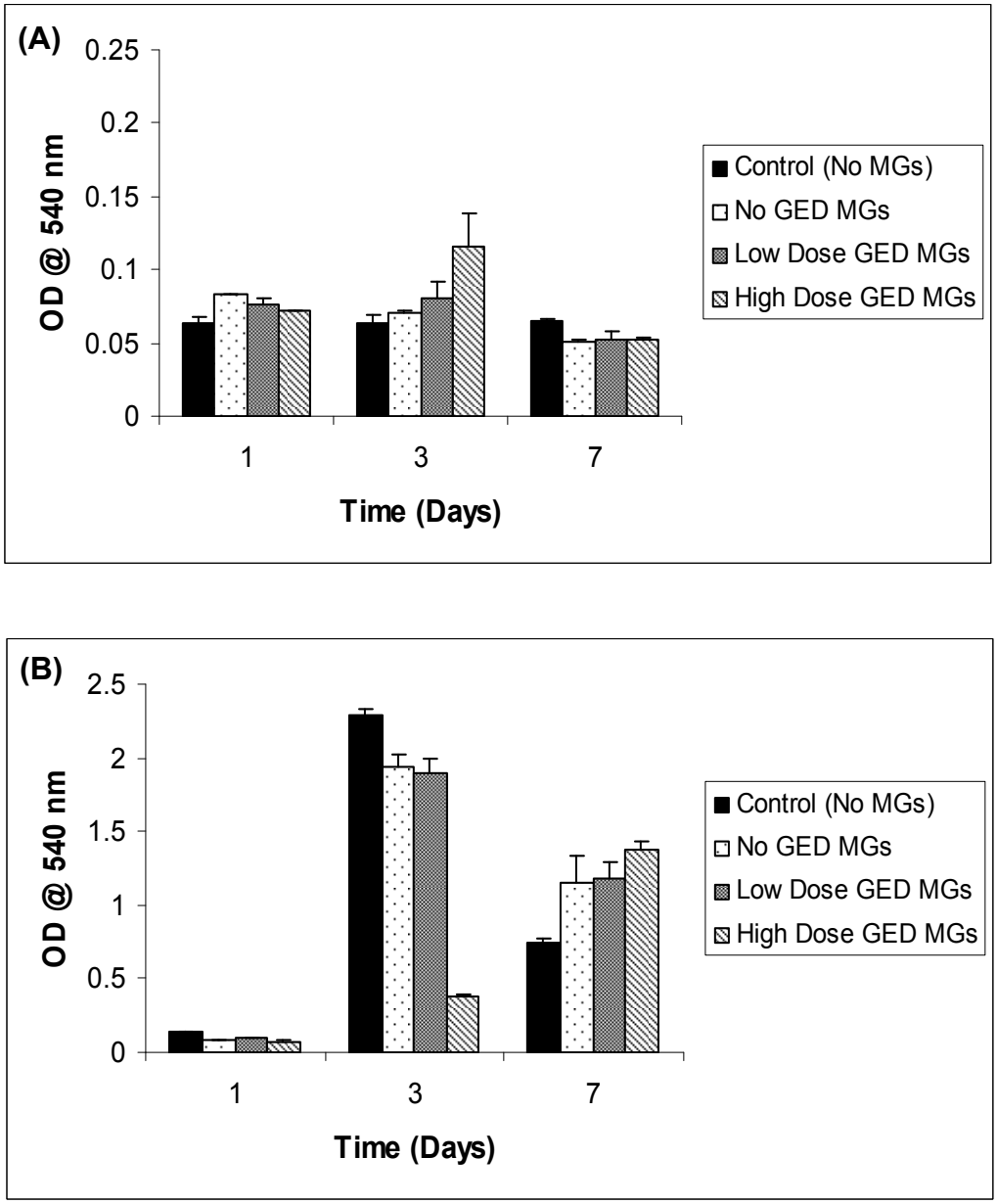

Figure 5.8: Nitrite measurement in macrophage cells that were either treated with microgels and/or cell culture media containing (A) no LPS, or (B) LPS (1 μg). The LPS was used to initiate a classically activated state in the macrophages. Nitrite levels were measured with the Greiss Assay and all nitrite levels were normalized to cell density (compared to control cells) at each time point (n=6). (No GED MGs = 0 μg GED/mg MGs; Low dose MGs = 6.3 μg GED/mg MG; High dose GED MGs = 63 μg GED/mg MGs)

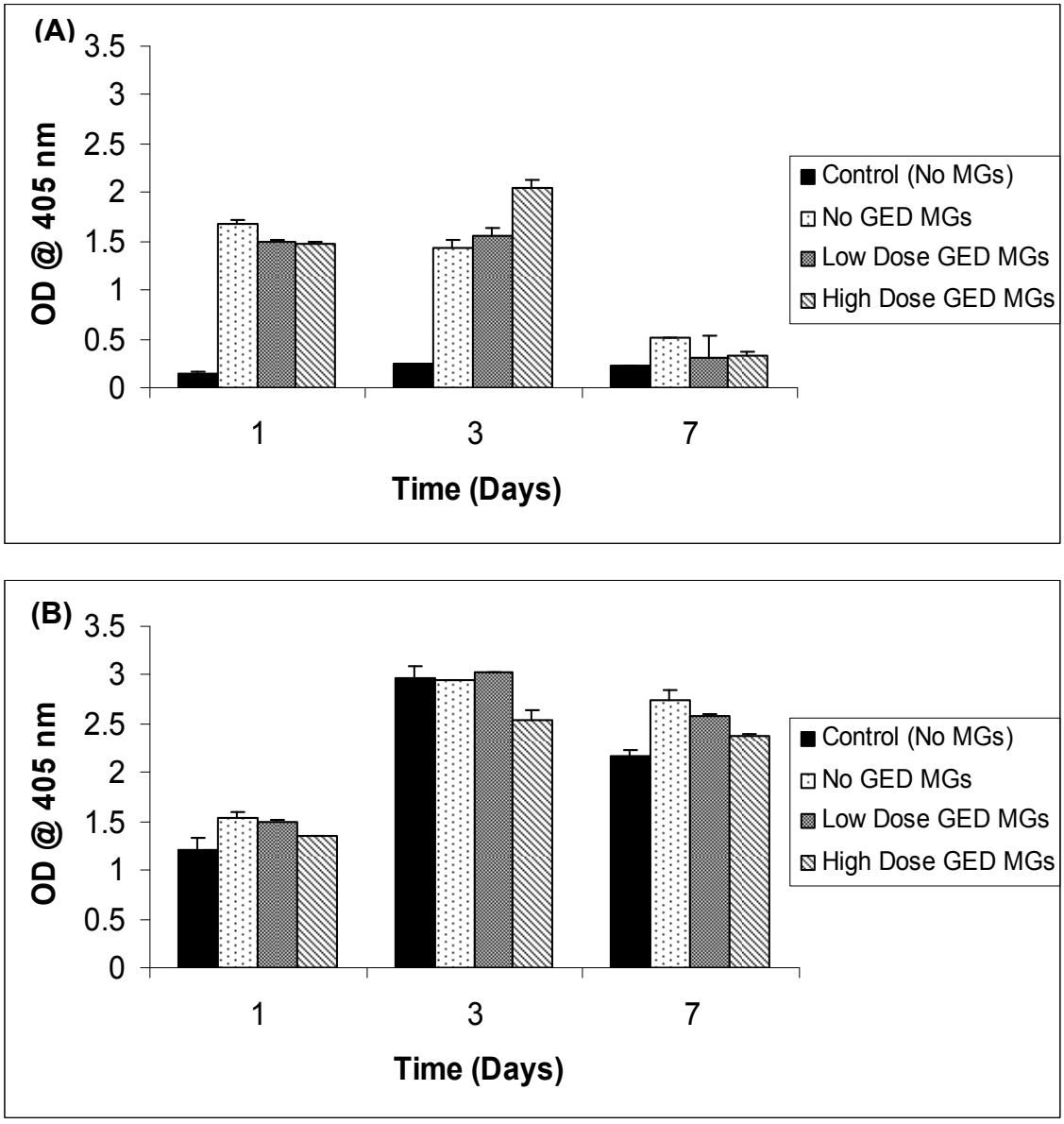

Figure 5.9: TNF-α measurement in macrophage cells that were either treated with microgels and/or cell culture media containing (A) no LPS, or (B) LPS (1 µg). The LPS was used to initiate a classically activated state in macrophages. The TNF-α levels were measured using an ELISA assay (n=3). (No GED MGs = 0 µg GED/mg MGs; Low dose MGs = 6.3 µg GED/mg MG; High dose GED MGs = 63 µg GED/mg MGs)

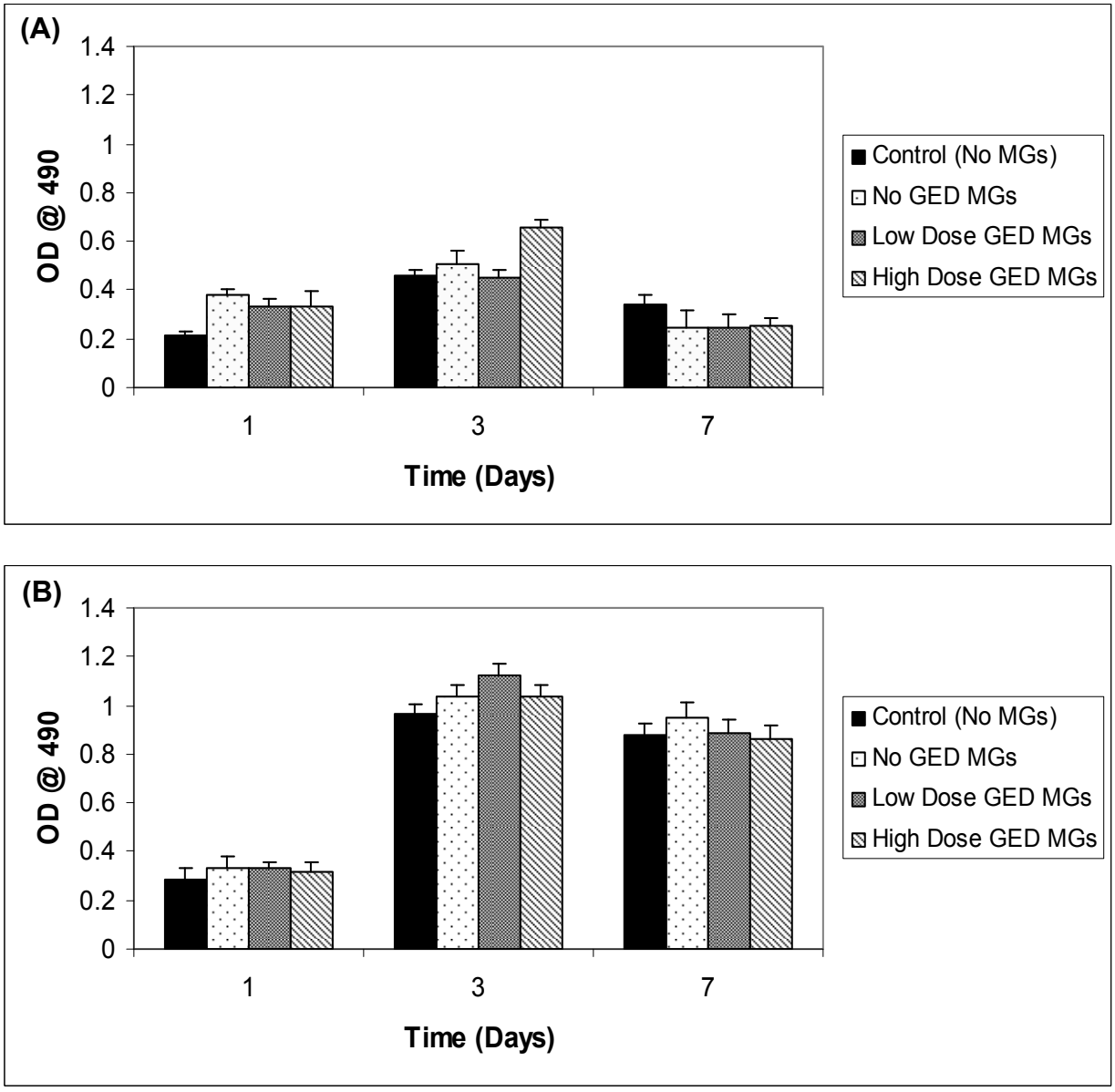

Figure 5.10: Metabolic activity (MTS assay) in macrophage cells that were either treated with microgels and/or cell culture media containing either (A) no LPS, or (B) LPS (1 µg). The LPS was utilized to produce a classically activated state in the macrophages. Error bars represent mean ± standard deviation of each treatment (n=6). (No GED MGs = 0 µg GED/mg MGs; Low dose MGs = 6.3 µg GED/mg MG; High dose GED MGs = 63 µg GED/mg MGs)

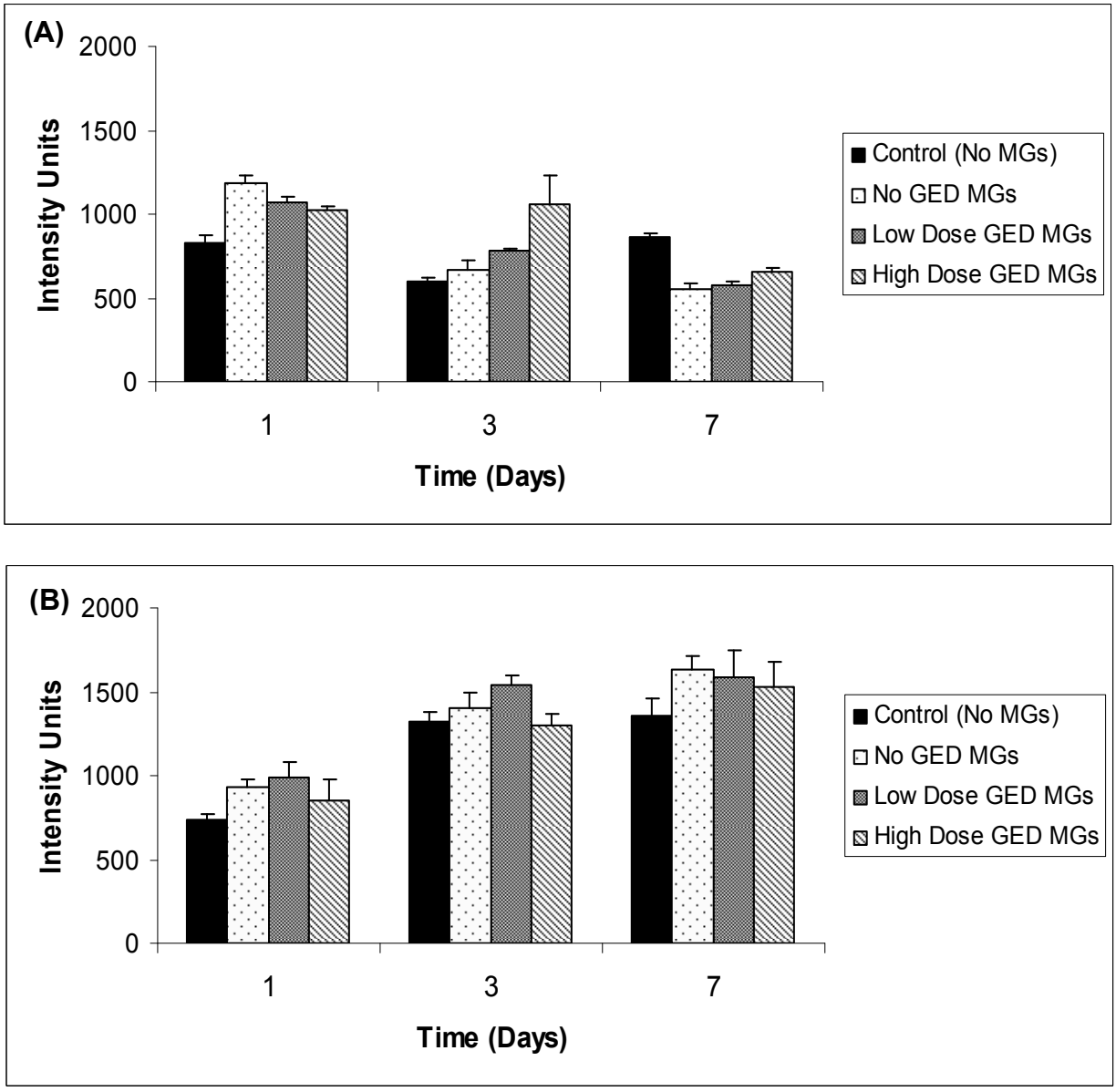

Figure 5.11: Reactive oxygen species (ROS) measurement in macrophage cells that were either treated with microgels and/or cell culture media containing either (A) no LPS, or (B) LPS (1 µg). The LPS was utilized to produce a classically activated state in the macrophages. The ROS levels were measured by incubating cells with DCFH-DA, lysing the cells, and then measuring the amount of DCFH that attached to cytoplasmic hydrogen peroxide (precursor to ROS). Error bars represent mean ± standard deviation of each treatment (n=3). (No GED MGs = 0 µg GED/mg MGs; Low dose MGs = 6.3 µg GED/mg MG; High dose GED MGs = 63 µg GED/mg MGs)

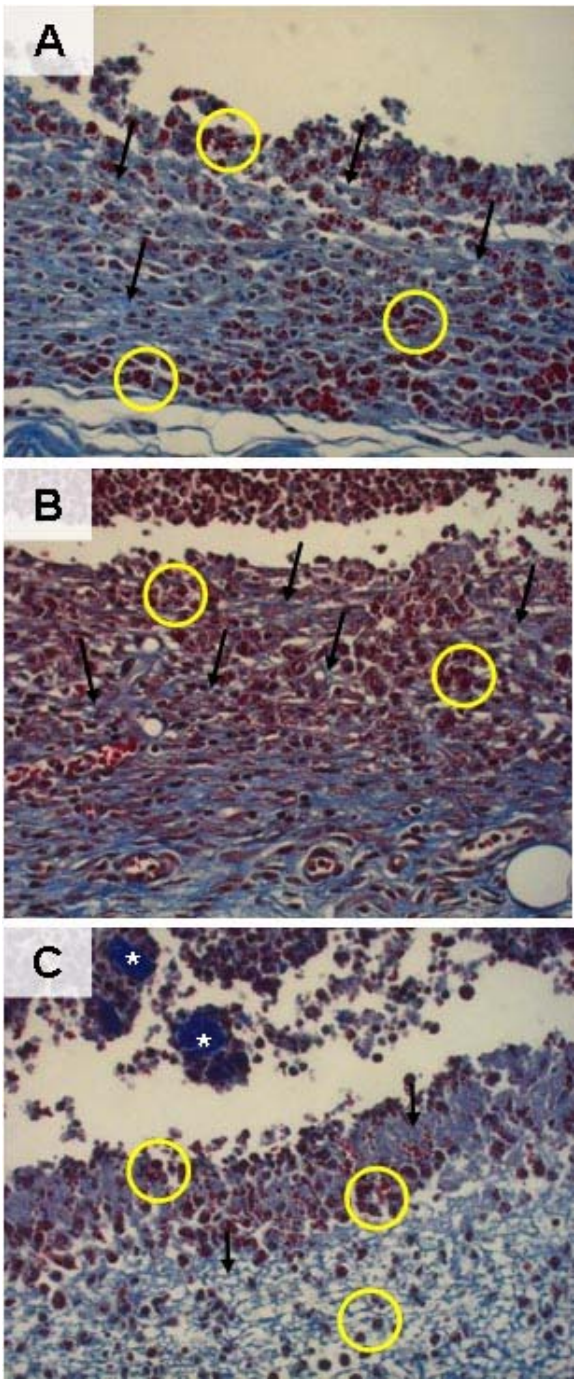

Figure 5.12: Cyst capsule cross sections of mice treated with Odex/CEC microgels and stained with Masson's trichrome method: (A) no GED microgels, (B) low dose GED microgels, (C) high dose GED microgels. Collagens are stained light blue with this staining method and the microgels stain red. Arrows point to fibrocytes containing soluble collagens in their cytoplasm. The yellow circles highlight the location of microgel-engorged macrophages at different depths of the cyst wall. White asterisks demonstrate residual, un-crosslinked oxidized dextran found mixed in with the microgels. These areas are surrounded by macrophages (Scale bar = 20 μm)

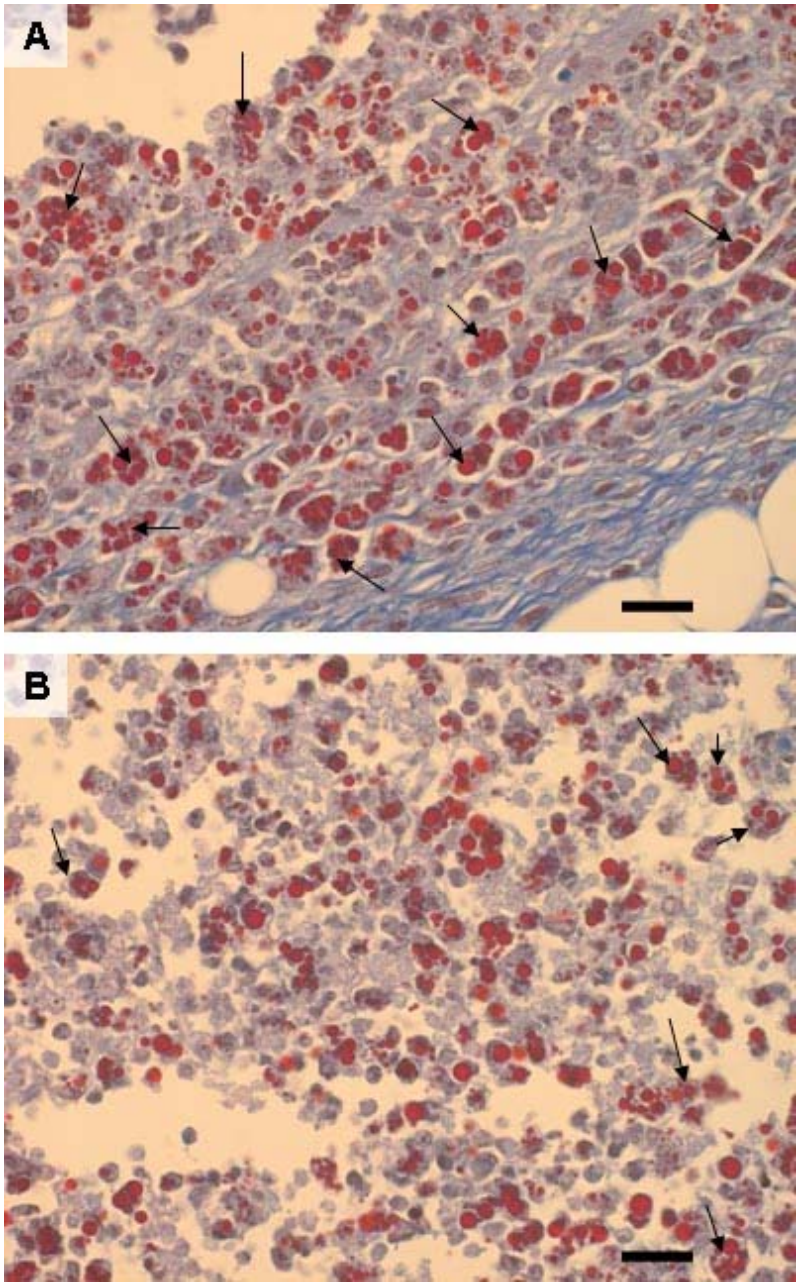

Figure 5.13: Macrophages phagocytosing multiple microgels in the (A) capsule surrounding the implant and (B) inside the implant zone. The animal was treated with microgels containing no GED for 7 days. Masson's trichrome staining was performed to highlight the microgels inside the macrophage cells (light blue cytoplasm). Arrows indicate some sample cells containing multiple microgels (Scale bar = 20 μm).

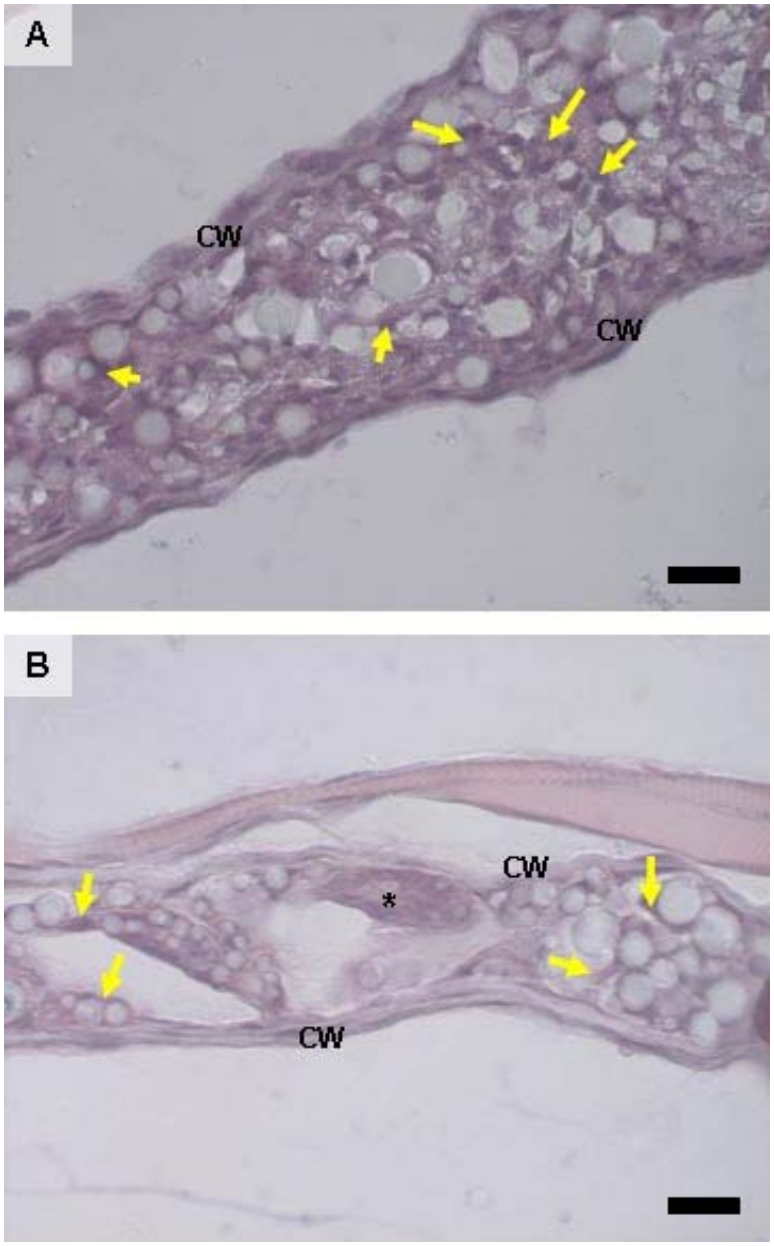

Figure 5.14: Implanted PLGA microspheres at (A) 7, and (B) 29 days post implantation. Sections at Day 7 show significant cell infiltration inside the implant area (yellow arrows). At 29 days, the amount of cellular infiltration has diminished. Also, a single foreign body giant cell (*) can be observed in the Day 29 sample. The cyst wall (CW) is also highlighted in both time point images. The tissue sections were stained with H&E (Scale bar = 20 μm).

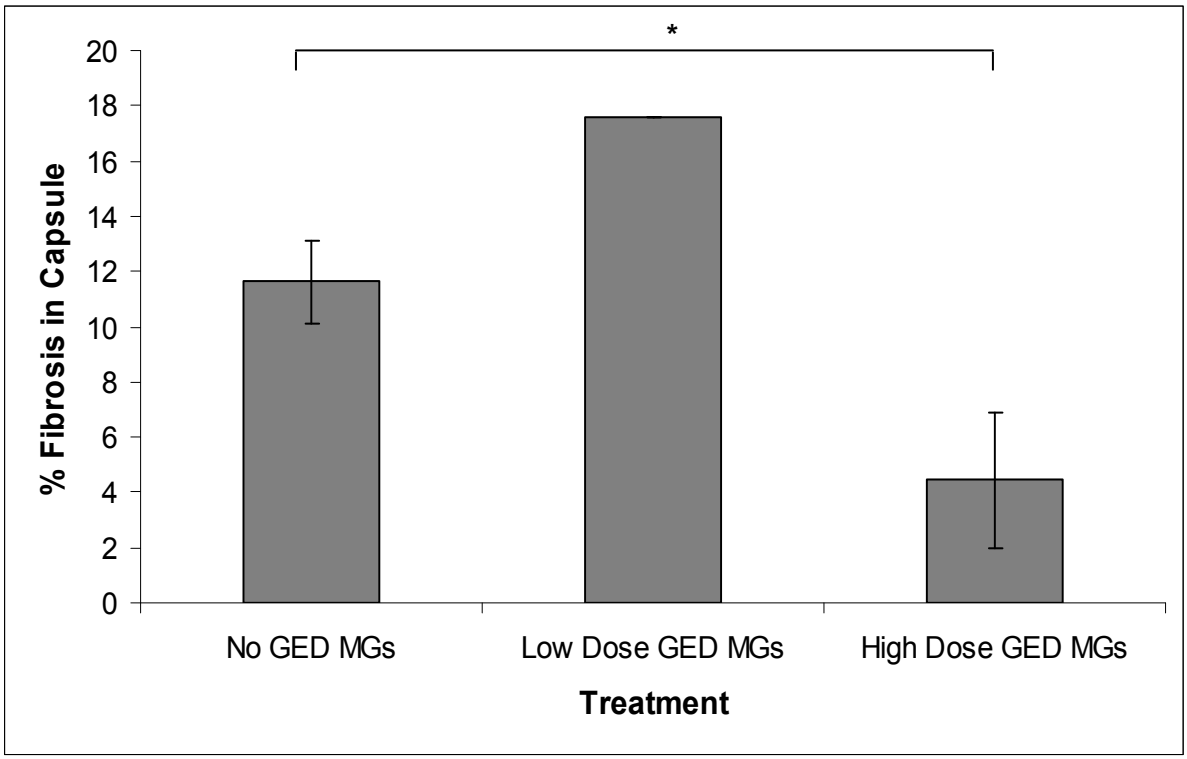

Figure 5.15: Area fraction of fibrosis involving Collagen type I at 29 days after microgel subdermal implant. A significant increase (p=0.013) in fibrosis inside and surrounding the implant capsule was seen in the microgel vehicle alone versus microgels with high dose GED (63 µg GED/mg microgels). Low dose microgels (6.3 µg GED/mg microgels) were not included in the statistical calculations because the sample number was too low (n=2). Saline treated animals (negative control) did not have a capsule area after 29 days and were excluded from analysis.

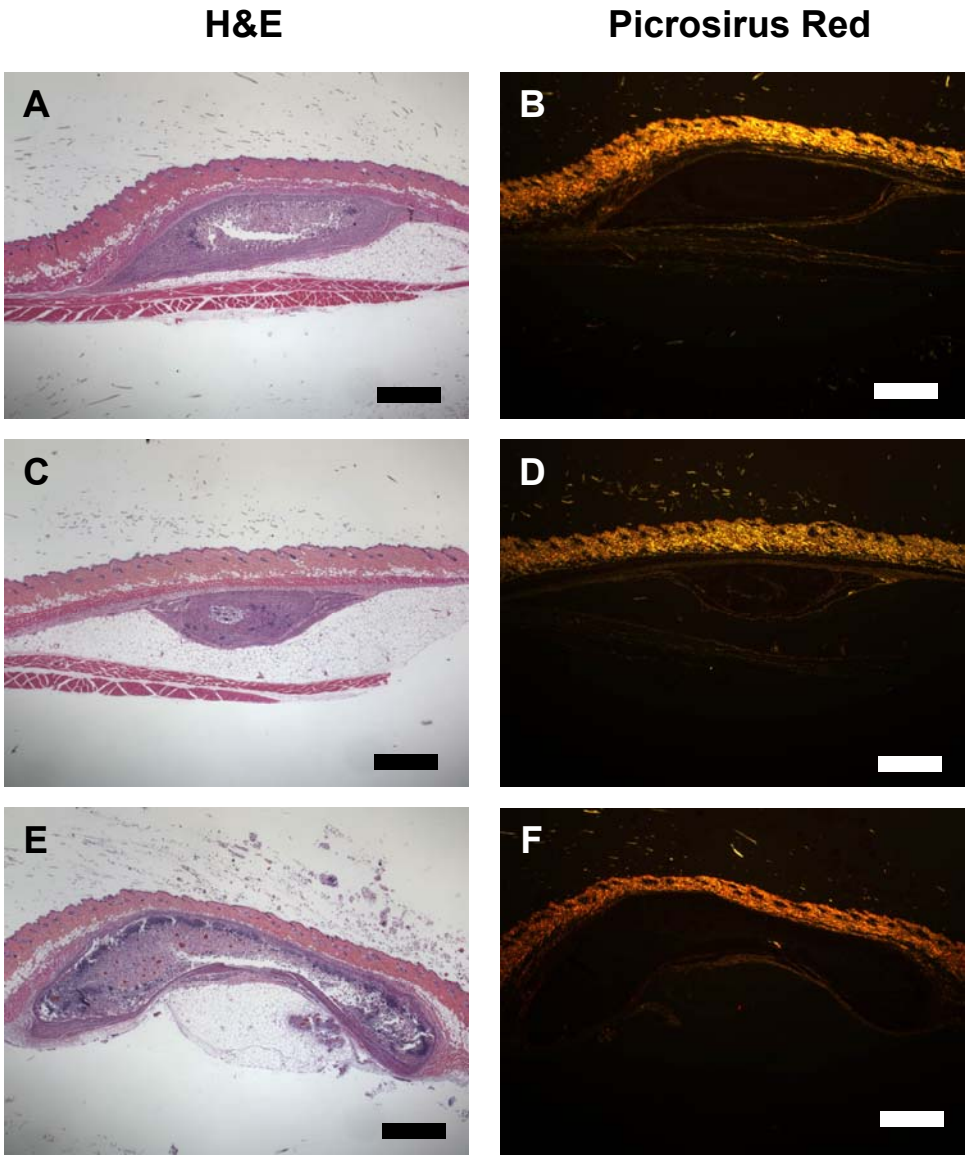

Figure 5.16: Picrosirius red staining to measure overall fibrosis inside implant area at Day 29. Images were captured at 2x magnification in both bright field and with linear polarized light. Microgels containing (A,B) no GED, (C,D) low dose GED, and (E,F) high dose GED are represented in these images (Scale bar = 1 mm).

Chapter 6

Conclusions and Future Studies

PLGA/PEG-g-CHN microspheres to deliver therapeutic proteins

In Chapter 2, PEG-g-CHN/PLGA blended microspheres were developed and tested as a delivery vehicle for a therapeutic protein, bFGF. The results of the study suggested that the PEG-g-CHN added to the PLGA polymer solution aided in the modulation of protein release. Fibroblast cell culture experiments demonstrated that bFGF released from microspheres after exposure to aqueous medium was bioactive and caused morphological changes similar to prepared solutions of native bFGF. *In vivo*, the PEG-g-CHN also reduced inflammation-associated microvascular dilation after placement in the hamster cheek pouch, with either encapsulated BSA or bFGF. Furthermore, chronic exposure to bFGF released from implanted microspheres enhanced endothelin expression in the blood vessel walls and augmented vasoconstriction. The results suggest that the endothelin produced by exposure to bFGF after vascular pre-conditioning with SNP acted as a negative feedback mechanism to reduce blood vessel dilation in this animal model.

The results of bFGF release kinetics show very low levels of conformationally correct protein released from the PLGA/5% PEG-g-CHN microspheres as determined by a receptor-based ELISA assay. In our microsphere synthesis protocol, we used a

standard water-in-oil-in-water (W/O/W) method that utilized both a strong organic solvent (chloroform) and high mechanical shear forces (impeller mixing) to produce the polymer droplets inside the continuous phase. Both parameters can damage proteins before the microspheres have had the time to harden [264]. In addition to structural damage, proteins that are released from the microspheres can adhere back onto the surface of the microspheres, thus removing them from the samples of aqueous release media [265]. A method to check the amounts of particle adhered proteins would be to add surfactants to the release medium, such as Tween20 [266,267]. Tween20 is a detergent that is used frequently to discourage released proteins from sticking to the polymer microspheres and the sample vessel walls. The use of this detergent may prevent released bFGF from being adsorbed back onto the PLGA/PEG-g-CHN microsphere surfaces and would allow for a more accurate quantification of bFGF release from the microspheres.

Future studies of protein encapsulation with PLGA/PEG-g-CHN microspheres should also examine the aggregation potential of released. The aggregation of proteins occurs when proteins are damaged and expose complementary binding sites to produce dimers and trimers of proteins after release [266]. Aggregates can also form inside the polymer microspheres during synthesis and prevent facile diffusion of proteins from the microsphere matrix [268,269]. A serious consequence of protein aggregation after release involves the production of antibodies and an allergic reaction due to the body's inability to recognize the aggregated proteins [270]. Previous studies of protein stability in PLGA microspheres after a W/O/W preparation used measurement tools such as size exclusion high performance liquid chromatography (SE-HPLC) [266]

and sodium dodecyl sulfate polyacrylamide gel electrophoresis (SDS-PAGE) [265,271]. SE-HPLC is a quantitative method of determining the concentration of aggregated proteins, whereas SDS-PAGE is a semi-quantitative measure. Both methods can also identify whether bFGF has been fragmented into smaller units. By quantifying the extent of bFGF aggregation, the amount of non-aggregated protein (quantified by ELISA) with the aggregation results can be compared. Even if there was significant aggregation of released bFGF, the aggregates did not increase the inflammatory potential of the bFGF-loaded microspheres in the hamster cheek pouch model.

HA film and CEC/Odex hydrogel adhesion barriers

In Chapter 3 and 4, two barrier materials were evaluated for the reduction of post surgical adhesions in an experimental model of bowel trauma in the rat. The HA film and the Odex/CEC hydrogel had significantly reduced adhesion severity compared with the untreated control animals at 21 days after surgery. The hydrogel did not show any significant advantage in adhesion reduction over the clinically available Seprafilm. However, the hydrogel has the advantage of adapting to complex geometries and small spaces inside the abdomen, which is a difficult task to accomplish with the brittle Seprafilm. The hydrogel could also be adapted to use in laparoscopic procedures. Future studies of laparoscopic applications would require that the mixed hydrogel not crosslink in the delivery catheter and clog it before the hydrogel reaches the visceral surface. In the hydrogel study, it was noted that the time for gelation of the autoclaved polymer solutions was slightly longer than non-autoclaved solutions from previous

studies. The laparoscopic study should include viscometry studies of the autoclaved solutions to determine how long it takes for the solution to gel at room temperature.

The goal of the HA film and Odex/CEC hydrogel barrier studies was focused on the long-term outcome of adhesions. Adhesions were assumed to be permanent and severe if they could not be separated with blunt dissection or without bleeding/visceral tearing at 21 days after surgery. As discussed in Chapters 2, 3, and 4, abdominal adhesions typically begin to form within the first 36 hours following surgery and strengthen several days later. At 21 days after surgery, it is assumed that any visceral or abdominal wall damage would be completely healed. Because the film and hydrogel treated animals demonstrated significantly lower adhesion scores, it is indicated that the barrier materials were present between the damaged tissues for at least the first several days following surgery. Multiple remnants of hydrogel were observed in some animals, and a nearly intact film on the cecum at 21 days after surgery in one animal. In the future, the localization and degradation rate of both the film and hydrogel should be investigated in the same rat cecum/abdominal wall injury model. The experiments could be performed by utilizing earlier sacrifice time points (e.g., 12 hours, 1 day, 3 days, 5 days, and 7 days). In addition to examining the state of the barrier materials after their placement, samples of the injured tissue in contact with the materials will yield insight into whether the material augments wound inflammation and how the materials interact with blood materials at the site of injury.

Although animal models of pelvic adhesions were not investigated in this dissertation, adhesions represent a pervasive problem that occurs after most reproductive surgical procedures. The repercussions from severe, fibrous, pelvic

adhesions can cause intense pain and infertility [272]. Even if the adhesions are lysed after they have been diagnosed, the recurrence rate is approximately 67% [273]. Both the HA film and Odex/CEC hydrogel barriers were effective barriers to adhesions in the abdomen, but they have not yet been tested in a gynecological surgical model. In Chapter 2, the commercially available adhesion barrier Interceed was initially approved for use in both abdominal and pelvic surgical applications. However, after reviewing the clinical data after abdominal implementation of Interceed, it was determined that the barrier had no significant improvement in adhesion scores compared to negative control patients. After gynecological surgeries, Interceed was found to be more effective in reducing severe adhesions. The FDA recommended that Interceed be utilized only during pelvic surgeries. The barriers used in our studies could encounter similar issues if applied in the pelvic cavity.

Post-surgical adhesions can form in other areas of the body besides the abdomen and pelvis. Adhesions of the pericardium after myocardial tissue damage due to ischemic events or surgical interventions also require an effective barrier material as a prophylactic. Similar to events in the abdomen, myocardial adhesions form by the accumulation of exudates/fibrin after injury, followed by the accumulation of inflammatory cells to the injury site, and the population of the fibrin bridges with collagen-fiber producing cells [274]. Naito et al. studied the application of Seprafilm in combination with a PTFE membrane for the reduction of pericardial adhesions after pericardial reconstruction and found that the HA films significantly reduced the adhesion severity scores when utilized in an animal model of open heart surgery [275]. The HA film studied in Chapter 3 would have several advantages over Seprafilm in this

application including ease of handling by the surgeon and the crosslinked film would withstand re-hydration without disintegrating.

Microgels synthesized from Odex and CEC to deliver an iNOS inhibitor

In Chapter 5, we synthesized microgels for the delivery of the iNOS inhibitor drug GED, and characterized their physical characteristics and inflammatory potential using a macrophage cell line and a murine subdermal implant model. The results of the study demonstrated the synthesis of microgel particles using a single water-in-oil emulsion method. The microgels exhibited an initial burst release of either GED or Toluidine Blue O (a model dye molecule) followed by a lesser, more moderate payload release over 9 days. When macrophage cells were co-incubated with whole microgels with or without GED *in vitro*, cells produced a complex response. The microgels, regardless of GED dose encapsulated, did not produce significantly high levels of nitrites (an indicator of classical inflammatory response in macrophage cells); however, the cells produced high levels of TNF-α compared with the negative control cells. This result indicated that the macrophage cells recognized the microgels as a foreign body, but they did not produce classical activation. When the microgels were implanted in a murine subdermal model, both the high and low dose GED microgels produced significantly higher inflammatory cell infiltration compared with animals receiving microgels without GED loaded at Day 7. On the final time point, Day 29, animals that received microgels with the highest GED dose maintained a high inflammatory cell infiltration score compared with low dose and no GED microgels at the same time point. This indicated that the GED may augment the acute inflammation phase following implantation and allow for additional PMN cells

(e.g. neutrophils) to migrate to the implant area. The fibrosis scores for the implanted microgels at Day 29 revealed that high dose GED microgels had significantly lower fibrotic content of the implant and capsule compared with microgels without GED. This result confers that the high dose of GED inhibited the assembly of Collagen I fibers. We also hypothesized that the use of GED with the microgel particles may produce an effective anti-fibrotic treatment in certain clinical applications.

After reviewing the cell culture data, we hypothesized that the microgel particles were producing some elements of classical inflammation. It was also observed that the cells decreased their output of TNF-α, a pro-inflammatory cytokine, after 7 days of culture with the microgels. We hypothesized that the macrophage cells were changing their activation states from classical to alternative. In future studies, a panel of ELISA assays or custom protein array should be performed to measure the levels of classical (IL-1, IL-6, matrix metalloproteinases) and alternative (IL-10 and TGF-β1) activation cytokines at each time point to further verify a change in macrophage activation states during the course of co-incubation of microgels.

The data from the subdermal implantation study suggested that GED can reduce the amount of Collagen-I formed and we hypothesized that this attribute can be utilized in certain medical situations where the initiation of the healing process and the formation of scar tissue need to be inhibited. One example of this is glaucoma, where it is advantageous to generate a non-healing wound in the eye to relieve excess pressure and preserve eyesight. Glaucoma affects about 70 million people worldwide [276,277] and 2.2 million people in the US [278,279]. The disease is characterized by optic neuropathy caused by increased intraocular pressure (IOP), which can lead total

blindness if left untreated [278,280,281]. IOP is regulated by aqueous humor production, resistance to aqueous humor outflow, and episcleral venous pressure [282]. Glaucoma can be controlled and vision loss slowed by lowering IOP through topical medication and laser treatments [278]. However, pharmaceutical interventions may not lower or stabilize IOP in some patients and surgical intervention (i.e., Trabeculectomy) is required to create an alternate draining route for excess aqueous humor to leave the anterior chamber and relieve the pressure focused on the optic nerves. The surgeon cuts a small pocket between the conjunctiva (outer membrane on eye surface) and the sclera (white outer wall of the eye) where the fluid is eventually absorbed by the blood or lymph vessels near the pocket [277]. The surgical procedure can provoke scar/fibrotic tissue formation at the bleb site that can close the bleb prematurely starting 12 hours after the surgery, similar to skin [283]. To keep the filter open for drainage and prevent scarring, the surgeon typically applies an anti-mitotic drug, such as 5-Fluorouracil (5-FU) or Mitomycin C (MMC), which slows healing of the filter opening [277,282,284,285] by reducing the number of cells involved in the wound healing pathway (i.e., fibroblasts, macrophages, endothelial cells) near the filter site and thus preventing fibrotic tissue from closing the filter within hours of the surgery [277,286]. Evidence presented by Daniels et al. also suggests that growth arrested Tenon's fibroblast cells can still produce bioactive growth factors that can affect the behavior of normal fibroblast cells; thus, even though the growth arrested cells are not proliferating, they can still participate in the scar tissue formation process [287]. It is possible that using an iNOS inhibitor after glaucoma surgery may reduce bleb scaring by decreasing

the number of macrophage cells and their associated cytokines that encourage fibroblast proliferation at the bleb site [288].

The local application of iNOS inhibitor drugs may decrease the fibrotic closure of Trabeculectomy blebs by directly targeting NO signaling of wound fibroblasts to produce collagen during the proliferative phase of healing. The exact mechanism behind the stimulation of collagen production through NO signaling is not exactly known. NO has been suggested as a regulator of the cytokine environment inside the wound bed [289]. The production of NO during the mid- to late-inflammatory stage may suppress the production of additional inflammatory cytokines through the direct suppression of transcriptional factor NF-kB [208]. It is also possible that NO affects collagen deposition by enhancing post-translational collagen synthesis rather than de novo transcription of relevant genes in wound fibroblasts [260]. In several small animal studies, the inhibition of iNOS activity, either through breeding an iNOS-knock out animal [290] or through the administration of iNOS inhibitor drugs [208,291], showed significant decreases in wound bed collagen content compared with wild type/untreated animals. Although iNOS inhibitors such as GED have not yet been tested as an anti-fibrotic treatment after Trabeculectomy procedures, future studies utilizing a standard rabbit eye model would be necessary to examine the connection between NO and fibrosis in the eye. Another aspect of GED application after glaucoma surgery is the experimentation needed to test different doses of the drug and how the fibrotic tissue cascade is affected. In the subdermal study, different GED doses produced different levels of fibrosis: low doses produced higher fibrosis, while high doses produced much lower fibrosis. Finding the optimal therapeutic range in an experimental animal model will help better modulate the

fibrosis occurring at the bleb site and allow excess aqueous humor to leave the anterior chamber of the eye.

Bibliography

1 Mabanta L, Valane P, Borne J, Frame MD: Initiation of remote microvascular preconditioning requires k(atp) channel activity. Am J Physiol Heart Circ Physiol 2006;290:H264-271.

2 Fox RJ, Frame MD: Arteriolar flow recruitment with vitronectin receptor stimulation linked to remote wall shear stress. Microvasc Res 2002;64:414-424.

3 Frame MD: Increased flow precedes remote arteriolar dilations for some microapplied agonists. Am J Physiol Heart Circ Physiol 2000;278:H1186-1195.

4 Frame MD: Conducted signals within arteriolar networks initiated by bioactive amino acids. Am J Physiol 1999;276:H1012-1021.

5 Karal-Yilmaz O, Serhatli M, Baysal K, Baysal BM: Preparation and in vitro characterization of vascular endothelial growth factor (vegf)-loaded poly(d,l-lactic-co-glycolic acid) microspheres using a double emulsion/solvent evaporation technique. Journal of microencapsulation;28:46-54.

6 Lochmann A, Nitzsche H, von Einem S, Schwarz E, Mader K: The influence of covalently linked and free polyethylene glycol on the structural and release properties of rhbmp-2 loaded microspheres. J Control Release;147:92-100.

7 Lee M, Wu BM, Stelzner M, Reichardt HM, Dunn JC: Intestinal smooth muscle cell maintenance by basic fibroblast growth factor. Tissue Eng Part A 2008;14:1395-1402.

8 Guan J, Stankus JJ, Wagner WR: Biodegradable elastomeric scaffolds with basic fibroblast growth factor release. J Control Release 2007;120:70-78.

9 Lee KW, Yoon JJ, Lee JH, Kim SY, Jung HJ, Kim SJ, Joh JW, Lee HH, Lee DS, Lee SK: Sustained release of vascular endothelial growth factor from calcium-induced alginate hydrogels reinforced by heparin and chitosan. Transplant Proc 2004;36:2464-2465.

10 Cote MF, Laroche G, Gagnon E, Chevallier P, Doillon CJ: Denatured collagen as support for a fgf-2 delivery system: Physicochemical characterizations and in vitro release kinetics and bioactivity. Biomaterials 2004;25:3761-3772.

11 Sahoo S, Ang LT, Goh JC, Toh SL: Growth factor delivery through electrospun nanofibers in scaffolds for tissue engineering applications. J Biomed Mater Res A 2010;93:1539-1550.

12 Nie H, Soh BW, Fu YC, Wang CH: Three-dimensional fibrous plga/hap composite scaffold for bmp-2 delivery. Biotechnol Bioeng 2008;99:223-234.

13 Choi JS, Yoo HS: Nano-inspired fibrous matrix with bi-phasic release of proteins. J Nanosci Nanotechnol 2010;10:3038-3045.

14 Crotts G, Park TG: Protein delivery from poly(lactic-co-glycolic acid) biodegradable microspheres: Release kinetics and stability issues. Journal of microencapsulation 1998;15:699-713.

15 Blanco D, Alonso MJ: Protein encapsulation and release from poly(lactide-co-glycolide) microspheres: Effect of the protein and polymer properties and of the co-encapsulation of surfactants. Eur J Pharm Biopharm 1998;45:285-294.

16 Shive MS, Anderson JM: Biodegradation and biocompatibility of pla and plga microspheres. Adv Drug Deliv Rev 1997;28:5-24.

17 Yang YY, Chung TS, Ng NP: Morphology, drug distribution, and in vitro release profiles of biodegradable polymeric microspheres containing protein fabricated by double-emulsion solvent extraction/evaporation method. Biomaterials 2001;22:231-241.

18 Bittner B, Witt C, Mader K, Kissel T: Degradation and protein release properties of microspheres prepared from biodegradable poly(lactide-co-glycolide) and aba triblock copolymers: Influence of buffer media on polymer erosion and bovine serum albumin release. J Control Release 1999;60:297-309.

19 Yang YY, Chia HH, Chung TS: Effect of preparation temperature on the characteristics and release profiles of plga microspheres containing protein fabricated by double-emulsion solvent extraction/evaporation method. J Control Release 2000;69:81-96.

20 Zheng X, Huang Y, Zheng C, Dong S, Liang W: Alginate-chitosan-plga composite microspheres enabling single-shot hepatitis b vaccination. The AAPS journal;12:519-524.

21 Yeo Y, Park K: Control of encapsulation efficiency and initial burst in polymeric microparticle systems. Arch Pharm Res 2004;27:1-12.

22 Kim JH, Taluja A, Knutson K, Han Bae Y: Stability of bovine serum albumin complexed with peg-poly(l-histidine) diblock copolymer in plga microspheres. J Control Release 2005;109:86-100.

23 Mallarde D, Boutignon F, Moine F, Barre E, David S, Touchet H, Ferruti P, Deghenghi R: Plga-peg microspheres of teverelix: Influence of polymer type on microsphere characteristics and on teverelix in vitro release. International journal of pharmaceutics 2003;261:69-80.

24 Hoffman AS, Ratner BD: Nonfouling surfaces; in Ratner BD, Hoffman AS, Schoen FJ, Lemons JE (eds): Biomaterials science: An introduction to materials in medicine. London, Elsevier Academic Press, 2004, pp 197-201.

25 Zheng CH, Gao JQ, Zhang YP, Liang WQ: A protein delivery system: Biodegradable alginate-chitosan-poly(lactic-co-glycolic acid) composite microspheres. Biochemical and biophysical research communications 2004;323:1321-1327.

26 Schoubben A, Blasi P, Giovagnoli S, Perioli L, Rossi C, Ricci M: Novel composite microparticles for protein stabilization and delivery. Eur J Pharm Sci 2009;36:226-234.

27 Wang Y, Gao JQ, Zheng CH, Xu DH, Liang WQ: Biodegradable and complexed microspheres used for sustained delivery and activity protection of sod. J Biomed Mater Res B Appl Biomater 2006;79:74-78.

28 Zheng C, Liang W: A one-step modified method to reduce the burst initial release from plga microspheres. Drug delivery;17:77-82.

29 Ouchi T, Nishizawa H: Aggregation phenomenon of peg-grafted chitosan in aqueous solution. Polymer 1998;39:5171-5175.

30 Jiang H, Fang D, Hsiao B, Chu B, Chen W: Preparation and characterization of ibuprofen-loaded poly(lactide-co-glycolide)/poly(ethylene glycol)-g-chitosan electrospun membranes. Journal of biomaterials science 2004;15:279-296.

31 Ray NF, Denton WG, Thamer M, Henderson SC, Perry S: Abdominal adhesiolysis: Inpatient care and expenditures in the united states in 1994. Journal of the American College of Surgeons 1998;186:1-9.

32 Ellis H: The clinical significance of adhesions: Focus on intestinal obstruction. Eur J Surg Suppl 1997:5-9.

33 Liakakos T, Thomakos N, Fine PM, Dervenis C, Young RL: Peritoneal adhesions: Etiology, pathophysiology, and clinical significance. Recent advances in prevention and management. Digestive surgery 2001;18:260-273.

34 diZerega GS, Campeau JD: Peritoneal repair and post-surgical adhesion formation. Hum Reprod Update 2001;7:547-555.

35 Boland GM, Weigel RJ: Formation and prevention of postoperative abdominal adhesions. The Journal of surgical research 2006;132:3-12.

36 Ar'Rajab A, Dawidson I, Sentementes J, Sikes P, Harris R, Mileski W: Enhancement of peritoneal macrophages reduces postoperative peritoneal adhesion formation. The Journal of surgical research 1995;58:307-312.

37 Milligan DW, Raftery AT: Observations on the pathogenesis of peritoneal adhesions: A light and electron microscopical study. The British journal of surgery 1974;61:274-280.

38 Markogiannakis H, Messaris E, Dardamanis D, Pararas N, Tzertzemelis D, Giannopoulos P, Larentzakis A, Lagoudianakis E, Manouras A, Bramis I: Acute mechanical bowel obstruction: Clinical presentation, etiology, management and outcome. World J Gastroenterol 2007;13:432-437.

39 Osada H, Takahashi K, Fujii TK, Tsunoda I, Satoh K: The effect of cross-linked hyaluronate hydrogel on the reduction of post-surgical adhesion reformation in rabbits. The Journal of international medical research 1999;27:233-241.

40 Tittel A, Treutner KH, Titkova S, Ottinger A, Schumpelick V: Comparison of adhesion reformation after laparoscopic and conventional adhesiolysis in an animal model. Langenbecks Arch Surg 2001;386:141-145.

41 Saravelos HG, Li TC: Physical barriers in adhesion prevention. J Reprod Med 1996;41:42-51.

42 Gago LA, Saed GM, Chauhan S, Elhammady EF, Diamond MP: Seprafilm (modified hyaluronic acid and carboxymethylcellulose) acts as a physical barrier. Fertility and sterility 2003;80:612-616.

43 Harris ES, Morgan RF, Rodeheaver GT: Analysis of the kinetics of peritoneal adhesion formation in the rat and evaluation of potential antiadhesive agents. Surgery 1995;117:663-669.

44 Haney AF, Doty E: Murine peritoneal injury and de novo adhesion formation caused by oxidized-regenerated cellulose (interceed [tc7]) but not expanded polytetrafluoroethylene (gore-tex surgical membrane). Fertility and sterility 1992;57:202-208.

45 DeCherney AH, diZerega GS: Clinical problem of intraperitoneal postsurgical adhesion formation following general surgery and the use of adhesion prevention barriers. The Surgical clinics of North America 1997;77:671-688.

46 Larsson B: Efficacy of interceed in adhesion prevention in gynecologic surgery: A review of 13 clinical studies. J Reprod Med 1996;41:27-34.

47 Robertson D, Lefebvre G, Leyland N, Wolfman W, Allaire C, Awadalla A, Best C, Contestabile E, Dunn S, Heywood M, Leroux N, Potestio F, Rittenberg D, Senikas V, Soucy R, Singh S: Adhesion prevention in gynaecological surgery. J Obstet Gynaecol Can;32:598-608.

48 Arnold PB, Green CW, Foresman PA, Rodeheaver GT: Evaluation of resorbable barriers for preventing surgical adhesions. Fertility and sterility 2000;73:157-161.

49 Best CL, Rittenhouse D, Vasquez C, Norng T, Subias E, Sueldo CE: Evaluation of interceed(tc7) for reduction of postoperative adhesions in rabbits. Fertility and sterility 1992;58:817-820.

50 Diamond MP: Reduction of adhesions after uterine myomectomy by seprafilm membrane (hal-f): A blinded, prospective, randomized, multicenter clinical study. Seprafilm adhesion study group. Fertility and sterility 1996;66:904-910.

51 Vrijland WW, Tseng LN, Eijkman HJ, Hop WC, Jakimowicz JJ, Leguit P, Stassen LP, Swank DJ, Haverlag R, Bonjer HJ, Jeekel H: Fewer intraperitoneal adhesions with use of hyaluronic acid-carboxymethylcellulose membrane: A randomized clinical trial. Annals of surgery 2002;235:193-199.

52 Goldberg EP, Burns JW, Yaacobi Y: Prevention of postoperative adhesions by precoating tissues with dilute sodium hyaluronate solutions. Prog Clin Biol Res 1993;381:191-204.

53 Burns JW, Skinner K, Colt J, Sheidlin A, Bronson R, Yaacobi Y, Goldberg EP: Prevention of tissue injury and postsurgical adhesions by precoating tissues with hyaluronic acid solutions. The Journal of surgical research 1995;59:644-652.

54 Chen WY, Abatangelo G: Functions of hyaluronan in wound repair. Wound Repair Regen 1999;7:79-89.

55 Nehls V, Hayen W: Are hyaluronan receptors involved in three-dimensional cell migration? Histol Histopathol 2000;15:629-636.

56 Tsai SW, Fang JF, Yang CL, Chen JH, Su LT, Jan SH: Preparation and evaluation of a hyaluronate-collagen film for preventing post-surgical adhesion. The Journal of international medical research 2005;33:68-76.

57 Belluco C, Meggiolaro F, Pressato D, Pavesio A, Bigon E, Dona M, Forlin M, Nitti D, Lise M: Prevention of postsurgical adhesions with an autocrosslinked hyaluronan derivative gel. The Journal of surgical research 2001;100:217-221.

58 Sikkink CJ, de Man B, Bleichrodt RP, van Goor H: Auto-cross-linked hyaluronic acid gel does not reduce intra-abdominal adhesions or abscess formation in a rat model of peritonitis. The Journal of surgical research 2006;136:255-259.

59 Grainger DA, Meyer WR, DeCherney AH, Diamond MP: The use of hyaluronic acid polymers to reduce post-operative adhesions. Journal of gynecologic surgery 1991;7:97-101.

60 Liu Y, Skardal A, Shu XZ, Prestwich GD: Prevention of peritendinous adhesions using a hyaluronan-derived hydrogel film following partial-thickness flexor tendon injury. J Orthop Res 2008;26:562-569.

61 Yeo Y, Highley CB, Bellas E, Ito T, Marini R, Langer R, Kohane DS: In situ cross-linkable hyaluronic acid hydrogels prevent post-operative abdominal adhesions in a rabbit model. Biomaterials 2006;27:4698-4705.

62 Kim AP, Yellen P, Yun YH, Azeloglu E, Chen W: Delivery of a vector encoding mouse hyaluronan synthase 2 via a crosslinked hyaluronan film. Biomaterials 2005;26:1585-1593.

63 Liu Y, Li H, Shu XZ, Gray SD, Prestwich GD: Crosslinked hyaluronan hydrogels containing mitomycin c reduce postoperative abdominal adhesions. Fertility and sterility 2005;83 Suppl 1:1275-1283.

64 Fda statement: Urgent global market withdrawal: Gynecare intergel adhesion prevention solution voluntarily withdrawn from the market by gynecare worldwide: http://www.fda.gov/Safety/MedWatch/SafetyInformation/SafetyAlertsforHumanMedicalProducts/ucm170010.htm November 11, 2010

65 Ikada Y: Biological materials; in Barbucci R (ed): Integrated biomaterial science. New York, Kluwer Academic/Plenum Publishers, 2002, pp 1-23.

66 Tomihata K, Ikada Y: In vitro and in vivo degradation of films of chitin and its deacetylated derivatives. Biomaterials 1997;18:567-575.

67 Kennedy R, Costain DJ, McAlister VC, Lee TD: Prevention of experimental postoperative peritoneal adhesions by n,o-carboxymethyl chitosan. Surgery 1996;120:866-870.

68 Krauland AH, Guggi D, Bernkop-Schnurch A: Thiolated chitosan microparticles: A vehicle for nasal peptide drug delivery. International journal of pharmaceutics 2006;307:270-277.

69 Rokhade AP, Shelke NB, Patil SA, Aminabhavi TM: Novel hydrogel microspheres of chitosan and pluronic f-127 for controlled release of 5-fluorouracil. Journal of microencapsulation 2007;24:274-288.

70 Zhou J, Elson C, Lee TD: Reduction in postoperative adhesion formation and re-formation after an abdominal operation with the use of n, o - carboxymethyl chitosan. Surgery 2004;135:307-312.

71 Yeo Y, Burdick JA, Highley CB, Marini R, Langer R, Kohane DS: Peritoneal application of chitosan and uv-cross-linkable chitosan. J Biomed Mater Res A 2006;78:668-675.

72 Weng L, Chen X, Chen W: Rheological characterization of in situ crosslinkable hydrogels formulated from oxidized dextran and n-carboxyethyl chitosan. Biomacromolecules 2007;8:1109-1115.

73 Jiang H, Wang Y, Huang Q, Li Y, Xu C, Zhu K, Chen W: Biodegradable hyaluronic acid/n-carboxyethyl chitosan/protein ternary complexes as implantable carriers for controlled protein release. Macromolecular bioscience 2005;5:1226-1233.

74 Draye JP, Delaey B, Van de Voorde A, Van Den Bulcke A, Bogdanov B, Schacht E: In vitro release characteristics of bioactive molecules from dextran dialdehyde cross-linked gelatin hydrogel films. Biomaterials 1998;19:99-107.

75 Weng L, Romanov A, Rooney J, Chen W: Non-cytotoxic, in situ gelable hydrogels composed of n-carboxyethyl chitosan and oxidized dextran. Biomaterials 2008;29:3905-3913.

76 Toda N, Nakanishi-Toda M: Nitric oxide: Ocular blood flow, glaucoma, and diabetic retinopathy. Progress in retinal and eye research 2007;26:205-238.

77 Lee RH, Efron D, Tantry U, Barbul A: Nitric oxide in the healing wound: A time-course study. The Journal of surgical research 2001;101:104-108.

78 Lohinai Z, Benedek P, Feher E, Gyorfi A, Rosivall L, Fazekas A, Salzman AL, Szabo C: Protective effects of mercaptoethylguanidine, a selective inhibitor of inducible nitric oxide synthase, in ligature-induced periodontitis in the rat. British journal of pharmacology 1998;123:353-360.

79 Padalko E, Ohnishi T, Matsushita K, Sun H, Fox-Talbot K, Bao C, Baldwin WM, 3rd, Lowenstein CJ: Peroxynitrite inhibition of coxsackievirus infection by prevention of viral rna entry. Proceedings of the National Academy of Sciences of the United States of America 2004;101:11731-11736.

80 Schaffer MR, Tantry U, Ahrendt GM, Wasserkrug HL, Barbul A: Stimulation of fibroblast proliferation and matrix contraction by wound fluid. The international journal of biochemistry & cell biology 1997;29:231-239.

81 Schaffer MR, Tantry U, van Wesep RA, Barbul A: Nitric oxide metabolism in wounds. The Journal of surgical research 1997;71:25-31.

82 Babich H, Zuckerbraun HL, Hirsch ST, Blau L: In vitro cytotoxicity of the nitric oxide donor, s-nitroso-n-acetyl-penicillamine, towards cells from human oral tissue. Pharmacology & toxicology 1999;84:218-225.

83 Paquette DW, Rosenberg A, Lohinai Z, Southan GJ, Williams RC, Offenbacher S, Szabo C: Inhibition of experimental gingivitis in beagle dogs with topical mercaptoalkylguanidines. Journal of periodontology 2006;77:385-391.

84 Schaffer MR, Efron PA, Thornton FJ, Klingel K, Gross SS, Barbul A: Nitric oxide, an autocrine regulator of wound fibroblast synthetic function. J Immunol 1997;158:2375-2381.

85 Schaffer MR, Tantry U, Gross SS, Wasserburg HL, Barbul A: Nitric oxide regulates wound healing. The Journal of surgical research 1996;63:237-240.

86 Cuzzocrea S, Zingarelli B, Hake P, Salzman AL, Szabo C: Antiinflammatory effects of mercaptoethylguanidine, a combined inhibitor of nitric oxide synthase and peroxynitrite scavenger, in carrageenan-induced models of inflammation. Free radical biology & medicine 1998;24:450-459.

87 Zingarelli B, Cuzzocrea S, Szabo C, Salzman AL: Mercaptoethylguanidine, a combined inhibitor of nitric oxide synthase and peroxynitrite scavenger, reduces trinitrobenzene sulfonic acid-induced colonic damage in rats. The Journal of pharmacology and experimental therapeutics 1998;287:1048-1055.

88 Bao F, DeWitt DS, Prough DS, Liu D: Peroxynitrite generated in the rat spinal cord induces oxidation and nitration of proteins: Reduction by mn (iii) tetrakis (4-benzoic acid) porphyrin. J Neurosci Res 2003;71:220-227.

89 Brahn E, Banquerigo ML, Firestein GS, Boyle DL, Salzman AL, Szabo C: Collagen induced arthritis: Reversal by mercaptoethylguanidine, a novel antiinflammatory agent with a combined mechanism of action. The Journal of rheumatology 1998;25:1785-1793.

90 Wilmott RW, Kitzmiller JA, Szabo C, Southan GJ, Salzman AL: Mercaptoethylguanidine inhibits the inflammatory response in a murine model of chronic

infection with pseudomonas aeruginosa. The Journal of pharmacology and experimental therapeutics 2000;292:88-95.

91 Szabo C, Bryk R, Zingarelli B, Southan GJ, Gahman TC, Bhat V, Salzman AL, Wolff DJ: Pharmacological characterization of guanidinoethyldisulphide (ged), a novel inhibitor of nitric oxide synthase with selectivity towards the inducible isoform. British journal of pharmacology 1996;118:1659-1668.

92 Szabo C, Ferrer-Sueta G, Zingarelli B, Southan GJ, Salzman AL, Radi R: Mercaptoethylguanidine and guanidine inhibitors of nitric-oxide synthase react with peroxynitrite and protect against peroxynitrite-induced oxidative damage. The Journal of biological chemistry 1997;272:9030-9036.

93 Southan GJ, Zingarelli B, O'Connor M, Salzman AL, Szabo C: Spontaneous rearrangement of aminoalkylisothioureas into mercaptoalkylguanidines, a novel class of nitric oxide synthase inhibitors with selectivity towards the inducible isoform. British journal of pharmacology 1996;117:619-632.

94 Freitas S, Merkle HP, Gander B: Microencapsulation by solvent extraction/evaporation: Reviewing the state of the art of microsphere preparation process technology. J Control Release 2005;102:313-332.

95 Agnihotri SA, Aminabhavi TM: Novel interpenetrating network chitosan-poly(ethylene oxide-g-acrylamide) hydrogel microspheres for the controlled release of capecitabine. International journal of pharmaceutics 2006;324:103-115.

96 Yun YH, Jiang H, Chan R, Chen W: Sustained release of peg-g-chitosan complexed DNA from poly(lactide-co-glycolide). Journal of biomaterials science 2005;16:1357-1378.

97 Mohamed F, van der Walle CF: Plga microcapsules with novel dimpled surfaces for pulmonary delivery of DNA. International journal of pharmaceutics 2006;311:97-107.

98 Khan A, Benboubetra M, Sayyed PZ, Ng KW, Fox S, Beck G, Benter IF, Akhtar S: Sustained polymeric delivery of gene silencing antisense odns, sirna, dnazymes and ribozymes: In vitro and in vivo studies. Journal of drug targeting 2004;12:393-404.

99 Zhang JX, Chen D, Wang SJ, Zhu KJ: Optimizing double emulsion process to decrease the burst release of protein from biodegradable polymer microspheres. Journal of microencapsulation 2005;22:413-422.

100 Waeckerle-Men Y, Allmen EU, Gander B, Scandella E, Schlosser E, Schmidtke G, Merkle HP, Groettrup M: Encapsulation of proteins and peptides into biodegradable poly(d,l-lactide-co-glycolide) microspheres prolongs and enhances antigen presentation by human dendritic cells. Vaccine 2006;24:1847-1857.

101 Hejazi R, Amiji M: Chitosan-based gastrointestinal delivery systems. J Control Release 2003;89:151-165.

102 King TW, Patrick CW, Jr.: Development and in vitro characterization of vascular endothelial growth factor (vegf)-loaded poly(dl-lactic-co-glycolic acid)/poly(ethylene glycol) microspheres using a solid encapsulation/single emulsion/solvent extraction technique. Journal of biomedical materials research 2000;51:383-390.

103 Cao X, Schoichet MS: Delivering neuroactive molecules from biodegradable microspheres for application in central nervous system disorders. Biomaterials 1999;20:329-339.

104 Zhang JX, Zhu KJ, Chen D: Preparation of bovine serum albumin loaded poly (d, l-lactic-co-glycolic acid) microspheres by a modified phase separation technique. Journal of microencapsulation 2005;22:117-126.

105 Diwan M, Park TG: Pegylation enhances protein stability during encapsulation in plga microspheres. J Control Release 2001;73:233-244.

106 Kang J, Schwendeman SP: Comparison of the effects of mg(oh)2 and sucrose on the stability of bovine serum albumin encapsulated in injectable poly(d,l-lactide-co-glycolide) implants. Biomaterials 2002;23:239-245.

107 Croll TI, O'Connor AJ, Stevens GW, Cooper-White JJ: A blank slate? Layer-by-layer deposition of hyaluronic acid and chitosan onto various surfaces. Biomacromolecules 2006;7:1610-1622.

108 Kumar MN, Mohapatra SS, Kong X, Jena PK, Bakowsky U, Lehr CM: Cationic poly(lactide-co-glycolide) nanoparticles as efficient in vivo gene transfection agents. J Nanosci Nanotechnol 2004;4:990-994.

109 Koning GA, Schiffelers RM, Wauben MH, Kok RJ, Mastrobattista E, Molema G, ten Hagen TL, Storm G: Targeting of angiogenic endothelial cells at sites of inflammation by dexamethasone phosphate-containing rgd peptide liposomes inhibits experimental arthritis. Arthritis Rheum 2006;54:1198-1208.

110 Yang A, Yang L, Liu W, Li Z, Xu H, Yang X: Tumor necrosis factor alpha blocking peptide loaded peg-plga nanoparticles: Preparation and in vitro evaluation. International journal of pharmaceutics 2007;331:123-132.

111 Li Y, Pei Y, Zhang X, Gu Z, Zhou Z, Yuan W, Zhou J, Zhu J, Gao X: Pegylated plga nanoparticles as protein carriers: Synthesis, preparation and biodistribution in rats. J Control Release 2001;71:203-211.

112 Felt O, Buri P, Gurny R: Chitosan: A unique polysaccharide for drug delivery. Drug development and industrial pharmacy 1998;24:979-993.

113 Montembault A, Tahiri K, Korwin-Zmijowska C, Chevalier X, Corvol MT, Domard A: A material decoy of biological media based on chitosan physical hydrogels: Application to cartilage tissue engineering. Biochimie 2006;88:551-564.

114 Zhang M, Li XH, Gong YD, Zhao NM, Zhang XF: Properties and biocompatibility of chitosan films modified by blending with peg. Biomaterials 2002;23:2641-2648.

115 Frame MD, Miano JM, Yang J, Rivers RJ: Localized adenovirus-mediated gene transfer into vascular smooth muscle in the hamster cheek pouch. Microcirculation 2001;8:403-413.

116 Nishimura S, Kohgo O, Kurita K, Kuzuhara H: Chemospecific manipulations of a rigid polysaccharide: Synthesis of novel chitosan derivatives with excellent solubility in common organic solvents by regioselective chemical modifications. Macromolecules 1991;24:4745-4748.

117 Berg BR, Sarelius IH: Functional capillary organization in striated muscle. Am J Physiol 1995;268:H1215-1222.

118 Frame MD, Sarelius IH: L-arginine-induced conducted signals alter upstream arteriolar responsivity to l-arginine. Circ Res 1995;77:695-701.

119 Snedecor GW, Cochran WG: Statistical methods, ed 6th. Ames, The Iowa State University Press, 1974.

120 Coleman AB, Momand J, Kane SE: Basic fibroblast growth factor sensitizes nih 3t3 cells to apoptosis induced by cisplatin. Molecular pharmacology 2000;57:324-333.

121 Ignjatovic N, Ninkov P, Kojic V, Bokurov M, Srdic V, Krnojelac D, Selakovic S, Uskokovic D: Cytotoxicity and fibroblast properties during in vitro test of biphasic calcium phosphate/poly-dl-lactide-co-glycolide biocomposites and different phosphate materials. Microscopy research and technique 2006;69:976-982.

122 Kang F, Singh J: Preparation, in vitro release, in vivo absorption and biocompatibility studies of insulin-loaded microspheres in rabbits. AAPS PharmSciTech 2005;6:E487-494.

123 Rucker M, Laschke MW, Junker D, Carvalho C, Schramm A, Mulhaupt R, Gellrich NC, Menger MD: Angiogenic and inflammatory response to biodegradable scaffolds in dorsal skinfold chambers of mice. Biomaterials 2006;27:5027-5038.

124 Enriquez de Salamanca A, Diebold Y, Calonge M, Garcia-Vazquez C, Callejo S, Vila A, Alonso MJ: Chitosan nanoparticles as a potential drug delivery system for the ocular surface: Toxicity, uptake mechanism and in vivo tolerance. Investigative ophthalmology & visual science 2006;47:1416-1425.

125 Obara K, Ishihara M, Fujita M, Kanatani Y, Hattori H, Matsui T, Takase B, Ozeki Y, Nakamura S, Ishizuka T, Tominaga S, Hiroi S, Kawai T, Maehara T: Acceleration of wound healing in healing-impaired db/db mice with a photocrosslinkable chitosan hydrogel containing fibroblast growth factor-2. Wound Repair Regen 2005;13:390-397.

126 Faure JP, Hauet T, Han Z, Goujon JM, Petit I, Mauco G, Eugene M, Carretier M, Papadopoulos V: Polyethylene glycol reduces early and long-term cold ischemia-reperfusion and renal medulla injury. The Journal of pharmacology and experimental therapeutics 2002;302:861-870.

127 Li P, Oparil S, Sun JZ, Thompson JA, Chen YF: Fibroblast growth factor mediates hypoxia-induced endothelin-- a receptor expression in lung artery smooth muscle cells. J Appl Physiol 2003;95:643-651; discussion 863.

128 Spieker LE, Flammer AJ, Luscher TF: The vascular endothelium in hypertension. Handb Exp Pharmacol 2006:249-283.

129 Samora JB, Frisbee JC, Boegehold MA: Growth-dependent changes in endothelial factors regulating arteriolar tone. Am J Physiol Heart Circ Physiol 2007;292:H207-214.

130 Sandow SL, Goto K, Rummery NM, Hill CE: Developmental changes in myoendothelial gap junction mediated vasodilator activity in the rat saphenous artery. J Physiol 2004;556:875-886.

131 Hellebrekers BW, Trimbos-Kemper GC, Bakkum EA, Trimbos JB, Declerck PJ, Kooistra T, Emeis JJ: Short-term effect of surgical trauma on rat peritoneal fibrinolytic activity and its role in adhesion formation. Thromb Haemost 2000;84:876-881.

132 Dou Q, Williams RS, Chegini N: Inhibition of transforming growth factor-beta 1 alters the growth, anchor-dependent cell aggregation and integrin mrna expression in human promonocytes: Implications for endometriosis and peritoneal adhesion formation. Mol Hum Reprod 1997;3:383-391.

133 Ishihara K, Yamaguchi Y, Okabe K, Ogawa M: Neutrophil elastase enhances macrophage production of chemokines in receptor-mediated reaction. Research communications in molecular pathology and pharmacology 1999;103:139-147.

134 Tulandi T: Adhesion prevention in laparoscopic surgery. Int J Fertil Menopausal Stud 1996;41:452-457.

135 Wiseman DM, Gottlick LE, Diamond MP: Effect of thrombin-induced hemostasis on the efficacy of an absorbable adhesion barrier. J Reprod Med 1992;37:766-770.

136 Numanoglu V, Cihan A, Salman B, Ucan BH, Cakmak GK, Cesur A, Balbaloglu H, Ilhan MN: Comparison between powdered gloves, powder-free gloves and hyaluronate/carboxymethylcellulose membrane on adhesion formation in a rat caecal serosal abrasion model. Asian journal of surgery / Asian Surgical Association 2007;30:96-101.

137 Menzies D, Ellis H: Intestinal obstruction from adhesions--how big is the problem? Annals of the Royal College of Surgeons of England 1990;72:60-63.

138 Menzies D: Postoperative adhesions: Their treatment and relevance in clinical practice. Annals of the Royal College of Surgeons of England 1993;75:147-153.

139 Ghellai AM, Stucchi AF, Lynch DJ, Skinner KC, Colt MJ, Becker JM: Role of a hyaluronate-based membrane in the prevention of peritonitis-induced adhesions. J Gastrointest Surg 2000;4:310-315.

140 Tuzuner A, Kuzu MA, Akin B, Karaca S, Hazinedaroglu S: The effect of hyaluronan-based agents on adhesion formation in an intraabdominal sepsis model. Dig Dis Sci 2004;49:1054-1061.

141 Schimizzi AL, Massie JB, Murphy M, Perry A, Kim CW, Garfin SR, Akeson WH: High-molecular-weight hyaluronan inhibits macrophage proliferation and cytokine release in the early wound of a preclinical postlaminectomy rat model. Spine J 2006;6:550-556.

142 Cashman J, Burt HM, Springate C, Gleave J, Jackson JK: Camptothecin-loaded films for the prevention of postsurgical adhesions. Inflamm Res 2004;53:355-362.

143 Park SN, Jang HJ, Choi YS, Cha JM, Son SY, Han SH, Kim JH, Lee WJ, Suh H: Preparation and characterization of biodegradable anti-adhesive membrane for peritoneal wound healing. Journal of materials science 2007;18:475-482.

144 Zong X, Li S, Chen E, Garlick B, Kim KS, Fang D, Chiu J, Zimmerman T, Brathwaite C, Hsiao BS, Chu B: Prevention of postsurgery-induced abdominal adhesions by electrospun bioabsorbable nanofibrous poly(lactide-co-glycolide)-based membranes. Annals of surgery 2004;240:910-915.

145 Falabella CA, Melendez MM, Weng L, Chen W: Novel macromolecular crosslinking hydrogel to reduce intra-abdominal adhesions. Journal of Surgical Research 2009;In Press

146 Leach RE, Burns JW, Dawe EJ, SmithBarbour MD, Diamond MP: Reduction of postsurgical adhesion formation in the rabbit uterine horn model with use of hyaluronate/carboxymethylcellulose gel. Fertility and sterility 1998;69:415-418.

147 Yaacobi Y, Israel AA, Goldberg EP: Prevention of postoperative abdominal adhesions by tissue precoating with polymer solutions. The Journal of surgical research 1993;55:422-426.

148 Liu Y, Zheng Shu X, Prestwich GD: Biocompatibility and stability of disulfide-crosslinked hyaluronan films. Biomaterials 2005;26:4737-4746.

149 Weng L, Pan H, Chen W: Self-crosslinkable hydrogels composed of partially oxidized hyaluronan and gelatin: In vitro and in vivo responses. J Biomed Mater Res A 2008;85:352-365.

150 Duranti F, Salti G, Bovani B, Calandra M, Rosati ML: Injectable hyaluronic acid gel for soft tissue augmentation. A clinical and histological study. Dermatol Surg 1998;24:1317-1325.

151 Kimmelman CP, Edelstein DR, Cheng HJ: Sepragel sinus (hylan b) as a postsurgical dressing for endoscopic sinus surgery. Otolaryngol Head Neck Surg 2001;125:603-608.

152 Kayaoglu HA, Ozkan N, Hazinedaroglu SM, Ersoy OF, Koseoglu RD: An assessment of the effects of two types of bioresorbable barriers to prevent postoperative intra-abdominal adhesions in rats. Surg Today 2005;35:946-950.

153 Boraldi F, Croce MA, Quaglino D, Sammarco R, Carnevali E, Tiozzo R, Pasquali-Ronchetti I: Cell-matrix interactions of in vitro human skin fibroblasts upon addition of hyaluronan. Tissue & cell 2003;35:37-45.

154 Longaker MT, Chiu ES, Adzick NS, Stern M, Harrison MR, Stern R: Studies in fetal wound healing. V. A prolonged presence of hyaluronic acid characterizes fetal wound fluid. Annals of surgery 1991;213:292-296.

155 Postoperative adhesion development after operative laparoscopy: Evaluation at early second-look procedures. Operative laparoscopy study group. Fertility and sterility 1991;55:700-704.

156 Alpay Z, Saed GM, Diamond MP: Postoperative adhesions: From formation to prevention. Semin Reprod Med 2008;26:313-321.

157 De Iaco PA, Muzzupapa G, Bigon E, Pressato D, Dona M, Pavesio A, Bovicelli L: Efficacy of a hyaluronan derivative gel in postsurgical adhesion prevention in the presence of inadequate hemostasis. Surgery 2001;130:60-64.

158 Mais V, Bracco GL, Litta P, Gargiulo T, Melis GB: Reduction of postoperative adhesions with an auto-crosslinked hyaluronan gel in gynaecological laparoscopic surgery: A blinded, controlled, randomized, multicentre study. Human reproduction (Oxford, England) 2006;21:1248-1254.

159 Lundorff P, van Geldorp H, Tronstad SE, Lalos O, Larsson B, Johns DB, diZerega GS: Reduction of post-surgical adhesions with ferric hyaluronate gel: A european study. Human reproduction (Oxford, England) 2001;16:1982-1988.

160 Hirano S: Chitin biotechnology applications. Biotechnology annual review 1996;2:237-258.

161 Khor E, Lim LY: Implantable applications of chitin and chitosan. Biomaterials 2003;24:2339-2349.

162 Mehvar R: Dextrans for targeted and sustained delivery of therapeutic and imaging agents. J Control Release 2000;69:1-25.

163 Hennink WE, van Nostrum CF: Novel crosslinking methods to design hydrogels. Adv Drug Deliv Rev 2002;54:13-36.

164 Buckenmaier CC, 3rd, Pusateri AE, Harris RA, Hetz SP: Comparison of antiadhesive treatments using an objective rat model. The American surgeon 1999;65:274-282.

165 Bancroft JD, Cook HC: Manual of histological techniques. Edinburgh, Churchill Livingstone, 1984.

166 S.diZerega GCJD: Peritoneal repair and post-surgical adhesion formation. Human Reproduction Update 2001;7:547-555.

167 Dunn R, Lyman MD, Edelman PG, Campbell PK: Evaluation of the spraygel adhesion barrier in the rat cecum abrasion and rabbit uterine horn adhesion models. Fertility and sterility 2001;75:411-416.

168 Cadee JA, van Luyn MJ, Brouwer LA, Plantinga JA, van Wachem PB, de Groot CJ, den Otter W, Hennink WE: In vivo biocompatibility of dextran-based hydrogels. Journal of biomedical materials research 2000;50:397-404.

169 Risberg B: Adhesions: Preventive strategies. Eur J Surg Suppl 1997:32-39.

170 Anderson JM: Inflammation, wound healing, and the foreign body response; in Ratner BD, Hoffman AS, Schoen FJ, Lemons JE (eds): Biomaterials science: An introduction to materials in medicine. San Diego, Elsevier Academic Press, 2004, pp 296-304.

171 Chuang YC, Fan CN, Cho FN, Kan YY, Chang YH, Kang HY: A novel technique to apply a seprafilm (hyaluronate-carboxymethylcellulose) barrier following laparoscopic surgeries. Fertility and sterility 2008

172 Packer MA, Porteous CM, Murphy MP: Superoxide production by mitochondria in the presence of nitric oxide forms peroxynitrite. Biochem Mol Biol Int 1996;40:527-534.

173 Pacher P, Beckman JS, Liaudet L: Nitric oxide and peroxynitrite in health and disease. Physiol Rev 2007;87:315-424.

174 Beckman JS: Oxidative damage and tyrosine nitration from peroxynitrite. Chem Res Toxicol 1996;9:836-844.

175 Okano H, Ogawa Y, Nakamura M, Kaneko S, Iwanami A, Toyama Y: Transplantation of neural stem cells into the spinal cord after injury. Semin Cell Dev Biol 2003;14:191-198.

176 Garbossa D, Fontanella M, Fronda C, Benevello C, Muraca G, Ducati A, Vercelli A: New strategies for repairing the injured spinal cord: The role of stem cells. Neurol Res 2006;28:500-504.

177 Yu D, Neeley WL, Pritchard CD, Slotkin JR, Woodard EJ, Langer R, Teng YD: Blockade of peroxynitrite-induced neural stem cell death in the acutely injured spinal cord by drug-releasing polymer. Stem Cells 2009;27:1212-1222.

178 Lakey JR, Suarez-Pinzon WL, Strynadka K, Korbutt GS, Rajotte RV, Mabley JG, Szabo C, Rabinovitch A: Peroxynitrite is a mediator of cytokine-induced destruction of human pancreatic islet beta cells. Laboratory investigation; a journal of technical methods and pathology 2001;81:1683-1692.

179 Suarez-Pinzon WL, Mabley JG, Strynadka K, Power RF, Szabo C, Rabinovitch A: An inhibitor of inducible nitric oxide synthase and scavenger of peroxynitrite prevents diabetes development in nod mice. Journal of autoimmunity 2001;16:449-455.

180 Zingarelli B, Day B, Crapo JD, Salzman AL, Szabo C: The potential role of peroxynitrite in the vascular contractile and cellular energetic failure in endotoxin shock. British journal of pharmacology 1997;120:259-267.

181 Satake K, Matsuyama Y, Kamiya M, Kawakami H, Iwata H, Adachi K, Kiuchi K: Nitric oxide via macrophage inos induces apoptosis following traumatic spinal cord injury. Brain Res Mol Brain Res 2000;85:114-122.

182 Southan GJ, Szabo C: Selective pharmacological inhibition of distinct nitric oxide synthase isoforms. Biochemical pharmacology 1996;51:383-394.

183 Falabella CA, Melendez MM, Weng L, Chen W: Novel macromolecular crosslinking hydrogel to reduce intra-abdominal adhesions. The Journal of surgical research 2009

184 Elfick AP, Green SM, McCaskie AW, Birch MA: Opsonization of polyethylene wear particles regulates macrophage and osteoblast responses in vitro. J Biomed Mater Res B Appl Biomater 2004;71:244-251.

185 ASTM: Standard practice for testing biological responses to particles in vitro. West Conshohocken, PA, ASTM International, 2010, F1903-10, pp 4.

186 Ingram JH, Stone M, Fisher J, Ingham E: The influence of molecular weight, crosslinking and counterface roughness on tnf-alpha production by macrophages in response to ultra high molecular weight polyethylene particles. Biomaterials 2004;25:3511-3522.

187 Claudio E, Segade F, Wrobel K, Ramos S, Lazo PS: Activation of murine macrophages by silica particles in vitro is a process independent of silica-induced cell death. Am J Respir Cell Mol Biol 1995;13:547-554.

188 Chapekar MS, Zaremba TG, Kuester RK, Hitchins VM: Synergistic induction of tumor necrosis factor alpha by bacterial lipopolysaccharide and lipoteichoic acid in combination with polytetrafluoroethylene particles in a murine macrophage cell line raw 264.7. Journal of biomedical materials research 1996;31:251-256.

189 Huang SL, Cheng WL, Lee CT, Huang HC, Chan CC: Contribution of endotoxin in macrophage cytokine response to ambient particles in vitro. J Toxicol Environ Health A 2002;65:1261-1272.

190 Weghofer M, Karlic H, Haslberger A: Quantitative analysis of immune-mediated stimulation of tumor necrosis factor-alpha in macrophages measured at the level of mrna and protein synthesis. Ann Hematol 2001;80:733-736.

191 Yim ES, Zhao B, Myung D, Kourtis LC, Frank CW, Carter D, Smith RL, Goodman SB: Biocompatibility of poly(ethylene glycol)/poly(acrylic acid) interpenetrating polymer network hydrogel particles in raw 264.7 macrophage and mg-63 osteoblast cell lines. J Biomed Mater Res A 2009;91:894-902.

192 Kwon YM, Xia Z, Glyn-Jones S, Beard D, Gill HS, Murray DW: Dose-dependent cytotoxicity of clinically relevant cobalt nanoparticles and ions on macrophages in vitro. Biomedical materials (Bristol, England) 2009;4:025018.

193 Suzuki Y, Nishiyama T, Hasuda K, Fujishiro T, Niikura T, Hayashi S, Hashimoto S, Kurosaka M: Effect of etidronate on cox-2 expression and pge(2) production in macrophage-like raw 264.7 cells stimulated by titanium particles. J Orthop Sci 2007;12:568-577.

194 Choi J, Zhang Q, Reipa V, Wang NS, Stratmeyer ME, Hitchins VM, Goering PL: Comparison of cytotoxic and inflammatory responses of photoluminescent silicon nanoparticles with silicon micron-sized particles in raw 264.7 macrophages. J Appl Toxicol 2009;29:52-60.

195 Scarfi S, Magnone M, Ferraris C, Pozzolini M, Benvenuto F, Benatti U, Giovine M: Ascorbic acid pre-treated quartz stimulates tnf-alpha release in raw 264.7 murine macrophages through ros production and membrane lipid peroxidation. Respir Res 2009;10:25.

196 Bailey LO, Lippiatt S, Biancanello FS, Ridder SD, Washburn NR: The quantification of cellular viability and inflammatory response to stainless steel alloys. Biomaterials 2005;26:5296-5302.

197 Goering PL, Kuester RK, Neale AR, Chapekar MS, Zaremba TG, Gordon EA, Hitchins VM: Effects of particulate and soluble cadmium species on biochemical and functional parameters in cultured murine macrophages. In vitro & molecular toxicology 2000;13:125-136.

198 ASTM: Standard practice for short term screening of implant materials. Philadelphia, PA, ASTM Committee, 1987, F763-87, pp 276-279.

199 Patil SD, Papadimitrakopoulos F, Burgess DJ: Dexamethasone-loaded poly(lactic-co-glycolic) acid microspheres/poly(vinyl alcohol) hydrogel composite coatings for inflammation control. Diabetes Technol Ther 2004;6:887-897.

200 Bridges AW, Garcia AJ: Anti-inflammatory polymeric coatings for implantable biomaterials and devices. J Diabetes Sci Technol 2008;2:984-994.

201 Anderson JM, Rodriguez A, Chang DT: Foreign body reaction to biomaterials. Semin Immunol 2008;20:86-100.

202 Jutila MA: Leukocyte traffic to sites of inflammation. APMIS 1992;100:191-201.

203 Black J: The inflammatory process; Biological performance of materials: Fundamentals of biocompatibility. Boca Raton, FL, Taylor and Francis, 2006, pp 139-162.

204 Tomazic-Jezic VJ, Merritt K, Umbreit TH: Significance of the type and the size of biomaterial particles on phagocytosis and tissue distribution. Journal of biomedical materials research 2001;55:523-529.

205 Dadsetan M, Jones JA, Hiltner A, Anderson JM: Surface chemistry mediates adhesive structure, cytoskeletal organization, and fusion of macrophages. J Biomed Mater Res A 2004;71:439-448.

206 Clark RAF: Wound repair: Overview and general considerations; in Clark RAF (ed): Molecular and cellular biology of wound repair. New York, Plenum Press, 1996, pp 3-50.

207 Mirza R, DiPietro LA, Koh TJ: Selective and specific macrophage ablation is detrimental to wound healing in mice. Am J Pathol 2009;175:2454-2462.

208 Schaffer MR, Tantry U, Thornton FJ, Barbul A: Inhibition of nitric oxide synthesis in wounds: Pharmacology and effect on accumulation of collagen in wounds in mice. The European journal of surgery = Acta chirurgica 1999;165:262-267.

209 Amadeu TP, Seabra AB, de Oliveira MG, Monte-Alto-Costa A: Nitric oxide donor improves healing if applied on inflammatory and proliferative phase. The Journal of surgical research 2008;149:84-93.

210 Witte MB, Barbul A: Role of nitric oxide in wound repair. Am J Surg 2002;183:406-412.

211 Amadeu TP, Costa AM: Nitric oxide synthesis inhibition alters rat cutaneous wound healing. J Cutan Pathol 2006;33:465-473.

212 Weng L, Ivanova ND, Zakhaleva J, Chen W: In vitro and in vivo suppression of cellular activity by guanidinoethyl disulfide released from hydrogel microspheres composed of partially oxidized hyaluronan and gelatin. Biomaterials 2008;29:4149-4156.

213 Ritger PL, Peppas NA: A simple equation for description of solute release i. Fickian and non-fickian release from non-swellable devices in the form of slabs, spheres, cylinders or discs. Journal of Controlled Release 1987;5:23-36.

214 Pozzi R, De Berardis B, Paoletti L, Guastadisegni C: Inflammatory mediators induced by coarse (pm2.5-10) and fine (pm2.5) urban air particles in raw 264.7 cells. Toxicology 2003;183:243-254.

215 Jalava PI, Salonen RO, Halinen AI, Penttinen P, Pennanen AS, Sillanpaa M, Sandell E, Hillamo R, Hirvonen MR: In vitro inflammatory and cytotoxic effects of size-segregated particulate samples collected during long-range transport of wildfire smoke to helsinki. Toxicol Appl Pharmacol 2006;215:341-353.

216 Flick DA, Gifford GE: Comparison of in vitro cell cytotoxic assays for tumor necrosis factor. J Immunol Methods 1984;68:167-175.

217 Bastos KR, Barboza R, Sardinha L, Russo M, Alvarez JM, Lima MR: Role of endogenous ifn-gamma in macrophage programming induced by il-12 and il-18. J Interferon Cytokine Res 2007;27:399-410.

218 Ross JA, Auger MJ: The biology of the macrophage; in Burke B, Lewis CE (eds): The macrophage (second edition). New York, Oxford University Press, 2002, pp 3-56.

219 LeBel CP, Ischiropoulos H, Bondy SC: Evaluation of the probe 2',7'-dichlorofluorescin as an indicator of reactive oxygen species formation and oxidative stress. Chem Res Toxicol 1992;5:227-231.

220 Lin PH, M.K. H, von Fraunhofer JA, Greisler HP: Wound healing and inflammatory response to biomaterials; in Chu CC (ed): Wound closure biomaterials and devices. New York, CRC Press, 1997, pp 7-24.

221 De Jong WH, Eelco Bergsma J, Robinson JE, Bos RR: Tissue response to partially in vitro predegraded poly-l-lactide implants. Biomaterials 2005;26:1781-1791.

222 Picrosirius red staining protocol for collagen: http://www.ihcworld.com/_protocols/special_stains /sirius_red.htm 10 May 2010

223 Tabata Y, Ikada Y: Effect of the size and surface charge of polymer microspheres on their phagocytosis by macrophage. Biomaterials 1988;9:356-362.

224 Ainslie KM, Tao SL, Popat KC, Daniels H, Hardev V, Grimes CA, Desai TA: In vitro inflammatory response of nanostructured titania, silicon oxide, and polycaprolactone. J Biomed Mater Res A 2009;91:647-655.

225 Kirby BJ, Hasselbrink EF, Jr.: Zeta potential of microfluidic substrates: 1. Theory, experimental techniques, and effects on separations. Electrophoresis 2004;25:187-202.

226 Prior S, Gander B, Blarer N, Merkle HP, Subira ML, Irache JM, Gamazo C: In vitro phagocytosis and monocyte-macrophage activation with poly(lactide) and poly(lactide-co-glycolide) microspheres. Eur J Pharm Sci 2002;15:197-207.

227 Jiang B, Hu L, Gao C, Shen J: Ibuprofen-loaded nanoparticles prepared by a co-precipitation method and their release properties. International journal of pharmaceutics 2005;304:220-230.

228 Huang YC, Chiang CH, Yeh MK: Optimizing formulation factors in preparing chitosan microparticles by spray-drying method. Journal of microencapsulation 2003;20:247-260.

229 Brandwood A, Noble KR, Schindhelm K: Phagocytosis of carbon particles by macrophages in vitro. Biomaterials 1992;13:646-648.

230 Yamaguchi K, Anderson JM: Biocompatibility studies of naltrexone sustained release formulations. Journal of Controlled Release 1992;19:299-314.

231 Morais JM, Papadimitrakopoulos F, Burgess DJ: Biomaterials/tissue interactions: Possible solutions to overcome foreign body response. The AAPS journal;12:188-196.

232 Onuki Y, Bhardwaj U, Papadimitrakopoulos F, Burgess DJ: A review of the biocompatibility of implantable devices: Current challenges to overcome foreign body response. J Diabetes Sci Technol 2008;2:1003-1015.

233 Anderson JM, Langone JJ: Issues and perspectives on the biocompatibility and immunotoxicity evaluation of implanted controlled release systems. J Control Release 1999;57:107-113.

234 Hwang SM, Chen CY, Chen SS, Chen JC: Chitinous materials inhibit nitric oxide production by activated raw 264.7 macrophages. Biochemical and biophysical research communications 2000;271:229-233.

235 Moller W, Hofer T, Ziesenis A, Karg E, Heyder J: Ultrafine particles cause cytoskeletal dysfunctions in macrophages. Toxicol Appl Pharmacol 2002;182:197-207.

236 Luzardo-Alvarez A, Blarer N, Peter K, Romero JF, Reymond C, Corradin G, Gander B: Biodegradable microspheres alone do not stimulate murine macrophages in vitro, but prolong antigen presentation by macrophages in vitro and stimulate a solid immune response in mice. J Control Release 2005;109:62-76.

237 Binker MG, Zhao DY, Pang SJ, Harrison RE: Cytoplasmic linker protein-170 enhances spreading and phagocytosis in activated macrophages by stabilizing microtubules. J Immunol 2007;179:3780-3791.

238 Cardona MA, Simmons RL, Kaplan SS: Tnf and il-1 generation by human monocytes in response to biomaterials. Journal of biomedical materials research 1992;26:851-859.

239 Hooper KA, Nickolas TL, Yurkow EJ, Kohn J, Laskin DL: Characterization of the inflammatory response to biomaterials using a rodent air pouch model. Journal of biomedical materials research 2000;50:365-374.

240 Thorns M, Benghuzzi H, Tucci M, Carson Z: The physiological response associated with large particles of tcp, ha, and alcap implants using raw 264.7 cells. Biomed Sci Instrum 2001;37:287-292.

241 Taffet SM, Singhel KJ, Overholtzer JF, Shurtleff SA: Regulation of tumor necrosis factor expression in a macrophage-like cell line by lipopolysaccharide and cyclic amp. Cell Immunol 1989;120:291-300.

242 Stuehr DJ, Marletta MA: Synthesis of nitrite and nitrate in murine macrophage cell lines. Cancer Res 1987;47:5590-5594.

243 Zhao F, Wang L, Liu K: In vitro anti-inflammatory effects of arctigenin, a lignan from arctium lappa l., through inhibition on inos pathway. J Ethnopharmacol 2009;122:457-462.

244 Jones JA, McNally AK, Chang DT, Qin LA, Meyerson H, Colton E, Kwon IL, Matsuda T, Anderson JM: Matrix metalloproteinases and their inhibitors in the foreign body reaction on biomaterials. J Biomed Mater Res A 2008;84:158-166.

245 Mantovani A, Sica A, Sozzani S, Allavena P, Vecchi A, Locati M: The chemokine system in diverse forms of macrophage activation and polarization. Trends Immunol 2004;25:677-686.

246 Mosser DM, Zhang X: Activation of murine macrophages. Curr Protoc Immunol 2008;Chapter 14:Unit 14 12.

247 Song E, Ouyang N, Horbelt M, Antus B, Wang M, Exton MS: Influence of alternatively and classically activated macrophages on fibrogenic activities of human fibroblasts. Cell Immunol 2000;204:19-28.

248 Anderson JM, Jones JA: Phenotypic dichotomies in the foreign body reaction. Biomaterials 2007;28:5114-5120.

249 Tawil NJ, Connors D, Gies D, Bennett S, Gruskin E, Mustoe T: Stimulation of wound healing by positively charged dextran beads depends upon clustering of beads and cells in close proximity to the wound. Wound Repair Regen 1999;7:389-399.

250 Sasaki A, Mueller RV, Xi G, Sipe R, Buck D, Hollinger J: Mast cells: An unexpected finding in the modulation of cutaneous wound repair by charged beads. Plastic and reconstructive surgery 2003;111:1446-1453.

251 Eppley BL, Summerlin DJ, Prevel CD, Sardove AM: Effects of a positively charged biomaterial for dermal and subcutaneous augmentation. Asethetic Plastic Surgery 1994;18:413-416.

252 Lemperle G, Morhenn VB, Pestonjamasp V, Gallo RL: Migration studies and histology of injectable microspheres of different sizes in mice. Plastic and reconstructive surgery 2004;113:1380-1390.

253 Liu P, Yin K, Nagele R, Wong PY: Inhibition of nitric oxide synthase attenuates peroxynitrite generation, but augments neutrophil accumulation in hepatic ischemia-reperfusion in rats. The Journal of pharmacology and experimental therapeutics 1998;284:1139-1146.

254 Lucas T, Waisman A, Ranjan R, Roes J, Krieg T, Muller W, Roers A, Eming SA: Differential roles of macrophages in diverse phases of skin repair. J Immunol;184:3964-3977.

255 Sanchez-Alcazar JA, Schneider E, Hernandez-Munoz I, Ruiz-Cabello J, Siles-Rivas E, de la Torre P, Bornstein B, Brea G, Arenas J, Garesse R, Solis-Herruzo JA, Knox AJ, Navas P: Reactive oxygen species mediate the down-regulation of mitochondrial transcripts and proteins by tumour necrosis factor-alpha in l929 cells. The Biochemical journal 2003;370:609-619.

256 Treuting PM, Albertson TM, Preston BD: Case series: Acute tumor lysis syndrome in mutator mice with disseminated lymphoblastic lymphoma. Toxicologic pathology 2010;39:476-485.

257 Bhardwaj U, Sura R, Papadimitrakopoulos F, Burgess DJ: Controlling acute inflammation with fast releasing dexamethasone-plga microsphere/pva hydrogel composites for implantable devices. J Diabetes Sci Technol 2007;1:8-17.

258 Cadee JA, Brouwer LA, den Otter W, Hennink WE, van Luyn MJ: A comparative biocompatibility study of microspheres based on crosslinked dextran or poly(lactic-co-glycolic)acid after subcutaneous injection in rats. Journal of biomedical materials research 2001;56:600-609.

259 Darmani H, Crossan JC, Curtis A: Single dose of inducible nitric oxide synthase inhibitor induces prolonged inflammatory cell accumulation and fibrosis around injured tendon and synovium. Mediators Inflamm 2004;13:157-164.

260 Luo JD, Chen AF: Nitric oxide: A newly discovered function on wound healing. Acta pharmacologica Sinica 2005;26:259-264.

261 Borkakoti N: Matrix metalloprotease inhibitors: Design from structure. Biochem Soc Trans 2004;32:17-20.

262 Visscher GE, Robison RL, Maulding HV, Fong JW, Pearson JE, Argentieri GJ: Biodegradation of and tissue reaction to 50:50 poly(dl-lactide-co-glycolide) microcapsules. Journal of biomedical materials research 1985;19:349-365.

263 Hooper KA, Macon ND, Kohn J: Comparative histological evaluation of new tyrosine-derived polymers and poly (l-lactic acid) as a function of polymer degradation. Journal of biomedical materials research 1998;41:443-454.

264 Schwendeman SP, Costantino HR, Gupta RK, Tobio M, Chang AC, Alonso MJ, Siber GR, Langer R: Strategies for stabilising tetanus toxoid towards the development of a single-dose tetanus vaccine. Dev Biol Stand 1996;87:293-306.

265 Zhu G, Mallery SR, Schwendeman SP: Stabilization of proteins encapsulated in injectable poly (lactide- co-glycolide). Nature biotechnology 2000;18:52-57.

266 Cleland JL, Mac A, Boyd B, Yang J, Duenas ET, Yeung D, Brooks D, Hsu C, Chu H, Mukku V, Jones AJ: The stability of recombinant human growth hormone in poly(lactic-co-glycolic acid) (plga) microspheres. Pharmaceutical research 1997;14:420-425.

267 Cleland JL, Jones AJ: Stable formulations of recombinant human growth hormone and interferon-gamma for microencapsulation in biodegradable microspheres. Pharmaceutical research 1996;13:1464-1475.

268 van de Weert M, Hennink WE, Jiskoot W: Protein instability in poly(lactic-co-glycolic acid) microparticles. Pharmaceutical research 2000;17:1159-1167.

269 Kim HK, Park TG: Comparative study on sustained release of human growth hormone from semi-crystalline poly(l-lactic acid) and amorphous poly(d,l-lactic-co-glycolic acid) microspheres: Morphological effect on protein release. J Control Release 2004;98:115-125.

270 Hermeling S, Crommelin DJ, Schellekens H, Jiskoot W: Structure-immunogenicity relationships of therapeutic proteins. Pharmaceutical research 2004;21:897-903.

271 van de Weert M, Hoechstetter J, Hennink WE, Crommelin DJ: The effect of a water/organic solvent interface on the structural stability of lysozyme. J Control Release 2000;68:351-359.

272 Diamond MP, Freeman ML: Clinical implications of postsurgical adhesions. Hum Reprod Update 2001;7:567-576.

273 Mettler L: Pelvic adhesions: Laparoscopic approach. Annals of the New York Academy of Sciences 2003;997:255-268.

274 Leak LV, Ferrans VJ, Cohen SR, Eidbo EE, Jones M: Animal model of acute pericarditis and its progression to pericardial fibrosis and adhesions: Ultrastructural studies. The American journal of anatomy 1987;180:373-390.

275 Naito Y, Shin'oka T, Hibino N, Matsumura G, Kurosawa H: A novel method to reduce pericardial adhesion: A combination technique with hyaluronic acid biocompatible membrane. J Thorac Cardiovasc Surg 2008;135:850-856.

276 Flanagan JG: Glaucoma update: Epidemiology and new approaches to medical management. Ophthalmic Physiol Opt 1998;18:126-132.

277 Gupta D: Glaucoma diagnosis and management. Philadelphia, Pa., Lippincott Williams & Wilkins, 2005.

278 Vision problems in the us: Prevalence of adult vision impairment and age-related eye disease in america: http://www.nei.nih.gov/eyedata/pdf/VPUS.pdf 10-08-07

279 Friedman DS, Wolfs RC, O'Colmain BJ, Klein BE, Taylor HR, West S, Leske MC, Mitchell P, Congdon N, Kempen J: Prevalence of open-angle glaucoma among adults in the united states. Archives of ophthalmology 2004;122:532-538.

280 Yee RW: The effect of drop vehicle on the efficacy and side effects of topical glaucoma therapy: A review. Current opinion in ophthalmology 2007;18:134-139.

281 The advanced glaucoma intervention study (agis): 7. The relationship between control of intraocular pressure and visual field deterioration.The agis investigators. American journal of ophthalmology 2000;130:429-440.

282 Allingham RR, Shields MB: Shields' textbook of glaucoma, ed 5th. Philadelphia, Lippincott Willliams & Wilkins, 2005.

283 Frankhanser F: Wound healing in glaucoma filtering surgery. New York, Kugler, 1992.

284 Occleston NL, Daniels JT, Tarnuzzer RW, Sethi KK, Alexander RA, Bhattacharya SS, Schultz GS, Khaw PT: Single exposures to antiproliferatives: Long-term effects on ocular fibroblast wound-healing behavior. Investigative ophthalmology & visual science 1997;38:1998-2007.

285 Belyea DA, Dan JA, Stamper RL, Lieberman MF, Spencer WH: Late onset of sequential multifocal bleb leaks after glaucoma filtration surgery with 5-fluorouracil and mitomycin c. American journal of ophthalmology 1997;124:40-45.

286 Cordeiro MF, Constable PH, Alexander RA, Bhattacharya SS, Khaw PT: Effect of varying the mitomycin-c treatment area in glaucoma filtration surgery in the rabbit. Investigative ophthalmology & visual science 1997;38:1639-1646.

287 Daniels JT, Occleston NL, Crowston JG, Khaw PT: Effects of antimetabolite induced cellular growth arrest on fibroblast-fibroblast interactions. Experimental eye research 1999;69:117-127.

288 Cordeiro MF, Siriwardena D, Chang L, Khaw PT: Wound healing modulation after glaucoma surgery. Current opinion in ophthalmology 2000;11:121-126.

289 Schwentker A, Vodovotz Y, Weller R, Billiar TR: Nitric oxide and wound repair: Role of cytokines? Nitric Oxide 2002;7:1-10.

290 Yamasaki K, Edington HD, McClosky C, Tzeng E, Lizonova A, Kovesdi I, Steed DL, Billiar TR: Reversal of impaired wound repair in inos-deficient mice by topical adenoviral-mediated inos gene transfer. J Clin Invest 1998;101:967-971.

291 Akcay MN, Ozcan O, Gundogdu C, Akcay G, Balik A, Kose K, Oren D: Effect of nitric oxide synthase inhibitor on experimentally induced burn wounds. J Trauma 2000;49:327-330.

292 Sze A, Erickson D, Ren L, Li D: Zeta-potential measurement using the smoluchowski equation and the slope of the current-time relationship in electroosmotic flow. J Colloid Interface Sci 2003;261:402-410.

293 Puchtler H, Meloan SN, Waldrop FS: Are picro-dye reactions for collagens quantitative? Chemical and histochemical considerations. Histochemistry 1988;88:243-256.

294 Dayan D, Hiss Y, Hirshberg A, Bubis JJ, Wolman M: Are the polarization colors of picrosirius red-stained collagen determined only by the diameter of the fibers? Histochemistry 1989;93:27-29.

295 Junqueira LC, Bignolas G, Brentani RR: Picrosirius staining plus polarization microscopy, a specific method for collagen detection in tissue sections. Histochem J 1979;11:447-455.

296 Borges LF, Gutierrez PS, Marana HR, Taboga SR: Picrosirius-polarization staining method as an efficient histopathological tool for collagenolysis detection in vesical prolapse lesions. Micron 2007;38:580-583.

Appendix A

Microgel Sample Preparation for Particle Size Analysis and Zeta Potential

A.1 Preparation for Particle Size Analysis

Equivalent diameter values were determined using dynamic light scattering (DLS) (ZetaPlus, Brookhaven Instruments, Brookhaven NY). The diameter measured using DLS is determined by both the core size of the particle and the velocity of the particle (translational diffusion) through the suspending medium. The measured velocities of the particles are then used to calculate the actual diameter of the particles using the following equation:

$$d(H) = \frac{\kappa T}{3\pi\eta D} \qquad \text{(A.1)}$$

where d(H) is the hydrodynamic diameter, D is the translational diffusion coefficient (particle velocity), κ is Boltzmann's Constant, T is temperature (absolute), and η is the viscosity of the suspending medium.

Approximately 2.5 mg of microspheres were placed in 4 mL of phosphate buffered saline (PBS, pH=7.4) solution and the vessel was placed in a sonicator bath for 5 minutes, with intermittent removal to decrease heating effects from sonication. The sonication step is necessary to produce separate particles and break up any aggregates that formed during sample re-suspension with PBS. The microsphere suspension (2 mL) was added to a disposable, 1 cm path-length, polystyrene cuvette and capped. The cuvette was placed in the zetasizer instrument and particle size analysis was initiated by the provided software and algorithm (ZetaPlus Particle Sizing Software v.4.10, Brookhaven Instruments, Brookhaven NY). The program ran 5 size measurements for 5 minutes total for each batch of microgels. Sizing was performed on 3 different batches of each GED loading. Average and standard deviation of effective diameter were used in statistical analysis.

A.2 Zeta Potential Analysis

Zeta potential describes the propensity of particles in suspension to flocculate by measuring the charge potential difference between the supernatant solution and the stationary fluid layer around the particle [292]. Zeta potential analysis was performed using the same instrument (ZetaPlus) as described in the particle sizing protocol. The zeta potential measurements were determined by utilizing phase analysis light scattering (PALS) technique and Smoluchowski Equation, calculated internally by the installed software package (PALS Zeta Potential Analyzer v.3.57, Brookhaven Instruments Corp., Brookhaven NY).

Samples for zeta analysis were prepared in a less turbid suspension than their particle size analysis counterparts. Approximately 2.5 mg of each microgel formulation was placed in 4 mL of PBS (pH=7.4) and sonicated for 5 minutes, with intermittent removal. After the microgels were suspended in PBS, a 1 mL aliquot of the microgel

suspension was further diluted into 3 mL of fresh PBS solution. Approximately 2 mL of each diluted suspension was added to a disposable, polystyrene cuvette, and the zeta electrode unit was inserted into the cuvette. Cycle number (specifying the number of times the voltage potential is switched between electrodes in Zeta unit) was set to 30 and 5 runs were performed in triplicate per formulation (No GED, low dose GED, and high dose GED). The microgel slurry was allowed to “rest” for 30 seconds between run sets to decrease the chance of over-heating the samples inside the cuvette. The zeta potential values from each run set were averaged and standard deviation was calculated.

Appendix B

Tissue Staining Theory and Methods

B.1 Masson's Trichrome Staining Method

This method stains any collagen present in tissue a light-to-dark blue color while other tissue elements will be stained red and nuclei will stain black. Masson's trichrome staining also highlights blood vessel formation by darkly staining the annular tissue layers surrounding the vessel structure. The staining process was performed by the author for all samples using prepared staining solutions from the Electron Microscopy Sciences (Hatfield, PA). For paraffin embedded samples, the sections were deparaffinized in xylene and rehydrated to distilled water using a series of ethanol solutions. Sections from cryosectioning were rehydrated directly with distilled water. All sections were briefly soaked in distilled water and then transferred to Weigerts iron hematoxylin working solution for 10 minutes. The slides were liberally rinsed with running tap water for 10 minutes and then placed in a solution of Biebrich scarlet-acid fuchsin solution for 15 minutes. After rinsing away excess Biebrich scarlet-acid fuchsin from the sections, the slides were then placed in a solution of phosphomolybdic-phosphotungstic acid for 15 minutes. The slides were then placed (un-rinsed) in aniline blue solution for 5 minutes. Slides were then rinsed briefly in distilled water before differentiating in a 1% acetic acid solution for 5 minutes. The sections were dehydrated in ethanol solutions and cleared in xylene before applying a xylene-based resin (Permount, Fisher Scientific). High magnification images of the cyst capsules helped localize the microgels. PLGA microsphere treated tissue was not dehydrated like the microgel treated tissue. Instead, the tissue sections were removed from the acetic acid soak and mounted with a coverslip using a drop of Fluoromount (Electron Microscopy Sciences, Hatfield, PA).

B.2 Picrosirius Red Staining for Collagen-I Formation

Although Masson's Trichrome staining can identify collagens in tissue, it does not differentiate between types of collagen or whether the collagens present are in the cytoplasm of fibroblasts or assembled into mature fibrils. Other staining methods for connective tissues include Van Gieson's method; however, the stain tends to fade within several months even with proper storage conditions [293]. Picrosirius red staining is a more stable and a stronger collagen-binding staining method than both Van Giesons and Masson's Trichrome. The thickness/alignment of collagen fibers is measured by observing birefringence of stained collagen fibers under polarizing light microscopy [294,295]. Thicker collagen fibers are colored red/light orange (Collagen type I) in polarized light, while thinner fibers are more yellow/green (Collagen type III) in color. In addition, the birefringence observed is only seen with Collagen type I or III; however, other molecules such as Collagen type IV (basal lamina) and mucosal

membranes will stain red with the dye, but they do not demonstrate birefringence under polarized light [222,295,296].

The picrosirius red staining method used in this study was modified from a previously published protocol [222] and performed by the author. To stain paraffin embedded sections, the tissue was deparaffinized in xylene and re-hydrated to distilled water through a series of ethanol solutions. The tissues were then stained in Weigert's hematoxylin for 8 minutes and then rinsed in running tap water for 10 minutes. After rinsing, the sections were placed in a solution of 0.1% Sirius red (Direct Red 80, Sigma Aldrich, St. Louis, MO) dissolved in an aqueous 0.1% saturated picric acid. The sections stained in the picrosirius red solution for 1 hour at room temperature. At the end of this staining step, the slides were rinsed in 2 changes of acidified water (0.5% glacial acetic acid in distilled water). The sections were then quickly dehydrated with absolute ethanol, cleared in xylene, and mounted with resinous mounting media (Permount, Fisher Scientific, Pittsburgh, PA). PLGA microsphere treated tissues were stained in a similar manner, except that the alcohol re/dehydration steps were omitted and an aqueous based mounting media, Fluoromount (Electron Microscopy Sciences, Hatfield, PA), was utilized instead of Permount.